MULTI-COLOUR ANALYSIS OF GALAXY CLUSTERS WITH RADIO HALOS AND/OR RELICS

L. S. Legodi

Supervisors:
Dr N. Oozeer (SKA Africa, AIMS, NWU)
& Prof. T. Jarrett (UCT)

Astronomy Department
University of Cape Town (UCT)

A research project submitted in partial fulfilment of the requirements for the National Astrophysics and Space Science Programme (NASSP) M.Sc. degree.

September 2014

This work is funded fully by the South African National Research Foundation (SA NRF) and the the Square Kilometre Array South Africa (SKA SA) project through their postgraduate student scholarship. Opinions expressed and conclusions made, are those of the author and not necessarily those of the SA NRF, SKA SA, NASSP and/or UCT.

Abstract

Galaxy clusters can be sites of considerable dynamic activity due to intra-cluster and inter-cluster interactions. These interactions include cluster-cluster mergers which are accompanied by large release of energy observed via thermal X-ray emission ($L_X \sim 10^{44}$ ergs/s). The work presented here focuses on clusters that exhibit extended ($\sim$ 1 Mpc) diffuse radio sources (low surface brightness $\sim 1-0.1$ μJy.arcsec^{-2} at 1.4 GHz) called radio relics and radio halos. The relics tend to be found in the peripheral regions of galaxy clusters while halos tend to be located at the central regions. These two types of sources share many of their characteristics but some of their key difference is radio polarization: relics tend to have polarised emission while halos do not. The observed polarisations and the non-thermal nature of the emission of these sources suggests the existence of large scale magnetic fields which permeate galaxy cluster volumes. Investigations into relic and halo sources may shed light into the formation of galaxy clusters and how they evolve. A way of analysing the evolution of clusters is to investigate the evolutionary state of their galaxy populations. This work aims to both characterise galaxy membership and probe galaxy evolution in these clusters through a spatial, kinematic and photometric analysis.

Archival databases are utilised for multi-wavelength data acquisition. Cluster member galaxies are determined through a Gaussian mixture model (GMM) algorithm applied to the spatial and radial velocity distributions of galaxy cluster member candidates. The main cluster sample comprises of 20 clusters of up to redshift $z \leqslant 0.1$, selected for completeness to be optimally approximated. The sample consists of 5 halo clusters, 4 clusters with both a halo and/or relic(s) and 11 clusters that host radio relics. Through the spatial and kinematic analysis, it is found that these clusters have significant spatial substructure and are dynamically disturbed. These findings are in accord with current published literature, suggesting that radio relics and halos are found in galaxy clusters that have recently ($\lesssim$ 1 Gyr) undergone or are going through a merger process or processes.

A photometric analysis on the optical colour-magnitude relation: r versus $(g-r)$, recovers the red sequence and blue cloud of galaxies with a linear relation of scatter $\sigma(g-r) \sim 0.02$ AB mag. This agrees with published literature where $\sigma(g-r) \approx 0.04$ AB mag. Relic cluster galaxies and those from clusters with both a halo and/or relic(s) show the red and blue clouds along with the green valley in the UV-optical colour-colour ($NUV-r, g-r$) distribution.

The UV-optical colour-colour-magnitude ($NUV-r, g-r, M_z$) distribution of galaxies showed that red cloud objects tend to have the brightest z-band luminosities. Green valley galaxies displayed z-band luminosities similar to both red and blue cloud galaxies supporting the notion that the green valley is composed of two distinct galaxy populations on different evolutionary paths. The WISE mid-IR colour-colour-morphology-SF (star formation) relation was also recovered: galaxies with colours akin to the earliest morphologies displayed the lowest obscured star formation (specific star formation (sSRF) $\lesssim 1 \times 10^{-12}$ yr^{-1}) and galaxies with late type colours showed the highest obscured star formation (sSFR $\gtrsim 1 \times 10^{-11}$ yr^{-1}). A very small fraction ($\lesssim 0.3\%$) of galaxies displayed AGN-like colours, which is expected from galaxy cluster populations. Another small but significant fraction of galaxies ($\sim 16\%$), was found to have some of the largest stellar masses ($M_\star \sim 1 \times 10^{11}$ M$_\odot$), lowest obscured star formation (sSFR $\sim 1 \times 10^{-13}$ yr^{-1} to $\sim 1 \times 10^{-15}$ yr^{-1}), peculiar radial velocities ~ 100 km/s to ~ 2000 km/s, and all galaxies located within projected radii ~ 1 Mpc – suggesting that these are passively evolving early type galaxies.

Keywords: Galaxy cluster, Abell cluster, radio halo, radio relic, cluster analysis, Gaussian Mixture Model, Kernel density estimator, Abell radius, radial velocity, galaxy colour, star formation, subcluster, velocity dispersion, bi-weight estimator and complex cluster.

Acknowledgements

This work is funded fully by the South African National Research Foundation (SA NRF) and the the Square Kilometre Array South Africa (SKA SA) project through their postgraduate student scholarship.

The help and guidance of my supervisors, Dr Nadeem Oozeer, and Prof. Tom Jarrett, was pivotal throughout my research.

Data Sources

This research has made use of data products from the Wide-field Infrared Survey Explorer, which is a joint project of the University of California, Los Angeles, and the Jet Propulsion Laboratory/California Institute of Technology, funded by the National Aeronautics and Space Administration. This research has made use of the VizieR catalogue access tool and the SIMBAD database, CDS, Strasbourg, France.

This research has made use of Sloan Digital Sky Survey Data release 9 (SDSS DR9). Funding for SDSS-III has been provided by the Alfred P. Sloan Foundation, the Participating Institutions, the National Science Foundation, and the U.S. Department of Energy Office of Science. The SDSS-III web site is http://www.sdss3.org/. SDSS-III is managed by the Astrophysical Research Consortium for the Participating Institutions of the SDSS-III Collaboration including the University of Arizona, the Brazilian Participation Group, Brookhaven National Laboratory, Carnegie Mellon University, University of Florida, the French Participation Group, the German Participation Group, Harvard University, the Instituto de Astrofisica de Canarias, the Michigan State/Notre Dame/JINA Participation Group, Johns Hopkins University, Lawrence Berkeley National Laboratory, Max Planck Institute for Astrophysics, Max Planck Institute for Extraterrestrial Physics, New Mexico State University, New York University, Ohio State University, Pennsylvania State University, University of Portsmouth, Princeton University, the Spanish Participation Group, University of Tokyo, University of Utah, Vanderbilt University, University of Virginia, University of Washington, and Yale University.

This research has made use of the NASA/IPAC Extragalactic Database (NED), which is operated by the Jet Propulsion Laboratory, California Institute of Technology, under contract with the National Aeronautics and Space Administration (NASA).

Use of ultra-violet observations from the Galaxy Evolution Explorer (GALEX) is hereby acknowledged. GALEX is a NASA Small Explorer, launched in April 2003. GALEX research is lead by the California Institute of Technology and further information can be found on the website: http://www.galex.caltech.edu/

This research has made use of the NASA/ IPAC Infrared Science Archive, which is operated by the Jet Propulsion Laboratory, California Institute of Technology, under contract with the National Aeronautics and Space Administration.

Plagiarism Declaration

I, Letjatji Samuel Legodi, know the meaning of plagiarism and hereby declare that all of the work in this document, save for that which is properly acknowledged, is my own.

Signature: ———————

Date: ———————

Contents

List of Figures

List of Tables

Chapter 1

Introduction

1.1 Galaxy Clusters: An introduction

Galaxy clusters, along with large scale (sizes of several Megaparcecs) filamentary structures, large scale voids, dark matter and clusters/groups of galaxy clusters, form constituents of the cosmic web – the observed large scale distribution of galaxies and dark matter. Cosmic voids (or just voids) are regions in space (large scale structure) that have significantly low cosmic mean densities which are roughly approximated as the number densities of galaxies within the regions (Neyrick 2008[173]). Clusters are the largest gravitationally bound systems in this cosmic web with masses of the order $\sim 10^{12} - 10^{16}$ $M_{\odot}$ and volumetric sizes of ~ 100 Mpc^3 (Feretti et al. 2012[78]). They are composed largely of dark matter ($\sim 80\%$) with a smaller fraction of baryonic/"normal" matter. The baryonic matter further divides into galaxies ($\lesssim 5\%$) and the intra-cluster medium (ICM). This ICM is hot ionized gas (energies of several keV) and X-ray bright and so it is primarily detected through X-ray observations (Feretti et al. 2012[78]).

The current formation paradigm of clusters is that which follows hierarchical structure formation (Kravtsov & Borgani 2012[144]). In this scenario individual galaxies and groups of galaxies merged in the early universe and accreted more mass through gravity. The cluster then grows through these recurring mergers of smaller units. Regions in space which have higher densities tend to form large scale filaments with clusters being formed and evolving within these high density regions. The environment inside the filaments leads to clusters constantly changing, either on small scales where individual galaxies and small galaxy groups are constantly being accreted from the surrounding regions or on larger scales with major cluster-cluster mergers (Ferrari et al. 2008[79], Feretti et al. 2012[78]). This constant state of dynamic activity drives the evolution of galaxy clusters and quite literally shocks the ICM and leads to substructure and energization of the ICM as clusters collide. The ICM displays high densities in the central regions, where the X-ray emission peaks, and decreasing densities in the peripheries (Feretti et al. 2012[78]). Kravtsov & Borgani (2012)[144] have given an extensive review of the formation of galaxy clusters with a description of current paradigms and highlights of highly accurate theoretical models for cluster formation.

The ICM is a global cluster constituent and thus is not attributable to individual galaxies or groups, however, Kravtsov & Borgani (2012)[144] show that some properties of galaxies and the ICM are correlated. The authors find

that the ICM mass is approximately an order of magnitude larger than that part of the cluster mass that is due to galaxies (stellar mass). The ICM may also influence the evolution of galaxies depending on the locations, within the cluster, of these galaxies. In the central regions of clusters, there tends to be large, massive and highly luminous elliptical galaxies grouped under the collective term of cD galaxies (Kormendy & Djorgovski 1989[142]). These galaxies are the brightest cluster members and are also called brightest cluster galaxies (BCGs). They are the most massive galaxies but they display the least amount of recent star formation in the entire cluster (Kravtsov & Borgani 2012[144]). On the other hand, irregular and spiral galaxies (late type galaxies) which are much more active in terms of star formation, are much less massive and reside away from the central regions of clusters (Poggianti 2002[190]). While the high density and hot (X-ray bright) regions of cluster centres is where bright massive early type galaxies (ellipticals) reside, the later types reside in lower density regions (e.g. Dressler 1980[56]). Late type galaxies that are in the process of being accreted into clusters tend to have enhanced star formation (starbursts) and disturbed morphologies (Porter et al. 2008[191]). These peripheral galaxies tend to have their gaseous disks bent by ram pressure[1] as they fall into the cluster. Outer galaxies have been observed to have enhanced star formation not only within the galaxy itself but also within the material that is being stripped due to ram pressure (Sun et al. 2007[229]). Cortese et al. (2007)[45] also show that this effect has not only been observed in the nearby clusters but also in distant systems.

Clusters are also classified into various types based on their galaxy populations and masses. Clusters which display large galaxy number densities are classified as rich (hundreds to thousands of galaxies, e.g. Coma cluster) and those on the opposite end of galaxy number densities ($\lesssim 100$ galaxies), are classified as poor clusters (Abell 1958[1], Zwicky et al. 1961[258]). Other classifications are based on the nature of the central galaxy population (Bautz-Morgan, BM, type – BM I are clusters with a single central cD BCG, BM II are those that have several central cDs and giant ellipticals, and BM III are clusters without a dominant central galaxy) (Bautz & Morgan 1970[15]) and the Rood-Sastry (RS) type (Rood & Sastry 1971[201]). The RS type describes the distribution of the ten brightest galaxies in a similar manner as the BM type.

1.2 Radio Emission

Cluster galaxy populations are diverse and within them exists powerful radio emitters such as active galaxies (active galactic nuclei galaxies, AGN). The primary radio emission components are free-free[2] and synchrotron[3] emission. The galaxial radio emission usually extends to hundreds of kiloparsecs, beyond the extent of the emitting galactic source (Feretti et al. 2012[78]), as radio jets. Observation have shown that these jets do in fact interact with the ICM (e.g. Clarke et al. 2014[37]) and one prominent example of such cases is that of tailed radio galaxies (e.g. Jetha et al. 2006[123]). The radio emission which emanates from the host radio galaxy, forms a lobe (or pair of lobes) and is observed to be bent as a result of interactions with the ICM, especially for those galaxies which are found in dense central cluster regions (e.g. O'Donoghue et al. 1993[176]). This radio emission can be directly attributed to galaxial sources or sources on scales of galaxies, unambiguously.

[1] The pressure due to the ICM, felt by a galaxy as it falls into a cluster. This pressure depends on the galaxy-ICM relative velocities and the ICM density (Gunn & Gott 1972[108]).
[2] Where weak electric interactions between electrons and hydrogen ions lead to radio emission.
[3] Emission of photons by relativistic electrons which are accelerated, in a spiral fashion, along magnetic field lines.

Just as galaxy radio emission is expected in clusters, diffuse extended and cluster wide radio emission is not, and yet there exists large scale ($\sim$ 1 Mpc) radio emission of very low surface brightness in some galaxy clusters. This emission is well beyond the sizes of any sources that can be attributed to galaxies and must somehow originate from the ICM (Feretti et al. 2012[78], Ferrari et al. 2008[79]). The very low surface brightness makes it very difficult to detect and it can only be positively identified if galaxy sources are ruled out and the host cluster can be identified (Nuza et al. 2012[175]). The emission has been attributed to a non-thermal component of the ICM with the main emission mechanism being synchrotron processes (e.g. Feretti & Giovannini 2008[76]; Cassano et al. 2011[32]). The thermal component of the ICM is composed of hot diffuse gas which is what is primarily observed in the X-ray. The non-thermal component suggests the existence of relativistic ICM particles which spiral along cluster scale magnetic fields to produce some of the observed diffuse and extended radio emission. The number densities of relativistic ICM constituents is much lower than that of the thermal component ($\sim 10^{-10}$ cm^{-3}) with Lorentz factors of $\gamma \gg 1000$, while the magnetic fields in these clusters are $\lesssim 1$ μG with non-thermal energy contributions of $\lesssim 1$ % (Ferrari et al. 2008[79]). This non-thermal ICM, even with it's low contribution to the total energy, is vital to the holistic understanding of ICM and cluster evolution.

The first observations indicating the existence of these sources was made by Large et al. (1959)[146] in the Coma cluster centre and these detections were later confirmed by Willson (1970)[249]. These sources are still not currently fully understood but have been found to exist in primarily dynamic, disturbed and merging cluster systems (e.g. Cortese et al. 2004[44]). They are classified according to the polarization nature of their emission, their location and shape within the cluster. The two main classes are reviewed in the following subsections.

1.2.1 Radio Halos

Radio halos are diffuse (low surface brightness $\sim 1 - 0.1$ μJy arcsec^{-2} at 1.4 GHz – Feretti et al. 2012[78]) extended ($\gtrsim$ 1 Mpc) radio sources which are found in the central regions of some clusters (Figure 1.1). They have a regular morphology and their emission is not polarised, likely due to internal or beam depolarisation (Feretti et al. 2012). Giovannini and Feretti (2002)[97] show that there is a correlation between the X-ray luminosity (i.e. thermal ICM emission) and the occurrence of radio halos (i.e. non-thermal ICM emission). The number of halos increases with X-ray luminosity reaching $\gtrsim 25$ % in clusters which have X-ray luminosities $L_X > 5 \times 10^{44}$ ergs/s. A puzzle is the collapse of this correlation for redshifts higher than $z = 0.35$, where halo numbers drop, which could point to a real lack of radio halos at earlier cosmological times, sensitivity limitations of current detectors or a combination of selection biases (Giovannini et al. 2009[95]; Feretti et al. 2012[78]).

Radio halos display a steep spectrum[4] with spectral indices $\alpha \gtrsim 1$ (Feretti et al. 2012). A steep spectrum means that these sources emit strongly in the low frequencies and have low luminosities at higher frequencies where there may be an upper frequency limit beyond which there is little or no emission. Feretti et al. (2012) report that the distribution of spectral indices for clusters with temperatures of $\sim$ 10 keV has an average index $\alpha \sim 1$ indicating

[4]The convention used through out this work is that the spectral energy distribution (S_ν) and the frequency (ν) of the radiation emitted are proportional through the relation $S_\nu \sim \nu^{-\alpha}$, where α is the spectral index.

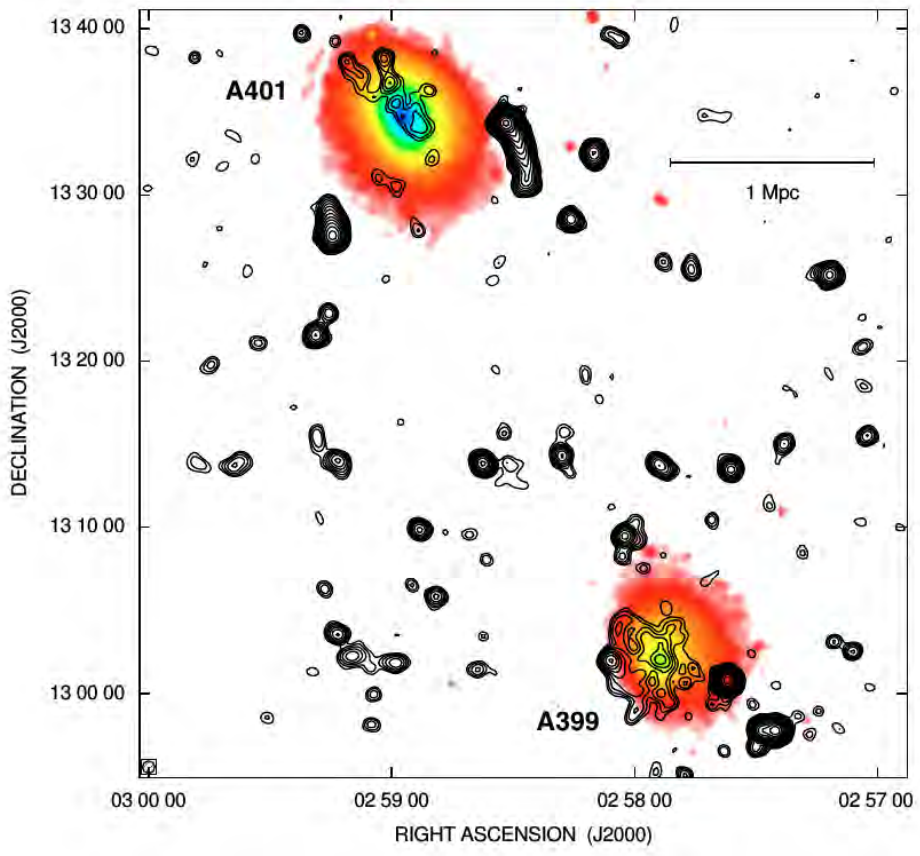

Figure 1.1: Radio halos in A0401 and A0399. Total intensity radio contours of the A0401-A0399 region. The contours are a Very Large Array (VLA) radio image taken at 1.4 GHz. The radio contours have a FWHM of $45'' \times 45''$. The first contour level is shown at 120 μJy/beam with a spacing of $\sqrt{2}$ for the other contours. The colour scale is the XMM X-ray image in the 0.2-12 keV band (Murgia et al. 2009[170]; Feretti et al. 2012[78]). The two halos (the diffuse emission in the central regions of both clusters) are among the faintest known, with the elongated one of A0401 confirmed as not due to a galactic source even given it position and morphology (Bacchi et al. 2003[8]). The elongated radio structure at the periphery of A0401 is due to a galaxy (a narrow angle tailed radio galaxy) and is not a relic.

that hot (X-ray luminous) clusters may have the most powerful radio halos. This correlation supports the notion that radio halos are associated with clusters which are massive and undergoing merger processes (Giovannini and Feretti 2002[97]). Buote (2001)[30] showed that the most powerful radio halos are found in clusters which are also very disturbed, but not all merging systems host halos and this bimodality in merging clusters is still poorly understood (Feretti et al. 2012).

There are also other "halos" which are much smaller than the megaparsec sizes of the halos described above. These are mini-halos and they tend to share the properties of *halos* except that they have sizes of $\sim$ 500 kpc. Their location at the central regions of some clusters increases the difficulty of identifying these sources as they may be misidentified with other diffuse radio sources such as radio bubbles produced by AGN in the cluster central regions. These sources are only identifiable once they are found to also form part of the ICM. Halos tend to share similar traits regardless of size, which indicates that these sources probably have a similar origin (Feretti et al. 2012).

The correlation between halos and X-ray properties of clusters also extends to the halo radio power and the X-ray luminosity. These two quantities are proportional which also supports a correlation between the cluster mass and the radio power of its halo (Govoni et al. 2001c[104]; Feretti 2003[73]).

1.2.2 Radio Relics

Radio relics are another class of diffuse and extended radio emission. They, however, have very irregular and often more elongated morphologies than halos. They are found at cluster peripheries and their emission is strongly polarised providing one of the best probes of cluster scale magnetic fields. Relics have been shown to be linked to relativistic particles accelerated at shock fronts located in cluster peripheries (e.g. Brüggen et al. 2011[26]) and are found both in merging clusters and cool-core clusters which are thought to be relaxed systems (Feretti et al. 2012; Giacintucci & Markevitch 2014[94]). Cluster mergers are categorised into minor mergers, where clusters of very different masses collide and the less massive one is incorporated into the more massive cluster, and major mergers where the merging clusters are of similar masses. Relics are found in clusters having undergone either or both types of mergers (e.g. Solovyeva et al. 2008[225]).

The relics come in two types: elongated and round relics. The elongated relics are more extended, irregular in shape, show the highest level of polarization among relics, and are found at peripheral cluster regions; while the roundish relics are less extended, more regular in shape and found nearer to the cluster central regions and also the periphery (Feretti et al. 2012). Radio relics are expected to come in pairs in the scenario that they result from major mergers. In this case the two relics should be located opposite each other along the merger axis (e.g. van Weeren et al. 2009[238]). van Weeren et al. (2011d)[236] showed this expected result through hydrodynamical simulations constrained by observations of a double radio relic observed in the cluster `CIZA J2242.8+5301`.

Systems with both a central halo and relic(s) also have been observed, with the Coma cluster being one of the earliest such clusters (Giovannini et al. 1991[99]; Giovannini et al. 1993[100]). Some of these systems also display a diffuse radio bridge between the relic and halo but the origin of this source is currently unknown. Feretti et al. (2012) show that in observations made so far, most relic sources are not accompanied by halos. This further supports the notion that relics form as a result of minor mergers which may not provide enough energy to produce a central halo along with the relic(s) while major merger systems can. Relics and halos also show similar correlations between the non-thermal radio power and thermal X-ray luminosity. This correlation starts to differ at low X-ray luminosities between the two classes of diffuse radio emission, with halos lacking as compared to relics.

1.2.3 Proposed Origins

Relics and halos provide a way to probe magnetic fields on the large scales of galaxy clusters. The diffuse radiation is attributed to synchrotron radiation by electrons in the ICM due to their interactions with a non-negligible magnetic field. The field is present through out the whole cluster. On smaller scales (less than about 100 kpc), magnetic fields can be probed through studying radiation from individual galaxies within or beyond the cluster. In this case Faraday rotation of the galaxy radiation is used to indirectly probe the magnetic field (Feretti et al., 2012[78]).

Magnetic fields of the order of μG are observed but the details of how these are linked to relics and halos are not trivially apparent. This is where the constituents of the ICM come under scrutiny. The ICM is composed mostly of a proton and electron plasma with the electrons suffering far greater radiation losses than the protons in the plasma

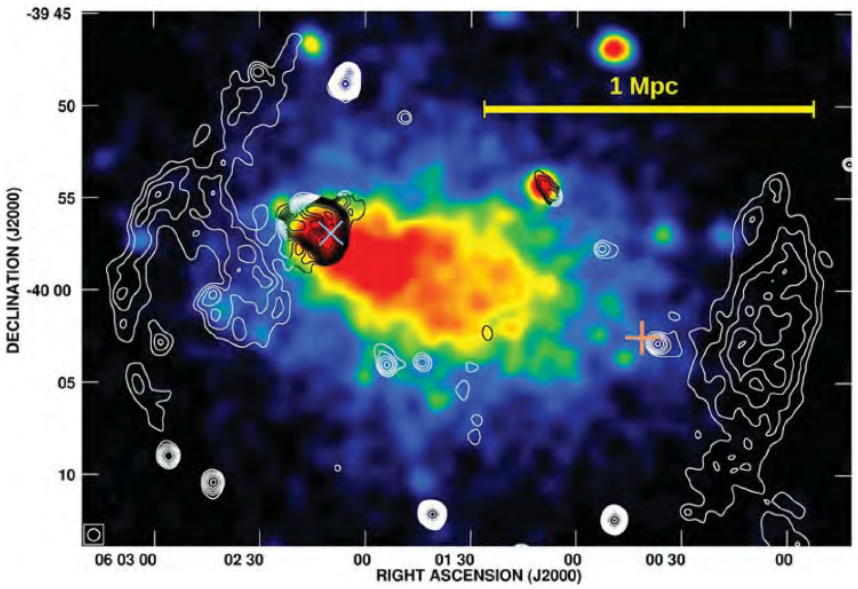

Figure 1.2: Radio relics in A3376. Giant Metrewave Radio Telescope (GMRT) 325 MHz radio image (contours) of A3376. The synthesised beam is $39'' \times 39''$ with contour levels drawn first at 5.8 mJy/beam and then progressively increased by a factor of $\sqrt{2}$. The colour gradient is an X-ray image from ROSAT in the band 0.1-2.4 keV. The cross marks the MRC 0600-399 (a bent double radio galaxy) and the plus sign marks the BCG (Kale et al. 2012[129]).

and thus most of the radiation emitted by the plasma must be due to the electrons. It then stands to reason that the non-thermal radiation from the ICM should be transient, short lived and not extended on the scales at which it is observed. This is due to the short radiative lifetimes of electrons. So where do these relativistic electrons come from?

Magnetic fields are a common feature in clusters and they have been attributed to the formation of clusters (Feretti et al., 2012[78]). These fields were produced during the times of large scale structure formation and major dynamical processes, such as cluster mergers, also serve to supply the energy required to amplify them to the levels at which they are observed at the current epoch (Ryu et al., 2008[204]). This evolution of the magnetic field proceeds parallel to the evolution of the parent cluster itself and so these fields are a common property of many clusters but the diffuse extended emission is not, suggesting that the relativistic electrons required to produce the observed synchrotron radiation might not be trivially accounted for.

Two main models to account for the production of relativistic electrons in the ICM have been suggested. These are the so called primary and secondary electron models. In the primary model, the electrons originate from the cluster galaxies. They are ejected from stellar evolution processes and nucleic activity in galaxies. On the other hand, secondary electrons are produced via proton-proton (p-p) collisions in the ICM plasma. These protons suffer far less radiation losses as compared to electrons and so they can spread through out the cluster volume (with the exception of cluster outskirts where the ICM particle densities are extremely low and so p-p collisions are rare) and produce electrons as they diffuse into the ICM (Feretti et al., 2012).

As electrons have very short radiative life spans, they require some way to be re-accelerated in order to explain the observed extended diffuse radio emission. The re-acceleration of these electrons can occur via two main channels, viz: magneto-hydrodynamic (MHD) turbulence and/or re-acceleration by shocks (Feretti et al., 2012). MHD turbulence, in

this case, is produced during cluster mergers and along with the amplification of magnetic fields, the ICM electrons can get accelerated to relativistic energies (Brunetti 2011[28]). This turbulence is a transient phenomenon and it occurs in a random nature through out the cluster and is thus not sustainable or substantially efficient in energizing the ICM electrons and as such, it is expected that the radiation from this channel is due to recent dynamical activity in the cluster i.e. recent merger processes. Suggested MHD turbulence models (Brunetti 2004[27]), in the case where only primary electrons are re-accelerated, produce results which are consistent with observed halo and mini-halo properties (Feretti et al., 2012).

Shock acceleration occurs most notably in regions around catastrophic explosions such as regions surrounding supernova remnants. Shocks tend to accelerate particles very near the shock boundary and the resulting spectrum (emission from the accelerated particles) gets steeper as the shock waves get larger and the Mach number increases. Skillman et al. (2008)[219] & Vazza et al., (2011)[243] observed this phenomena, of a steepening spectrum as one moves from cluster centres to the peripheries. Shocks are largely associated with relics (Sarazin 1999[209]) as they result in radiation that is very localised to the shock boundary.

These electron production methods have some short falls, especially the secondary model. Highly energetic gamma radiation is produced in the p-p collisions but this radiation has not been conclusively identified and linked to any extended radio emission (Ackermann et al. 2010[3]; Jeltema & Profumo 2011[122]; and Fermi 2011). Also, secondary electrons are produced through out the history of the cluster and do not come about because of anything other than the p-p collisions in the ICM which rather suggests that halos should be observed in all clusters but this too is not so. Feretti et al. (2012) suggest that this may point to a model that includes both primary and secondary electrons which might fare better in describing the origin of the ICM electrons responsible for relics and halos.

1.3 Galaxy Colours and Environmental Influences

In order to understand the environment of these halos and relics, one can make use of the colours of the galaxy members. The colours of galaxies reveal physical properties in an easily quantifiable and robustly reproducible manner. This is required for understanding the evolution of these systems in all environments in which they are found (Baloch et al., 2004[11]).

1.3.1 Colour-Magnitude Relation and Colours

One of the most readily noticeable properties of all galaxies in colour-colour space, is the existence of bimodality in the colour distribution where predominantly passively evolving (not star-forming) galaxies and their actively evolving (star forming) counter parts are located at different regions of colour-colour space and thus form two distinct populations: the red (early type galaxies) and blue (late types) populations. Menci et al. (2005[165], 2006[164]) show that this bimodal distribution may be due to the two galaxy populations having two distinct star-formation histories which may be affected by feedback mechanisms[5] differently.

[5]Feedback is the injection of energy, mass and heavy elements into the surrounding environment by supernovae and/or active-galactic nucleic (AGN) activity

Salimbeni et al. (2007)[207] perform a study on the bimodality in the U-V colour of blue and red galaxy populations with redshifts of up to $z \sim 3$. Their data is made up of galaxies from the Great Origins Observatory Deep Survey Multicolour South Infrared Catalogue catalogue (GOODS MUSIC). The authors found that the luminosity functions of the red and blue galaxies differ in that the blue luminosity function is well described by the analytic Schechter function[6](Press and Schechter 1974[193]) while the red luminosity function is well fitted by galaxies at low and intermediate redshifts but deviates from the Schechter function at higher redshifts. Salimbeni et al. (2007)[207] attributed this behaviour to the evolutionary paths of each population and not to environmental influences. They make this assertion based on their finding that early type galaxies have larger stellar masses as compared to late types in any B band luminosity class and that the early type galaxies are more centrally concentrated as compared to late types of the same class. Both late and early type galaxies that are faint, however, show similar spatial distributions and thus the different environmental distributions do not seem to be of great importance to the luminosity functions of galaxies.

Baloch et al. (2004)[11] also found this weak dependence of the galaxy colour distribution on environment, they showed that the mean and scatter in the colour of the two galaxy populations has a strong dependence on luminosity and thus galaxy mass, which is expected for the red population from the morphology-density relation[7] and is in agreement with the Tully-Fisher relation[8](Tully and Fisher, 1977)[234]. They illustrated the bimodality of galaxy colours by fitting two Gaussian distributions to the colour distribution of their sample of Sloan digital Sky Survey (SDSS) sources and their models agree with their data, showing two distinct populations in colour space. They also show the strong environmental dependence of late types in the form of a morphology-density relation for their data.

1.3.2 Colours in Different Environments

The colour-magnitude relations (CMR) of late and early type galaxies differ in that the colours of early type galaxies are systematically redder and the early types tend to have a much tighter CMR (e.g. Visvanathan & Sandage, 1977[248]). The slope of the CMR has been shown to be indicative of star-formation history, through mean stellar metallicity (Kodama & Arimoto 1997[139]), while its scatter has information on the age of galaxies (Kodama, Bower & Bell 1999[140]; Pimblet et al., 2002[186]; De Propris et al., 2013[52]).

In the hierarchical cluster formation scenario, clusters form and evolve from the accretion of galaxies and/groups thus the galaxy population of clusters should progressively get younger (i.e. bluer) as one looks at an increasing radial distance from the cluster core. The morphology-density relation would then suggest that star-formation could be altered (perhaps halted) as galaxies are accreted into the cluster environment leading to the assertion made by Pimbblet et al. (2002)[186] that studies of cluster peripheral galaxy population as a function of redshift (thus cosmic time) can give information on the effects of environment on the evolution of clusters which are evolving over Hubble time.

[6] A parametric description of the space density of galaxies as a function of their intrinsic luminosity (Press and Schechter 1974[193]).
[7] Progression of galaxy population from late to early type domination as the environmental density in which the galaxies reside increases (Dressler 1980[56]).
[8] Positive linear correlation between the rotational speed of spirals and their luminosity (Tully and Fisher, 1977)[234].

Pimbblet et al. (2002)[186] performed a photometric study of the variation in galaxy colour with environment on a sample of 11 X-ray bright galaxy clusters with $0.07 \leq z \geq 0.16$. They found that the CMR is a common feature among galaxy clusters and that the CMR of cluster cores changes with redshift. The authors found that the colours of galaxies forming the CMR agree with those of galaxies that formed their stellar backbone at high redshift $z \gg 2$. They also showed that galaxy colours vary as a function of radial distance from the cluster core (for a fixed luminosity) and that galaxy colours depend weakly on the local environment. The authors attributed the scatter in the CMR as due to quiescent early type spirals (late type S0 galaxies) noting that the CMR of a normal cluster consists of a red quiescent passively evolving population (S0 and elliptical galaxies), late type S0 galaxies and star-forming spirals. The findings of Jaffé et al. (2011) on the CMR of galaxies are in agreement with Pimmblet et al. (2002). Jaffé et al. (2011)[118] also found a small population of faint early type galaxies bluer than the CMR. The origin of these faint blue early types may be due to (as suggested by the authors) minor mergers which would trigger star-formation near the central regions of the galaxies. This star formation would then lead to a build up of a spheroidal galactic bulge and eventually a change in the morphology and colours to those galaxies, leading to similarities with red population galaxies.

1.4 Galaxy Colours and Evolution

The colours of galaxies indicate the dominant sources of light in galaxies i.e. the dominant stellar population (modulated by galaxy geometry, dust and gas content). These colours can also be linked to galaxy morphology and star-formation (e.g. Terlevich, Caldwell & Bower 2001[232]; Chilingarian & Zolotukin 2012[35]). Star formation activity can be used as a proxy for galaxy evolution and there are various photometric indicators of star formation such as the ultra-violet (UV) continuum due to massive young stars and emitted at $\lambda \sim 912 - 3000$ Å mid-infrared light from warm dust and molecular (polycyclic hydrocarbons – PAHs) emission and also far-infrared (far-IR) light from dust heated by UV radiation of young stars (e.g. Arnouts et al. 2013[6]). Below are colours in combined ultra-violet, optical and infrared (IR) magnitudes chosen as probes of these galaxy properties.

1.4.1 UV and Optical colours

Optical colour-magnitude diagrams (CMDs) show a narrow red sequence, made up mostly of passively evolving galaxies, and a broad blue cloud made up primarily of star-formers. For example: the optical $(g-r, M_r)$ CMD displays a narrow red sequence with $\sigma(g-r) \sim 0.04$ mag (e.g. Strateva et al. 2001[227]) largely made up of early type galaxies (ellipticals and lenticular galaxies). This CMD can be used to select early-type galaxies in clusters and groups. This, however, is simply not always trivial (e.g. Strateva et al. 2001[227]; Baldry et al. 2004[10]). There is ambiguity in the correlation between galaxy morphology and galaxy positions in optical colour-colour space. The red sequence consists of ~ 25 % late type and weakly star-forming galaxies and on the other hand, post-starburst galaxies contaminate the blue cloud – these galaxies display spectra with features of a k-star (typical of early type galaxies) and features of young massive A-stars (Dressler & Gunn 1983[57]). The post-starburst galaxies have blue colours but early morphologies (Chilingarian & Zolotukin 2012[35]), a clear conflict in the current paradigm of bimodality in galaxy colours.

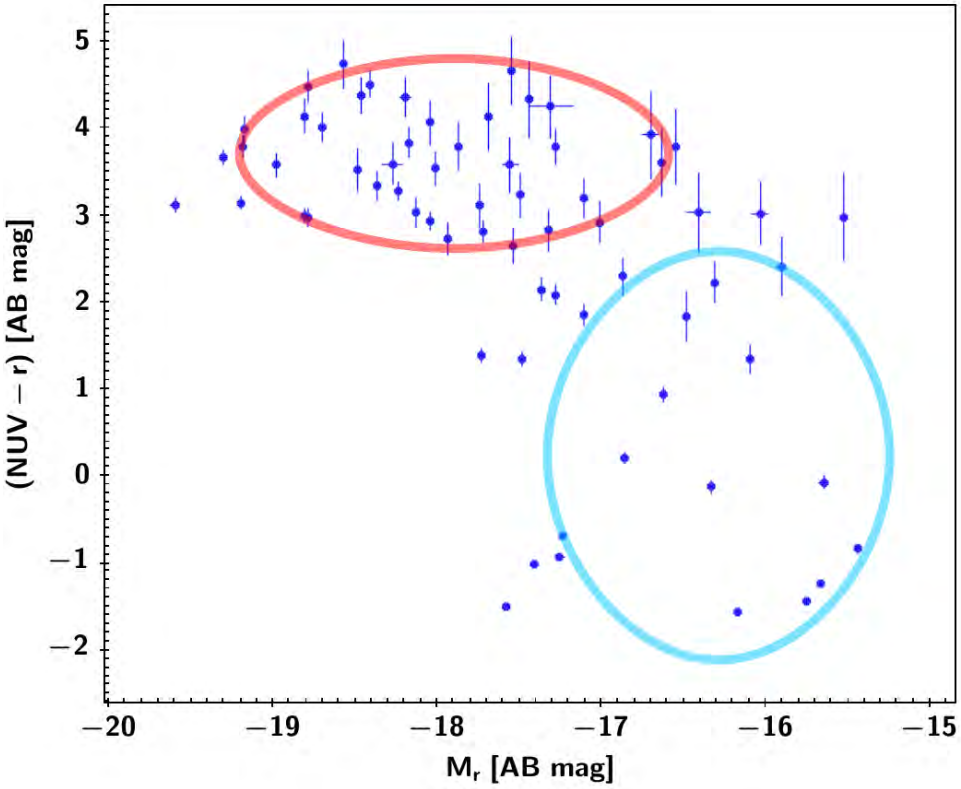

Figure 1.3: UV-optical colour-magnitude diagram of the Coma cluster. NUV is the GALEX near-ultraviolet apparent magnitude and r is the SDSS r-band apparent magnitude. (NUV-r) is the rest frame colour. The red and blue ellipses show the red sequence and blue cloud regions, respectively.

The red sequence and blue cloud become apparent in the UV-optical CMD, but again some ambiguity arises due to increased broadness of these two regions (Wyder et al. 2007[253]). For example: the near UV(NUV)-optical CMD $(NUV - r, M_r)$ displays pronounced regions of the red sequence and blue cloud but these are much broader in colour space as compared to the optical CMR ($\sigma(NUV - r) \sim 2$ mag). The GALEX (Galaxy Evolution Explorer) NUV band is significantly more sensitive to young stellar populations than any of the optical bands (Barway et al. 2013[14]) but this sensitivity also introduces ambiguity due to contamination of the blue cloud by early type galaxies which have small populations of young massive stars (Kaviraj et al. 2007[133]).

Chilingarian & Zolotukin (2012) show that the combination of optical and UV colours as a function of luminosity (using use absolute magnitudes) eliminates most of the above challenges. The authors find that in colour-colour-magnitude space there is a much tighter relation with reduced contamination in regions of the blue cloud, red sequence and regions where post-starburst galaxies are expected. This relation is found in the $(NUV - r, g - r, M_r)$ colour-colour-magnitude diagram. The relation persists when the $(NUV - r, g - r)$ colour-colour diagram is projected onto any of the optical r, i, z Sloan Digital Sky Survey (SDSS) bands.

1.4.2 Infra-red colours (IR)

Different objects have different IR colours as well. This extends to galaxies where different morphologies, and hence evolutionary histories, can be divided and recognised through their IR colours. Mid-infrared (MIR) colours, such

as those from the Wide-field Infrared Survey Explorer (Wright et al. 2010[252]) have been found to be essential in this respect. MIR wavebands are sensitive to processed starlight that is due to young stars which are hidden from our line sight by galaxy ISM. The WISE $W3$ band has an effective central wavelength of 12 micron, making it ideal for probing star formation that is obscured by the molecular component of the ISM (poly-cyclic hydrocarbons/PAH emission peaking at 11.3 micron) while the $W4$ band (22 micron) is more sensitive to the warm dust component of the ISM (Jarrett et al. 2012[121]). $W4$ band is best for probing star formation but has a lower signal to noise ratio and so the $W3$ band can be used to quantify global obscured star formation rates of galaxies (e.g. Jarrett et al. 2013[121]; Cluver et al. 2014[42]).

1.5 Cluster Kinematics

Apart from colour diagrams, cluster kinematics allow us to understand the dynamics inside the cluster environment. It is well accepted that the universe is expanding and that things, on the largest scales of galaxies and beyond, are receding form each other (Hubble 1929[115]). The clumping of matter through out the universe due to gravity, however, introduces internal dynamics whose effects can be observed in gravitationally interacting systems. These *peculiar* motions can be used to probe the connection between individual constituents (of gravitationally interacting systems) and gravity in that system (e.g. Davis & Scimegeour 2014[50]). The dispersions of these velocities can be used to probe the overall mass of the system under certain assumptions (e.g. Richmond 2012[9]).

1.5.1 Peculiar Velocity

There are various methods to determine the peculiar velocities (e.g. Davis & Scimegeour 2014[50]) and in this work the peculiar velocity of the $i-$th galaxy in a cluster with mean redshift z_{mean} is given by

$$v_i = c\left(\frac{z_i - z_{mean}}{1 + z_{mean}}\right), \tag{1.1}$$

where c is the speed of light. The cluster's X-ray centroid's redshift or BCG redshift may also be used but for the purposes of probing the peculiar velocities of all cluster galaxies.

The perculiar motion of galaxies in a cluster can be used to probe the nature of the gravitational interactions that those galaxies are undergoing and this notion can also be extended to the cluster BCG. BCGs (cD galaxies and BCGs will be used interchangeably) have a profound link with the evolution of clusters or galaxy groups as cD galaxies are found primarily in such environments (Hill & Oegerle 1993[114]). cD galaxies are thought to have formed through the hierarchical merging of galaxies in the central regions of groups and clusters (e.g. Lin & Mohr 2004[151]). A majority of these galaxies are observed to host AGN and also forms the largest population of radio loud/luminous galaxies among ellipticals (Best et al. 2007[18]). Their location at cluster centres suggests that they should be located at the bottom of their cluster's potential well and should be at rest within the cluster (Hill & Oegerle 1993[114]). Observations show that this is not so and BCGs are actually found to have peculiar velocities in the range $6 - 700$ km/s (e.g. Pimbblet et al. 2006[185] and references therein). Venturi et al. (2013)[245] found that the Abell 3560

[9] http://spiff.rit.edu/classes/phys440/lectures/glob_clus/glob_clus.html

cluster[10] BCG has a peculiar velocity of $\sim$ 1000 km/s, a significant deviation from observations of BCGs in relaxed (so called virialised) systems. Peculiar velocities of these magnitudes suggest that these BCGs are in dynamically disturbed clusters (Hill & Oegerle 1993[114]).

1.5.2 Velocity Dispersion

The galaxy velocity dispersion σ_v is a statistical measure of deviations in the radial velocities of galaxies from a mean radial velocity. It can be used as a probe for cluster mass especially for relaxed spheroidal systems where the virial theorem[11] can be reasonably applied. The velocity dispersion can also be used to probe cluster kinematics based on its statistical properties (e.g. Oegerle et al. 1995[177]). The velocity dispersion, σ_v, of a sample of N galaxies is given by

$$\sigma_v = \sqrt{\frac{\sum_{i=1}^{N} v_i^2}{N-1}}, \tag{1.2}$$

where v_i is defined in equation 1.1.

1.6 Cluster Membership

In order to make a reasonable analysis on the cluster kinematics and environment, one needs to determine the cluster members. Identifying patterns and similarities is one of the most basic and vital diagnostic tools which can be used in this particular analysis. This allows the grouping and ordering of the data into meaningful sets. This is most important in cases such as when considering galaxy clusters and their members. The single most important aspect of a cluster analysis would be the answer to the question "what defines a cluster?". In the case of this research, we want to extract those galaxies that form part of a cluster in terms of being bound to the cluster gravitationally and so the spatial distributions of the cluster member candidate galaxies are analysed to identify the most probable cluster members. Throughout this thesis, we shall use the term galaxy clusters to refer to clusters of galaxy gravitational bound together and clusters to statistical clustering algorithm.

1.6.1 Clustering Algorithms

Cluster analysis methods vary from trial and error methods to those which are more formal and make use of statistical models. They form two main categories: those which are hierarchical in nature and those which rather relocate cluster member candidates among existing groups/partitions/sub-clusters (Fraley & Raftery 1998[84]). In this analysis, hierarchical clustering methods will be employed as minimal prior information is assumed regarding the structure of the clusters in our sample. The initial assumptions we make are that galaxy clusters are composed of component(s) that are themselves normally distributed in terms of their spatial properties (RA, Dec and redshift/radial velocity). Hierarchical methods are divided into two main groups: agglomerative clustering – where larger groups form from

[10] A rich cluster in the A3558 complex which forms part of the Shapley Concentration (Bardelli et al. 2002[13]).

[11] This theorem relates the kinetic and potential energy of a self gravitating system by stating that the two should be comparable with a factor of two.

smaller groupings – and partitioning methods – where groups form by the breaking down of a larger partition.

Partitioning hierarchical cluster analysis requires some knowledge of the way in which to constrain the number of partitions formed, while in the case of agglomerative clustering each cluster candidate starts off as a seed made up of just one member and then these are merged until an optimum distribution is realised.

Gaussian mixture models (GMM) are a general way of modelling systems which consist of a number of superimposed normal distributions making up a non-relaxed cluster such as one undergoing a merger. GMM algorithms use expectation maximisation (EM) to select the optimal parameters that characterise the data. EM maximises the likelihood of a certain set of parameters in the model. The algorithm used here also employs the Bayesian information criterion (BIC) to robustly go about expectation maximisation. The BIC (Schwarz 1978[214]) is a criterion for comparing and selecting models according to maximum likelihood. Models can be made to fit data better by increasing the number of parameters used which may lead to misrepresentation of the information in the data; i.e over-fitting. The BIC combats this by introducing a penalty to the likelihood of progressively complex parametrisations. The most likely model has the largest absolute[12] BIC value. The BIC has the advantage that different models can be compared based on their parametrisations, number of components or both.

1.6.2 Statistical Tools Used

The statistical tools used to represent and characterise data are described in the subsections that follow.

1.6.2.1 *Histogram & Kernel Density Estimate (KDE)*

The representation of data is often the first step at an analysis and must always be performed in the most optimum way possible so as to get the most conclusive and comprehensible understanding of the data that is at one's disposal. At this initial level of analysis, density estimation tools such as the histogram come in very handy. The histogram is a one dimensional representation of the density of a given quantity – it simply gives the number of occurrences of the values of said quantity in specific sub-intervals (bins) into which the numerical range of the above quantity has been divided. These sub-intervals have the same width, the bin width, which is a free parameter and must be handled in the most optimised manner as to represent the data in the most accurate manner. As such, there are several ways in which one can choose the bin-width and the method employed here is that of Freedman & Diaconis 1981[86]

$$h = 2(IQR)/\sqrt{n}, \tag{1.3}$$

where h is the bin-with, IQR is the inter-quartile range[2] and n is the sample size. This method of estimating the bin-width has the advantage that it is sensitive to the true distribution of the sample and will explicitly show where outliers lie in relation to the main sample. The histogram, however, has the disadvantage that it is not continuous and smooth by definition and it also depends on the end points of the bins, thus some behaviour of the data might be

[12] Different authors use different sign conventions, either positive (Fraley & Raftery 1998[84]) or negative (Kass & Raftery 1995[132]).
[2] The difference between the upper and lower quartiles.

lost in the coarseness of the representation.

A higher order method that is similar to the histogram but lacks some of its disadvantages is the Kernel density estimation (KDE). This is a non-parametric estimation of the probability density function of the data. The KDE is independent of the bin-end points and is a smooth and continuous function. While the histogram groups data points discretely into bins, the KDE centres a kernel function (the kernel in this context is a symmetric function which integrates to unity – and the Gaussian kernel is chosen here for its well understood mathematical properties and the suspected Gaussian behaviour of galactic photometry and the nature of the GMM[13] which will be the principal foci of analysis in this work) on each of the data points in the sample and then these centred kernels are summed to give the kernel density estimate (Silverman 1986[218]; Scott 1979[215]). The bin-width (in the case of KDE this is often referred to as the band-width and dented as h below) is still a free parameter and will need to optimised for the most meaningful representation of the data. Mathematically, the KDE is defined by:

$$f(x) = \frac{1}{nh}\Sigma_{i=1}^{n}\left(K\frac{x-x_i}{h}\right), \tag{1.4}$$

where K is the kernel function and $x_i \in [x_1; x_2; ...; x_n]$ is an element of our data sample. In this work, and for the Gaussian kernel, the optimal choice of h is (Silverman's rule of thumb – Silverman (1986)[218]

$$h = \left(\frac{4}{3n}\sigma^5\right)^{\frac{1}{5}}, \tag{1.5}$$

where σ is the standard deviation.

1.6.2.2 *Location and Scale Estimators*

Estimators of location give an approximation of a representative value among a set of data while estimators of scale give an indication of the uncertainty in that representative value. A prime example is the mean/average and the standard deviation of the mean. These are good approximations for normal distributions but may not optimally represent the representative values in distributions with significantly non-normal components.

Mean and Median

The mean/average is one of the most widely used measures of location when it comes to basic statistical analysis. It is sensitive to skewness in data distribution and so will be significantly affected by outlying data, especially for small sample sizes. It can thus be used to rule out outliers under certain assumptions such as requiring the data to be normal to some degree of confidence. Weighting factors which favour data points nearest to the mean can be applied in these cases so that outliers or data points far away from the mean are more easily excluded. Real observations are, however, not necessarily Gaussian and assumptions made which request Gaussianity in the data may be biased and lead to erroneous conclusions.

[13] Bimodal colour distribution and Gaussian mixtures expected from clusters of galaxies.

The median is another commonly used measure of location. It is midpoint of the data with half the data values larger and the other half smaller. It is more robust than the mean/average as it is less sensitive to outliers and in the case of Gaussianity the two statistics agree. Only when one half of the data is heavily contaminated/skewed will the median be significantly affected by outlying values. Several modifications of the median have been constructed which exploit and improve on its robustness. Some of these include the broadened median (Andrews et al. 1972[5]), and the tri-median (Beers et al. 1990[16]).

Bi-weight Estimators

A robust location estimator which combines the strengths of both the mean and median is the biweight location estimator (C_{BI}) first proposed by Tukey (1958)[233]. It was suggested as an improvement to the normal distribution which includes significantly non-Gaussian components. It is defined as

$$C_{BI} = M + \left[\frac{\sum_{|u_i|<1}(x_i - M)(1-u_i^2)^2}{\sum_{|u_i|<1}(1-u_i^2)^2} \right], \tag{1.6}$$

where M is the median, x_is are the data points and

$$u_i = \frac{x_i - M}{c_t \cdot MAD}. \tag{1.7}$$

MAD is the sample median absolute deviation – defined as the median of the absolute deviations from the sample median, and c_t is the so called tuning constant. The tuning constant is chosen to ensure high efficiency of C_{BI} for a variety of distributions with the optimal value being $c_t = 6.0$. This includes data for up to 4σ (Mosteller & Tukey 1977[169]). C_{BI} outperforms any other estimators for sample sizes larger than about 50 and has an efficiency of greater than about 80 % for sample sizes of about 10^{14} (Beers et al. 1990[16]). C_{BI} approaches the mean in the case of a normally distributed dataset.

The biweight scale estimator (S_{BI}) is another robust statistic proposed for non-normal datasets. It takes the role of the standard deviation in the case of a skew distribution and like C_{BI}, approaches its Gaussian counterpart in the case of a normal distribution. It is defined by

$$S_{BI} = \sqrt{n} \left[\frac{\sqrt{\sum_{|u_i|<1}(x_i - M)^2(1-u_i^2)^4}}{\sum_{|u_i|<1}(1-u_i^2)(1-5u_i^2)} \right], \tag{1.8}$$

for u_i as defined above and tuning constant $c_t = 9.0$. This statistic also performs well for small samples, $n \sim 10$, (Goodall 1983[103]).

1.6.2.3 *Quartile-Quartile Plot*

A quartile-quartile or QQ plot is a non-parametrized method of comparing the correlation between two distributions. It is a scatter plot with one distribution on the y-axis and the other on the x-axis with the two distributions often plotted in terms of their quantiles. The two distributions are compared along the line $y = x$ and those points that differ from the line show disagreements between the models, while those which lie on the line agree. If two models have

[14] Assuming that the sample mean is 100 % efficient for a normal distribution but rapidly falls off in efficiency in the presence of small deviations from normality.

a linear relationship which differs from $y = x$ then the QQ plot will have points which lie on a line that is different from $y = x$. The plot can also shed some light on the relative skewness of the two distributions. If the distribution of points is above the $y = x$ line then the distribution on the y-axis is more skewed than that on the x-axis. The same is true for the x-axis, if the points are distributed below the $y = x$ line then the distribution on the x-axis is more skewed. In most cases the plot has points in an arc or an "S" shape indicating that one distribution is more skewed than the other. The QQ plot here, is used to compare the observed redshift distribution to a normal distribution.

1.7 Aims and Objectives

The availability of readily accessible multi-wavelength data allows for studies that are ever increasing in depth and extent, exploring a large array of physical properties. This work consists of utilising multi-wavelength data to both characterise galaxy cluster membership and analyse the evolution of galaxy cluster members as a function of environment.

1.8 Thesis Structure

This thesis is organised as follows:

- Chapter 2: (*Sample Selection*) An overview of the sample is given as well as a discussion of already known features in the selected clusters as obtained from the literature survey and virtual observatory (VO) data mining. The various data mining procedures are also discussed in this chapter. The tools used to characterise cluster membership are also discussed in this chapter and a dynamical analysis of complex clusters is performed.
- Chapter 3: (*Multi-colour Analysis*) A UV-optical and IR multi-colour analysis is performed in this chapter.
- Chapter 4: (*Star Formation*) The obscured (molecular ISM component) star formation of galaxies is analysed in this chapter.
- Chapter 5: (*Summary and Conclusions*) Results obtained from the analysis carried out on the sample will be summarised and discussed in this chapter. Conclusions of the dissertation will be given here together with suggestions for future work.

Chapter 2

Sample Selection

2.1 Cluster Selection

Feretti et al. (2012)[78] published a review on galaxy clusters which were known, as of the end of 2011, to have extended diffuse radio emission i.e. radio relics, radio halos and mini-halos. The authors review the observational properties of these clusters and those of the diffuse emission, the origins of the relics and halos, and the implications with regard to the content of the intra-cluster medium (ICM) and the nature of large scale magnetic fields. Feretti et al. (2012)[78] compile a short catalogue of the relic and halo host clusters collected from published multi-wavelength work by various researchers and groups (see references in Table 2.1).

Struble & Rood (1999)[228] have compiled 1572 redshifts and 395 velocity dispersions for Abell, Corwin, and Olowin (ACO) clusters. Their velocity dispersions are corrected to the reference frame of the cluster and will be used in this work as the reference measurements of cluster velocity dispersions for the majority of the cluster sample of Table 2.1.

The sample used for the analysis in this thesis is taken from the above review (Feretti et al. 2012)[78]. The selection criterion applied is that the largest cluster redshift (z_c or z_{Xc} in Table 1, the two are used interchangeably) be $z_c \sim 0.1$ so that we may lessen the Malmquist bias. A complete sample of cluster galaxies, where the sample is truly representative of the true galaxy population, is required to probe the different galaxy populations in the different cluster environments. This puts constraints on the clusters selected hence the cluster sample used in this work has an upper limit on redshifts of approximately 0.1. This is chosen because the primary source of optical photometry used is the ninth data release of the Sloan Digital Sky Survey (SDSS DR9, henceforth DR9) whose observations are significantly biased in favour of the most luminous objects for redshifts larger than approximately 0.2 (Ahn et al. 2012)[4]. This effect is due to the Malmquist bias, where the brightest of objects are observed the deeper in redshift that observations go, and progressively less of the very faint objects are detected (Malmquist 1920)[156] with increasing redshift observations. The restriction put on redshifts is in an attempt to have photometric completeness for the limited cluster sample. Only clusters having photometric data (from sources mentioned in Chapter 2.3.) were chosen in this study.

Table 2.1: Cluster sample (Feretti et al. 2012): Positions of the BCGs and Cluster centres for which $z \lesssim 0.1$. The sample of BCGs and possible cluster members was obtained from the CDS/SIMBAD database while the redshifts of the individual galaxy cluster candidates were obtained from NED.*

Cluster	RA_{Xc} [hh mm ss]	DEC_{Xc} [deg mm ss]	z_{Xc}	BCG	RA_{bcg} [hh mm ss]	DEC_{bcg} [deg mm ss]	z_{bcg}	Ref
A1213H	11 16 29	+29 16 35	0.0469	4C_29.41	11 16 35	+29 15 17	0.0470	1
A1367R	11 44 45	+19 41 59	0.0217	NGC3862	11 45 05	+19 36 23	0.0217	14
A0013R	00 13 38	-19 30 19	0.0943	2MASXI_J0013385-193000	00 13 39	-19 30 01	0.0943	11
A2048R	15 15 17	+04 22 47	0.0972	SDSS_J151514.10+042310.3	15 15 14	+04 23 10	0.0980	15
A2061R	15 21 21	+30 40 15	0.0784	2MASX_J15212054+3040154	15 21 21	+30 40 15	0.0789	16
A2063R	15 23 02	+08 38 22	0.0349	MCG+02-39-020	15 23 05	+08 36 33	0.0342	17
A2255R	17 12 47	+64 03 11	0.0806	2MASXI_J1712287+640338	17 12 29	+64 03 39	0.0734	7
A2255H	17 12 47	+64 03 11	0.0806	2MASXI_J1712287+640338	17 12 29	+64 03 39	0.0734	6
A2256R	17 03 43	+78 43 03	0.0581	UGC_10726	17 04 27	+78 38 26	0.0592	8
A2256H	17 03 43	+78 43 03	0.0581	UGC_10726	17 04 27	+78 38 26	0.0592	8
A2319H	19 20 45	+43 57 43	0.0557	MCG+07-40-004	19 21 10	+43 56 44	0.0542	9
A3376R-W	06 01 46	-39 59 34	0.0456	ESO_307-13	06 01 41	-40 02 40	0.0463	18
A3376R-E	06 01 46	-39 59 34	0.0456	ESO_307-13	06 01 41	-40 02 40	0.0463	18
A3562H	13 33 32	-31 40 23	0.0499	ESO_444-72	13 33 35	-31 40 20	0.0492	10
A0399H	02 57 56	+13 00 59	0.0718	UGC_2438	02 57 53	+13 01 51	0.0712	2
A0401H	02 58 57	+13 34 56	0.0737	UGC_2450	02 58 58	+13 34 58	0.0747	3
A4038R	23 47 31	-28 12 10	0.0282	IC_5358	23 47 45	-28 08 27	0.0291	11
A0548R-NW	05 47 02	-25 36 59	0.0424	6dFGS_gJ054429.7-260332	05 44 30	-26 03 32	0.0424	12
A0548R-N	05 47 02	-25 36 59	0.0424	6dFGS_gJ054429.7-260332	05 44 30	-26 03 32	0.0424	12
A0610R	07 59 16	+27 06 48	0.0954	2MASX_J07591712+2709159	09 08 32	+27 09 16	0.1049	13
A0754H	00 41 38	-09 20 33	0.0542	2MASX_J09083238-0937470	00 41 51	-09 18 11	0.0549	3
A0754R	00 41 38	-09 20 33	0.0542	2MASX_J09083238-0937470	00 41 51	-09 18 11	0.0549	3
A0085R	00 41 50	-09 18 07	0.0551	MCG-02-02-086	00 41 51	-09 18 11	0.0554	11
A3667R-NW	20 12 31	-56 49 55	0.0552	IC_4965	20 12 27	-56 49 36	0.0557	19
A3667R-SE	20 12 31	-56 49 55	0.0552	IC_4965	20 12 27	-56 49 36	0.0557	19
A1656R	12 59 49	+27 58 50	0.0231	NGC4889	13 00 08	+27 58 37	0.0220	5
A1656H	12 59 49	+27 58 50	0.0231	NGC4889	13 00 08	+27 58 37	0.0220	4

Col. 1: Cluster name with the last letter indicating a halo "H" or relic "R". The letters that follow a hyphen indicate the direction of a relic/halo with respect to the cluster centre on the sky. Col. 2, 3 & 4: Right ascension, declination & redshift of the cluster's X-ray centroid, respectively. Col. 5: BCG name. Col. 6, 7 & 8: Right ascension, declination & redshift of the cluster's BCG, respectively. Col. 9: Literature reference code of the halo/relic: (1) Giovannini et al. (2009)[95], (2) Murgia et al. (2010a)[171]; (3) Bacchi et al. (2003)[8]; (4) Kim et al. (1990)[135]; (5) Giovannini et al. (1991)[99]; (6) Govoni et al. (2005)[105]; (7) Feretti et al. (1997a)[75]; (8) Clarke & EnBlin (2006)[39]; (9) Feretti et al. (1997b)[77]; (10) Venturi et al. (2003)[244]; (11) Slee et al. (2001)[220]; (12) Feretti et al. (2006)[74]; (13) Giovannini & Feretti (2000)[96]; (14) Gavazzi & Trinchieri (1983)[92]; (15) van Weeren et al. (2011b)[239]; (16) van Weeren et al. (2011a)[237]; (17) Komisssarov & Gubanov (1994)[141]; (18) Bagchi et al. (2006)[9]; (19) Röttgering et al. (1997)[202].
*NED adopts the best published positions of all objects. The database uses optical positions for sources associated with galaxies and galaxy clusters and this is due to NED's source hierarchy which is based on physical models for each extra-galactic source (http://ned.ipac.caltech.edu/help/faq3.html#3b).

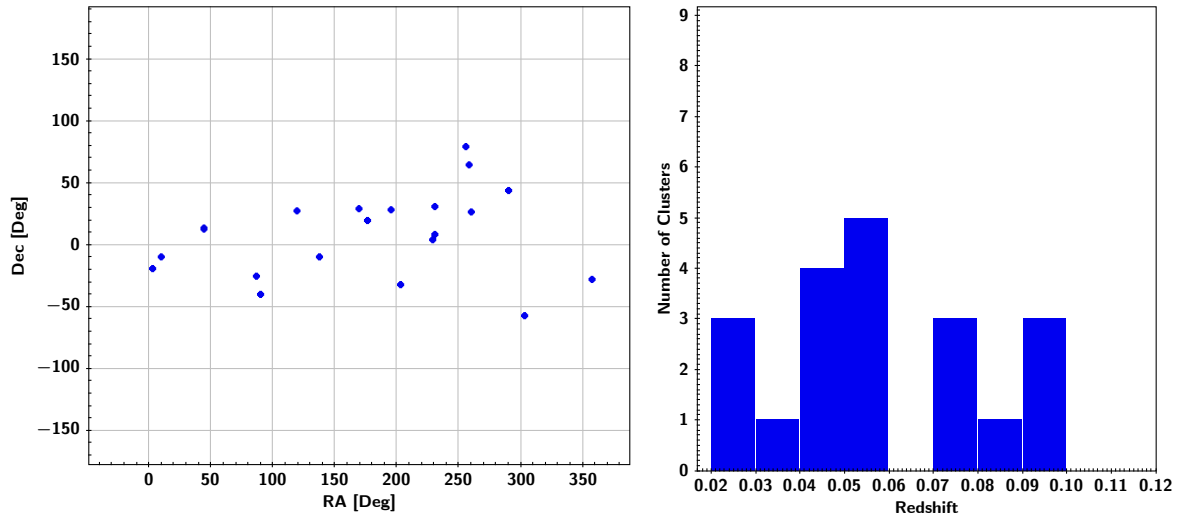

Figure 2.1: Left panel: The RA and Dec distribution of our cluster sample. Right panel: The cluster redshift distribution. The the lack of radio halo/relic clusters at redshifts $z \sim 0.06 - 0.07$ is also seen in the sample of Feretti et al. (2012)[78].

2.2 Cluster Sample

A brief review of each cluster, detailing the known published multi-wavelength and other physical properties, is given in this section. This information is used for comparison and reference with the analysis made in the later sections of this thesis.

A1213

A1213, with velocity dispersion $\sigma_v \simeq 566$ km/s (Hernández-Fernández et al. 2012)[113] is located at redshift $z_c \simeq 0.0469$ and a cosmologically corrected scale of 3.24 Mpc/degree[1](NED), is a poor cluster whose BCG is a dumbbell radio galaxy[2], 4C 29.41 (Fanti et al. 1982)[72]. The radio morphology of the BCG is similar to that of a Fanaroff & Rilley (FR) II[3] (Fanaroff & Rilley 1974)[71] radio galaxy. This cluster has been found to have a low X-ray luminosity (Giovannini et al. 2009)[95] and was discovered in X-ray observations by the Einstein and ROSAT missions (Jones et al. 2003)[127]. Optical and X-ray observations suggest that the cluster is dynamically disturbed (Giovannini et al. 2009)[95]. The cluster hosts a number of discrete radio loud sources including the BCG, but these cannot account for the extended diffuse emission that is observed in the radio. This extended emission makes up a large part of the cluster's halo while some smaller parts of this emission are made up of a filamentary structure which is directed at the BCG but is not connected to the BCG itself (Giovannini et al. 2009). The radio halo in this cluster is small, similar to a mini-halo (Feretti et al. 2012)[78], and asymmetric about the cluster centre. This cluster displays an exceptional scenario in challenge of the more observationally supported assertion that diffuse and extended radio emission is positively correlated with high X-ray luminosity. The cluster may hint at the existence of a new class of galaxy cluster (Giovannini et al. 2009).

A1367

A1367 has a velocity dispersion $\sigma_v \sim 879$ km/s (Moss et al. 1998)[168]. The cluster is located at redshift $z_c \simeq 0.0217$, with a cosmologically corrected scale of 1.61 Mpc/degree, and is situated at the intersection of two filamentary structures connecting to the Virgo and Coma galaxy clusters (Cortese, Gavazzi, & Boselli 2004[44], hereafter CGB). CGB assert that the cluster is dynamically young, undergoing a merger, due to its irregular X-ray morphology, large population of actively star forming spiral galaxies and low galaxy density at the central region of the cluster. The merger scenario of the cluster is supported by X-ray observations where an ICM shock has been observed (with ASCA[4] , Donnelly et al. 1998[55]) and a stream of cool gas moving toward the cluster's centre (Chandra observations by Sun & Murray 2002b[230] and XMM observations analysed by Forman et al. 2003[83]). Optical and radio observations also show an infall of galaxies (CGB) with Gavazzi et al. (1995[90], 2001[89]) having observed two infalling spiral galaxies with enhanced HII regions located on their leading edges and also a group of infalling starburst galaxies observed by Gavazzi et al. (2003b)[91] (CGB).

[1]The NASA/IPAC Extragalactic Database (NED: http://ned.ipac.caltech.edu/) is operated by the Jet Propulsion Laboratory, California Institute of Technology, under contract with the National Aeronautics and Space Administration.
[2]Two elliptical galaxies of approximately the same luminosity which share a common envelope (Wirth et al. 1982)[251]
[3]Radio loud galaxies with highly luminous (hotspots) regions dominating the emission from their radio lobes.
[4]The Advanced Satellite for Cosmology and Astrophysics.

A0013

A13 (A0013), with velocity dispersion $\sigma_v \simeq 886$ km/s (Mazure et al. 1996[163]), hosts a radio relic with a considerably steep radio spectrum ($\alpha \sim 4$) with a linear polarisation of $\sim 12\%$ at 1425 MHz (Slee et al. 2001)[220]. This cluster has an Abell richness of 2 (80 - 129 member galaxies[1]), and is of BM type II (Bautz & Morgan 1970[15]). This is an X-ray bright cluster with L_X(0.5-10 keV) $\sim 1.18 \times 10^{44}$ ergs/s (Slee et al. 2001). It is located at redshift $z \simeq 0.0943$ with a cosmologically corrected scale of 5.99 Mpc/degree. The cluster's radial velocity distribution suggests a spatial bimodality in the galaxy population as it has two of its brightest galaxies separated by ~ 2621 km/s in radial velocity space (Quintana & Ramirez 1995)[196]. The radial velocity distribution has a 16 galaxy component with dispersion $\sigma_v = 361^{+53}_{-35}$ km/s and a 21 galaxy component with dispersion $\sigma_v = 515^{+104}_{-81}$ km/s (Fadda et al. 1996[70]). Fadda et al. (1996) report a global cluster dispersion of $\sigma_v = 896^{+85}_{-73}$ km/s in agreement with that of Mazure et al. (1996)[163].

A2048

This cluster is a relic host located at redshift $z \simeq 0.0972$ where it's cosmologically corrected scale is 6.26 Mpc/degree. It is a BM type III poor cluster and Abell richness class 1 (50 - 79 member galaxies[1]). The radio relic, VLSS J1515.1+0424, is morphologically complex and located east of the cluster core (van Weeren et al. 2011b[240]). van Weeren et al. (2011b) find no polarisation in the relic and that its radio spectrum is steep with an average $\alpha \sim -1.7$ between 1425 and 325 MHz. Substructure is detected in the X-ray, with ROSAT[5], located east of the cluster's centre, suggesting that the cluster may have been dynamically disturbed (van Weeren et al. 2009b)[241].
Shen et al. (2008)[216] report a dispersion $\sigma_v \sim 857$ km/s and bolometric X-ray luminosity $L_X \simeq 1.9 \times 10^{44}$ ergs/s. Other authors report lower dispersions: $\sigma_v \sim 668$ km/s for 25 galaxies (den Hartog et al. 1995)[53] while van Weeren et al. (2011b) predict $\sigma_v \simeq 765 \pm 40$ km/s based on the X-ray-velocity relation ($L_X - \sigma_v$) of Shen et al. (2008). The latter authors determine their dispersion for galaxies with the A2048 virial radius.

A2061

A2061 is a poor cluster (Abell richness class 1), of BM type III. It is located at redshift $z \simeq 0.0784$ where its cosmologically corrected scale is 5.15 Mpc/degree. This cluster hosts a radio relic (Kempner & Sarazin 2001)[134], located at ~ 1.5 Mpc from the cluster centre (van Weeren et al. 2011a[242]), and may also host a central halo (Rudnick & Lemmerman 2009)[203]. It has X-ray luminosity L_X(0.1-2.4 keV) $\sim 3.95 \times 10^{44}$ ergs/s (Ebeling et al. 1998)[63] and velocity dispersion $\sigma_v = 673^{+49}_{-40}$ km/s (Oegerle & Hill 2001)[178]. The cluster has considerable structure and X-ray observations, obtained from ROSAT (van Weeren et al. 2011a), show an elongation in the north-east to south-west direction, the cluster has also been associated with Corona Borealis supercluster (Small et al. 1998[223]; Marini et al. 2004[157]). The spatial galaxy distribution also displays substructure with three prominent structures located in a north-east south-west axis (van Weeren et al. 2011a[242]). Marini et al. (2004) report a global tem-

[5]Röntgen Satellite: http://heasarc.gsfc.nasa.gov/docs/rosat/rosgof.html.

perature $kT = 4.53^{+48}_{-38}$ keV but the authors also find a region, to the north of the cluster, of higher temperature $kT = 10.67^{+3.90}_{-2.47}$ keV which may suggest an internal shock (van Weeren et al. 2011a).

A2061 is in close proximity to the cluster A2067 (~ 1.8 Mpc/h separation) (van Weeren et al. 2011a). The two have a systematic velocity difference of ~ 1600 km/s (Oegerle & Hill 2001)[178] suggesting that these two clusters may be interacting or even gravitationally bound (van Weeren et al. 2011a). Marini et al. (2004) show that there is extended X-ray emission from A2061 towards A2067 and the authors assert that the clusters may be merging and are in a phase of the merger where their cores have not yet collided. The authors make this assertion based on the absence of a merger shock which is expected for a post core-collision system (van Weeren et al. 2011a).

A2063

A2063 is a rich cluster with a radio relic and of BM type II. It is located at redshift $z \simeq 0.0349$ with a cosmologically corrected scale of 2.44 Mpc/degree. The cluster has temperature $kT \sim 4$ keV and bolometric X-ray luminosity $L_X \simeq 1.48 \times 10^{44}$ ergs/s (Jones & Forman 1984[126]; David et al. 1993[48]; Peres et al. 1998[181]). A2063 is a cool-core cluster (Kanov et al. 2006[131]) with a core ICM gas temperature $kT \sim 2$ keV (Hudson et al. 2010[116]) – early ICM X-ray observations showed that cluster cores tend to have dense ICM gas whose cooling time was much less than Hubble time which led to the development of the cooling flow (CF) model (e.g Lea et al. 1973[147]; Cowie & Binney 1977[46]; Fabian & Nulsen 1977[69]; Mathews & Bregman 1978[162]). In the CF model, the dense core ICM gas cools hydrostatically and hot peripheral ICM gas flows into the core region to replace the dense ICM gas, which is also being compressed by the weight of the overlaying gas. This flow would then lead to cooling times of the dense ICM gas that were much shorter than Hubble time. This CF model prediction is not well supported by observations as central ICM gas is not observed to cool at the rates predicted (e.g Peterson et al. 2001[182], Sanders et al. 2008)[208] thus clusters with dense ICM gas in their core regions which is cooler than cluster peripheral ICM gas are called cool-core clusters (Molendi & Pizzolato 2001[167]; Hudson et al. 2010[116]).

The cluster has velocity dispersion $\sigma_v \simeq 659$ km/s (Hill & Oegerle 1993[114]; den Hartog & Katgert 1996)[54], total mass $M_{tot} \simeq (1.31 \pm 0.06) \times 10^{13}$ $M_\odot$ and gas mass $M_{gas} \simeq (1.69 \pm 0.03) \times 10^{11}$ $M_\odot$ within a radius of 66 kpc (Kanov et al. 2006)[131]. The cluster's velocity dispersion profile has also been observed to decrease with radius suggesting that A2063 is dynamically disturbed (Krempéc-Krygier & Krygier 1999)[145].

A2255

A2255 is a rich nearby cluster at redshift $z_c \simeq 0.0806$ (Struble & Rood 1999)[228] with a cosmologically corrected scale of 5.25 Mpc/degree and velocity dispersion $\sigma_v \sim 1266$ km/s (Chen et al. 1998)[33]. It hosts both a radio halo and a relic (Burns et al. 1995[31]; Feretti et al. 1997a)[75]. The cluster has various attributes which suggest that it is complex: it has seven head-tail radio galaxies which are located both in the central region and in the peripheral region ($\gtrsim 2$ Mpc) (Pizzo et al. 2011)[188]. Its radio halo displays significant polarisation suggesting the presence of a well ordered magnetic field (Govoni et al. 2005)[105]. X-ray observations (XMM-Newton[6] observations by Sakelliou &

[6]The European Space Agency's (ESA) X-ray Multi-Mirror Mission (XMM-Newton)(http://xmm.esac.esa.int/; Jansen et al. 2001[119]).

Ponman 2006)[206] show a complex ICM temperature structure which is characteristic of a cluster that has recently (< 1 Gyr) undergone a merger event (Sakelliou & Ponman 2006). It has also been shown that at radii larger than about 10 Mpc, there are galaxy groups that are in orbit of the cluster core (Yuan et al. 2003)[255]. These multi-wavelength studies suggest that the cluster is very active and complex (Sakelliou & Ponman 2006).

A2256

A2256 is a rich cluster of BM type II-III. It is located at redshift $z_c \simeq 0.0581$ where its cosmologically corrected scale is 3.88 Mpc/degree. This cluster is in the process of a merger and hosts both a radio halo and relic (Enβlin 2006[67]; Brentjens 2008[23]; Kale & Dwarakanath 2010[128]; Clarke et al. 2011[38]). The merger is also observed in the cluster's X-ray emission which suggest that it is not in dynamic equilibrium (e.g Sun et al. 2002[231]). The core ICM has temperature $kT \sim 7 - 8$ keV (Clarke et al. 2011). Clarke et al.(2011) report two regions with cooler ICM temperatures of $kT \sim 4$ keV located north-west and south-east of the cluster core. A2256 has X-ray luminosity L_X(0.1-2.4 keV)$\simeq 3.70 \times 10^{44}$ ergs/s (Clarke & Enβlin 2006[39]), velocity dispersion $\sigma_v \simeq 1376$ km/s for 116 galaxies (Chen et al. 1998[33]), and a virial mass $M \sim 8 \times 10^{14}$ $M_\odot$ (Markevitch & Vikhlinin 1997[159]).

A2319

A2319 is poor cluster (Abell richness class 1) of BM type II-III. This cluster hosts a radio halo and is also a merging system (Feretti et al. 1997b)[77]. It is located at redshift $z \simeq 0.0557$ where it has a cosmologically corrected scale of 3.70 Mpc/degree. This is a complex cluster (substructure) with a bimodal radial velocity distribution of galaxies (Oegerle et al. 1995 [177]). The cluster has been reported to have an ICM temperature $kT \simeq 8.9 \pm 0.6$ keV (Gruber & Raphaeli 2001[107]) which includes both thermal and non-thermal components. The cluster has been found to have velocity dispersion $\sigma_v \simeq 1770$ km/s (Oergele et al. 1995 [177]), X-ray luminosity $L_X(0.1 - 2.4 \text{ keV}) \simeq 8.46 \times 10^{44}$ ergs/s (Feretti et al. 1997b[77]).

A3376

A3376 is a merging cluster with two giant (~ 1.6 Mpc) radio relics located East and West of the cluster core (Bagchi et al. 2006[9]). The cluster is of BM type I and Abell richness class 1. It is located at redshift 0.0456 where it has a cosmologically corrected scale of 3.12 Mpc/degree. The BCG for this cluster is located $\gtrsim 0.9$ Mpc from the cluster X-ray centroid (cluster "core") which further supports the merger scenario of this cluster (Bagchi et al. 2006[9]). Simulations suggest that the A3376 merger resulted from a head on collision of structures with a mass ratio of 6:1 (Machado & Lima Neto 2013[154]). Durret et al. (2013)[62] reported a dynamical mass of $\sim 5.3 \times 10^{14}$ $M_\odot$ with a velocity dispersion $\sigma_v \simeq 862$ km/s from a sample of 120 galaxies. The cluster has X-ray luminosity $L_X(0.1 - 2.4$ keV$) \simeq 1.08 \times 10^{44}$ ergs/s (Bagchi et al. 2006[9]) and temperature $kT \sim 4$ keV (Fukazawa et al. 2004 [87]; Bagchi et al. 2006[9]).

A3562

A3562 is a member of the Shapley super cluster and, along with two other clusters (A3556 and A3558), it is located in the central region of the super cluster (see e.g. Proust et al. 2006[195] and references therein). The cluster is of BM type I and Abell richness class 2. It is located at redshift 0.0499 with a cosmologically corrected scale of 3.37 Mpc/degree. Bardelli et al. (1998a)[12] found this cluster to be composed of three subclusters with dispersions $\sigma_{v1} \simeq 1113$ km/s (with 35 galaxies), $\sigma_{v2} \simeq 880$ km/s (with 8 galaxies) and $\sigma_{v3} \simeq 337$ km/s (with 20 galaxies). Ettori et al. (2000)[68] have determined an emission-weighed gas temperature of $kT = 5.1 \pm 0.2$ keV and a virial mass $M_{vir} = 3.9(\pm 0.4) \times 10^{14}\ h_{50}^{-1} M_{\odot}$. The cluster, along with its neighbour, A3556, are reported to be on the way to a three-way merger with A3558 (Ettori et al. (2000)[68]). Mazure et al. (1996)[163] reported a velocity dispersion $\sigma_v \simeq 1048$ km/s and Venturi et al. (2003)[244] have reported a radio halo and a cluster X-ray luminosity $L_X(0.1-2.4$ keV$) \simeq 1.57 \times 10^{44}$ ergs/s.

A0399 and A0401

A0399 and A0401 form a bound pair of rich clusters with radio halos (Sakelliou & Ponman 2004[205]). They both have Abell richness of 2 and A0399 is of BM type I-II while A0401 is of BM type I. A0399 is located at redshift $z \simeq 0.0724$ with a cosmologically corrected scale of 4.69 Mpc/degree and A0401 is located at redshift $z \simeq 0.0737$ with a cosmologically corrected scale of 4.80 Mpc/degree. Murgia et al. (2010a)[171] reported an ICM temperature $kT \simeq 7.2$ keV and an X-ray luminosity $L_X(0.1-2.4$ keV$) \simeq 3.80 \times 10^{44}$ ergs/s for A0399 while Bacchi et al. (2003)[8] reported an ICM temperature $kT \simeq 8.5$ keV and an X-ray luminosity $L_X(0.1-2.4$ keV$) \simeq 6.52 \times 10^{44}$ ergs/s for A0401. The two clusters are in the process of merging and are separated by a physical distance of ~ 3 Mpc (Sakelliou & Ponman 2004[205]). Hill & Oegerle (1993)[114] reported a velocity dispersion of 1130 km/s for A0401 while the velocity dispersion of A0399 was reported to be 1186 km/s (Hill & Oegerle 1993[114]; den Hartog & Katgert 1996[54]).

A4038

A4038 is a rich Southern cluster, also known as Klemola 44 (Klemola 1969[137]), of BM type I and Abell richness class 2 (Kiuchi et al. 2009[136]). The cluster is located at redshift $z \simeq 0.0282$ with a cosmologically corrected scale of 1.89 Mpc/degree. This is a regular (unimodal spatial galaxy distribution) cluster (Girardi et al. 1997[101]). It is also a radio relic host with an unusually small extent of the relic (~ 0.13 Mpc) which is also located very near ($\lesssim 50$ kpc) the cluster BCG (Slee & Roy 1998[221]). The proximity of the relic to central bright galaxies and its extent may suggest that this radio source is in fact a remnant of radio lobes from a radio loud AGN which is no longer active and that is now displaced from the radio source ("relic"), but it still fits the criteria of radio relics and it is classified as such (Slee & Roy 1998[221]).

The cluster has been found to have virial temperature $kT \simeq 3.14$ keV (Eckert et al. 2001[64]), an X-ray luminosity $L_X(0.1-2.4$ keV$) \simeq 1.97 \times 10^{44}$ ergs/s (Slee et al. 2001[220]), an estimated total mass $M_{tot} \sim 2 \times 10^{14}\ M_{\odot}$ (Vikhlinin et al. 2009[246]) and a velocity dispersion $\sigma_v \simeq 882$ km/s (Chen et al. 1998[33]).

A0548

A0548 is a rich cluster (richness class 1 and BM type III) with a bimodal spatial distribution of galaxies and an extent of $\sim$ 8 Mpc/h (Davis et al. 1995[49]). A spatial analysis of the cluster shows that it is elongated along the North-East (NE) to South-West (SW) direction relative to the cluster core region (Dressler & Schectman 1988b[58]) with its X-ray peak North-West of the core. The cluster shows a complex X-ray structure with sources associated with gas from galaxy groups, individual galaxies and also a diffuse source (Davis et al. 1995[49]). A0548 hosts a pair of confirmed radio relics which are located in the same region on the outskirts ($\gtrsim$ 400 kpc NW of the cluster centre) (Feretti et al. 2006[74]). Another region of diffuse radio emission is in the core region but this source has a pair of radio galaxies associated with it and thus may or may not be a relic source[74].
The cluster has X-ray luminosity L_X(0.1-2.4 keV)$\simeq$ 0.15 $\times$ 10^{44} ergs/s[74], σ_v $\simeq$ 842 km/s (den Hartog 1995)[53], redshift $z \simeq 0.0424$[74] and a cosmologically corrected scale of 2.85 Mpc/degree.

A0610

A0610 is a poor cluster at redshift $z_c \simeq 0.0954$ (Giovannini et al. 2009)[95] and it hosts both radio relic and radio halo (Giovannini & Feretti 2000[96]; Valentijn 1979[235]). It has a cosmologically corrected scale of 6.16 Mpc/degree. It is located behind the richer Zw0752.9+2833 cluster ($z \sim 0.15$). Valentijn (1979) mention that the existence of a radio halo is challenged by the presence of head-tail radio sources (associated with some ellipticals in the central region of the cluster) as these could also be used to describe the diffuse emission that has been classified as the radio halo thus only the radio relic has been considered here and the disputed detection of a central halo will be neglected.
The cluster has velocity dispersion $\sigma_v \sim 496$ km/s (Boschin et al. 2008[22]), 2σ upper limit X-ray luminosity of L_X(2-6 keV)$\simeq 0.58 \times 10^{44}\ h_{75}^{-1}$ergs/s (Kowalski et al. 1984[143]), and virial mass $M_{vir} \simeq 2.3^{+0.8}_{-0.6} \times 10^{14}$ $M_\odot/h_{70}$ within a virial radius $R_{vir} \simeq 1.15$ Mpc/h_{70} (Boschin et al. 2008[22]).

A0754

A0754 is a rich cluster of BM type I-II and Abell richness class 2. It is located at redshift $z \simeq 0.0542$ with a cosmologically corrected scale of 3.71 Mpc/degree. Chen et al. (1998)[33] reported a velocity dispersion $\sigma_v \simeq 931$ km/s. The cluster has been found to be in the process of a major merger with evidence from optical (Zabludoff & Zaritsky 1995[256]) and X-ray (Henry & Briel 1995[112]; Henriksen & Markevitch 1996[111]) observations. Henriksen & Markevitch (1996)[111] have reported a mean cluster temperature $kT \sim 9$ keV with a hotter ($kT \gtrsim 12$ keV) region located North-west of the cluster core. The authors found evidence suggesting that the cluster is a non-head on collision of two structures while Markevitch et al. (2000)[160] suggested that the cluster may be undergoing a 3 body merger. The cluster, with an X-ray luminosity L_X(0.1-2.4 KeV)$\simeq 2.21 \times 10^{44}\ h_{75}^{-1}$ergs/s, hosts both a radio halo and a relic (Bacchi et al. 2003[8]).

A0085

A0085 (or just A85) is a rich cluster (Abell richness class 3) of BM type I. The cluster is located at redshift $z \simeq 0.0551$ with a cosmologically corrected scale of 3.63 Mpc/degree and velocity dispersion $\sigma_v \simeq 969$ km/s (Mazure et al. 1996[163]). This cluster forms part of a cluster complex made up of A85, A87 and A89 (Durret et al. 2005[60]). The main cluster is fairly regular in shape, with an approximately unimodal distribution of galaxy radial velocities (Girardi et al. 1997[101]). The cluster is not without substructure, optical (Durret et al. 1998a[59]; Slezak et al. 1998[222]) and X-ray (Pislar et al. 1997[187]; Lima Neto et al. 1997[150]; Lima Neto et al. 2001[149]) observations suggest that there is complexity in the cluster – a structure (probably a group) located South of the main cluster and a filament ($\gtrsim 4$ Mpc in extent) are observed (Durret et al. 2005[60]).

Slee et al. (2001)[220] reported that this cluster hosts a radio relic and that it has an X-ray luminosity L_X(0.1-2.4 keV)$\simeq 4.10 \times 10^{44}$ ergs/s. The cluster has a total mass $M_{tot} \simeq 7.6 \times 10^{14}$ $M_\odot$, temperature $kT \simeq 7.0$ keV (Reiprich & Böhringer 2002[198]; Durret et al. 2005[60]).

A3667

A3667 is an X-ray bright, L_X(0.4 - 2.4 keV) $\sim 5 \times 10^{44}$ erg/s, nearby ($z = 0.0556$ with cosmologically corrected scale of 3.71 Mpc/degree) and hot cluster with $kT \sim 6$ keV (Knopp et al. 1996[138]; Röttgering et al. 1997[202]). This cluster shows evidence of a highly energetic merger scenario (Markevitch et al. 1999[158]; Owers et al. 2009[179]) with a pair of radio relics situated North-West (NW) and South-East(SE) of the cluster centre (Röttgering et al. 1997). The relics are very extended from the cluster core reaching approximately $\gtrsim 2$ Mpc/h (Röttgering et al. 1997). The NW relic is the brightest diffuse radio source yet to be detected with $F(\lambda = 20$ cm$) \simeq 3.7$ mJy (Johnson-Hollitt 2003[124]). X-ray observations show a steep gradient in the X-ray surface brightness which suggest that the region in question is a merger shock (Sarazin et al. 2013[210]). The SE sub-cluster displays a surface brightness discontinuity which was initially interpreted as suggestive of a shock front (Markevitch et al. 1999) but was later found to be a cold front due to dense cold gas travelling through the ICM at sound speed (Vikhlinin et al. 2001a)[247].

The cluster has Abell richness of 2 and a BM I-II type (Abell et al. 1989[2]). It has a virial mass $M_V \sim 1.2 \times 10^{15}$ $M_\odot$/h for a sample of 154 galaxies in a radius of 2.2 Mpc/h (Girardi et al. 1998)[102]. Girardi et al. (1998) calculate a velocity dispersion $\sigma_v \simeq 971$ km/s for their sample of member galaxies while other authors report higher σ_v values: $\sigma_v \simeq 1100 - 1400$ for smaller samples of galaxies, however, (Proust et al. 1988[194]; Sodre et al. 1992[224]).

A1656 (Coma Cluster)

A1656 (the Coma cluster) is the richest cluster (BM type II and Abell richness class 5) in the nearby universe. It is located at redshift $z \simeq 0.0231$ with a cosmologically corrected scale of 1.67 Mpc/degree. It is morphologically complex (substructures) – this has been shown by X-ray studies where turbulence, galaxy infall and dynamical disturbance are evident (e.g. Wilson 2012[250]; Planck Collaboration et al. 2013[189]). The cluster is the first to be found to host a radio halo (Willson 1970[249]) and a relic (Giovannini et al. 1985[98]). It has been found to have mass

$M \sim 1 \times 10^{15}$ $M_{\odot}$ and temperature $kT \simeq 8$ keV (Wilson 2012[250]). The cluster has velocity dispersion $\sigma_v \simeq 1008$ km/s (Chen et al. 1998[33]) and an X-ray luminosity $L_X(0.1\text{-}2.4\ \text{keV}) \simeq 3.99 \times 10^{44}$ ergs/s (Giovannini et al. 1991[99]).

2.3 Archival Data

Archival data was acquired by use of the Vizier[7] and NASA/IPAC Infrared Science Archive (IRSA)[8] catalogue access tools. Vizier was used to access near and far ultra-violet (NUV and FUV) photometry from the Galaxy Evolution Explorer (GALEX)[9](Bianchi et al. 2011[19]) and optical u, g, r, i and z photometry from the Sloan Digital Sky Survey data release 9 (SDSS DR 9)[10](Ahn et al. 2012[4]) while IRSA was used to access near and mid-infrared photometry from the Wide-field Infrared Survey Explorer (WISE)[11](Wright et al. 2010[252]; Cutri et al. 2014[47]).

GALEX is an ultraviolet space telescope launched in 2003. It observes in 2 ultraviolet bands, FUV (bandwidth 1344-1786 Å, effective wavelength 1538.6 Å) and NUV (bandwidth 1771-2831 Å, effective wavelength 2315.7 Å). The SDSS utilises a dedicated 2.5 m wide-field optical telescope (Sloan Foundation Telescope, Gunn et al. 2006[109]) to conduct deep surveys of the sky. SDSS observes in 5 photometric bands, u (effective wavelength 3543 Å), g (effective wavelength 4770 Å), r (effective wavelength 6231 Å), i (effective wavelength 7625 Å) and z (effective wavelength 9134 Å). WISE is a NASA Medium Class Explorer mission that has conducted a digital imaging survey of the entire sky in the 3.4 μm ($W1$), 4.6 μm ($W2$), 12 μm ($W3$) and 22 μm ($W4$) mid-IR μm. The manner in which data was extracted from the above archives is outlined below.

2.3.1 Data Acquisition

We use the CDS/SIMBAD database[12] and the NASA/IPAC Extragalactic Database (NED)[13] to extract galaxy positions and redshifts for galaxies in the regions around clusters in our sample (Table 2.1). Galaxies which are found to be cluster members are cross matched with the archives mentioned above to obtain multi-wavelength photometry. Our cluster sample is of nearby clusters and so we extract Petrosian magnitudes (Petrosian 1976[183]; Graham et al. 2005[106]) from the SDSS DR 9. Petrosian magnitudes take into account the fact that galaxies are extended objects and so their light needs to be measured within a representative radius so that a constant fraction of the galaxy light is measured.

From GALEX we extract calibrated AB magnitudes while from WISE we extract photometry for both "point" sources (unresolved) and extended (resolved) sources. This was done by placing restrictions on the reduced χ^2 of the profile-fit photometry measurement for the $W1$ bandpass viz.: a resolved source is that with $\chi^2(W1) > 2$, otherwise the source is unresolved (see Cluver et al. 2014[42]). Eleven arcsecond radius aperture magnitudes were then extracted from the WISE All-sky catalogue. These are the calibrated source brightnesses measured in an 11 arcsecond radius circular

[7] http://vizier.u-strasbg.fr/viz-bin/VizieR
[8] http://irsa.ipac.caltech.edu/
[9] http://www.galex.caltech.edu/
[10] http://www.sdss3.org/
[11] http://irsa.ipac.caltech.edu/Missions/wise.html
[12] http://simbad.u-strasbg.fr/simbad/
[13] http://ned.ipac.caltech.edu/

aperture centred on the source position on the Atlas Image. These apertures, however, do not have any foreground star removal, and hence may suffer from stellar contamination. The corresponding WISE colours should then be treated with caution.

2.4 Membership Characterisation

In the new era of huge datasets, one inevitably has to go through data mining. Data mining is the process of analysing data from different perspectives and summarising it into useful information. In this section we discuss the various tools that have been used to characterise galaxy candidates that form part of a particular galaxy cluster.

2.4.1 Cluster Analysis

The statistical computing and graphics package **R**[197] has a suite of useful functions dedicated to cluster analysis; such as `cluster` (Maechler et al. 2013[155]) for hierarchical clustering, `Mclust` (Fraley & Raftery 2012[85]) for model based clustering, `flexclust` (Leisch 2006[148]) for partition clustering analysis and many more in these three cluster analysis methodologies: hierarchical, model based and partitioning cluster analysis. The availability of such a vast suite allows for the exploration of various methods of cluster analysis and the one considered here is model based cluster analysis via `Mclust` as the cluster sample used is expected to be made up of individuals comprising of multiple Gaussian components.

The package, `Mclust`, applies multivariate Gaussian mixture models to find clustering in data i.e. the data is assumed to be made up of a combination of mixtures (components or groups) which are distributed according to unique Gaussian models (Fraley & Raftery 2012 [85]). The choice of the model(s) is based on likelihood maximisation using the expectation maximisation (EM) algorithm. The EM algorithm aims to maximise likelihood in cases of "incomplete" data. It is an iterative process where the parameter estimates which maximize likelihood are determined from models which depend on latent (derived) variables. The data, in EM, is considered to be composed of an observed part $\mathbf{x_i}$ and a "missing" part $\mathbf{z_i}$ and thus the "complete" data is taken as y_i=($\mathbf{x_i}$, $\mathbf{z_i}$) (Fraley & Raftery 1998 [84]). The "missing" data $\mathbf{z_i} = (z_{i1}, ..., z_{iG})$ constitute the conditional probabilities that the i-th observation belongs to one of G components (G specifies the number of mixture components) viz:

$$z_{ik} = \begin{cases} 1 : \mathbf{x_i} \in \text{group } k \\ 0 : \text{otherwise} \end{cases}$$

`Mclust` then uses the Bayesian Information Criterion (BIC) to select the model(s) which maximise the likelihood as calculated via EM.

The BIC (Schwarz 1978 [214]) is a criterion for comparing and selecting models according to maximum likelihood. Models can be made to fit data better by increasing the number of parameters used which may lead to misrepresentation of the information in the data, i.e over-fitting. The BIC combats this by introducing a penalty to the likelihood of

progressively complex parametrisations. The most likely model has the largest absolute BIC value. The BIC has the advantage that different models can be compared based on their parametrisations, number of components or both.

The clustering analysis, applied here, consists of two main parts. The first is a model based Gaussian mixture model (GMM) with the cluster region assumed to be made up of normally distributed galaxy groups/cluster components. This method is used for both membership characterisation and subcluster identification. The second part analyses the clustering structure of the cluster member sample, selected in the first part, using hierarchical agglomerative clustering methods. In the agglomerative clustering case, each galaxy is initially taken to make up an entire subcluster and then these subclusters are merged until only the main cluster (containing all individuals) remains. The mergers are made according to the smallest average distance between two neighbouring subclusters and the process is continued until the final stage.

The two methods are both realised largely through the use of the `R` programming language. The GMM analysis was implemented using the `R` package *`Mclust`* and the agglomerative clustering analysis implemented with the function *`AGNES`* [14] (Maechler et al. 2013[155]) from the package *`cluster`* . Further analysis was done using the `Python` programming language – most notably *`Astropy`* [15].

2.4.2 Application of the Gaussian Mixture Model (GMM)

This section details the steps taken to characterise cluster membership and and also identify complex clusters, those that have subclusters within the sample of galaxies which are selected as cluster members, for further analysis.

2.4.2.1 The Algorithm

The complete clustering algorithm applied to our sample is outlined in the flow diagram shown in Figure 2.2. The steps taken are explained below and results for each step are presented.

i. **Mine the VO for galaxies in cluster region**:

- Mine NED and SIMBAD for galaxies within 5 Mpc of the cluster center (Feretti et al. 2012 [78]) using the coordinates given in Table 2.1.
- Combine the two data sets, making sure to keep only one instance of any galaxies found in both catalogues. This was done through a table cross-match of the mined data.
- Extract galaxy redshifts, positions and galaxy-center projected angular separations. The projected physical distances where then calculated by multiplying the cosmologically corrected scale of a cluster (as given in the NED database) with the projected angular distance of the galaxies in the region of the cluster.

ii. **Select region of interest**:

[14] http://stat.ethz.ch/R-manual/R-patched/library/cluster/html/agnes.html
[15] Astropy Collaboration, 2013 (http://www.astropy.org).

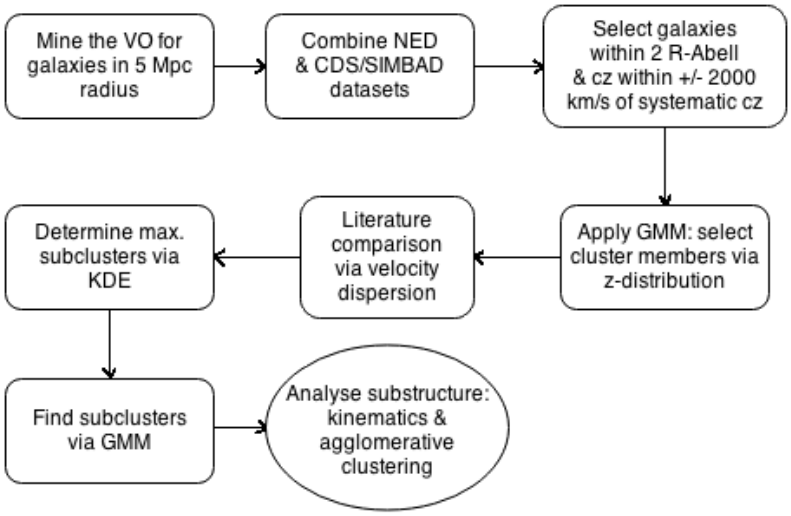

Figure 2.2: A summary of complete clustering algorithm and related steps. R-Abell is the Abell radius defined as $1.72/z$ *arcminutes for a cluster at redshift* z *(Abell 1958[1]). The final cluster members are selected by choosing only those galaxies which fall within 95 % (*$\sim 2\sigma$*) confidence bands of a uni-modal normal distribution.*

- Select galaxies whose projected distance from the cluster centre was less than 2 Abell radii (Abell 1958[1]) centred on the cluster and also on the BCG to include galaxies that may be well beyond the cluster core and falling into the cluster due to some kind of merger activity. This was done with the expectation that these halo and/or relic systems are primarily found in merging clusters where the BCG is significantly displaced from the X-ray centroid (e.g Buote 2001[30]; Feretti et al. 2012[78]). Abell (1958)[1] defined a typical cluster "radius", the so called Abell radius, containing at least 50 cluster galaxies within $1.72/z_c$ arcminutes, where z_c is the cluster redshift.

- Select galaxies whose radial velocities (cz) were within 2000 km/s of the cluster's systematic radial velocity (cz_{Xc}) and also that of the BCG. This accounts for the expected large peculiar velocities of galaxies expected in these dynamically active systems. Merritt (1988)[166] has shown that the radial velocity distribution of rich dynamic clusters (using A1656) can span $\sim$ 2000 km/s around the systematic radial velocity of the cluster. See Figure 2.3 for the results of this analysis applied to galaxies in the region of the A1213 cluster.

iii. **Optimise and test clustering algorithm**:

- Generate mock data with single component normally distributed RA, Dec and redshift. Mean redshifts, RA, Dec and standard deviations are chosen to be similar to those of each cluster in the sample. These parameters were obtained by fitting a single component Gaussian "mixture" to each cluster member candidate sample. The result is a sample of mock clusters modelled to be similar to our cluster sample but each "cluster" consisting of a single Gaussian component. The above steps were then applied to the mock samples which were then analysed with the GMM algorithm (as described in step (iv) below). The expected results were seen: uni-modal normally distributed galaxies for each mock cluster with every input galaxy forming part of the final cluster. The results are presented for the case of an A3667 mock cluster in Appendix A.

iv. **Select cluster members: Gaussian mixture model**

- Select galaxies whose redshifts fall within 95 % confidence bands ($\sim 2\sigma$) of a uni-modal normal distribution. The result of the comparison between the redshift distribution and a normal distribution are illustrated on a

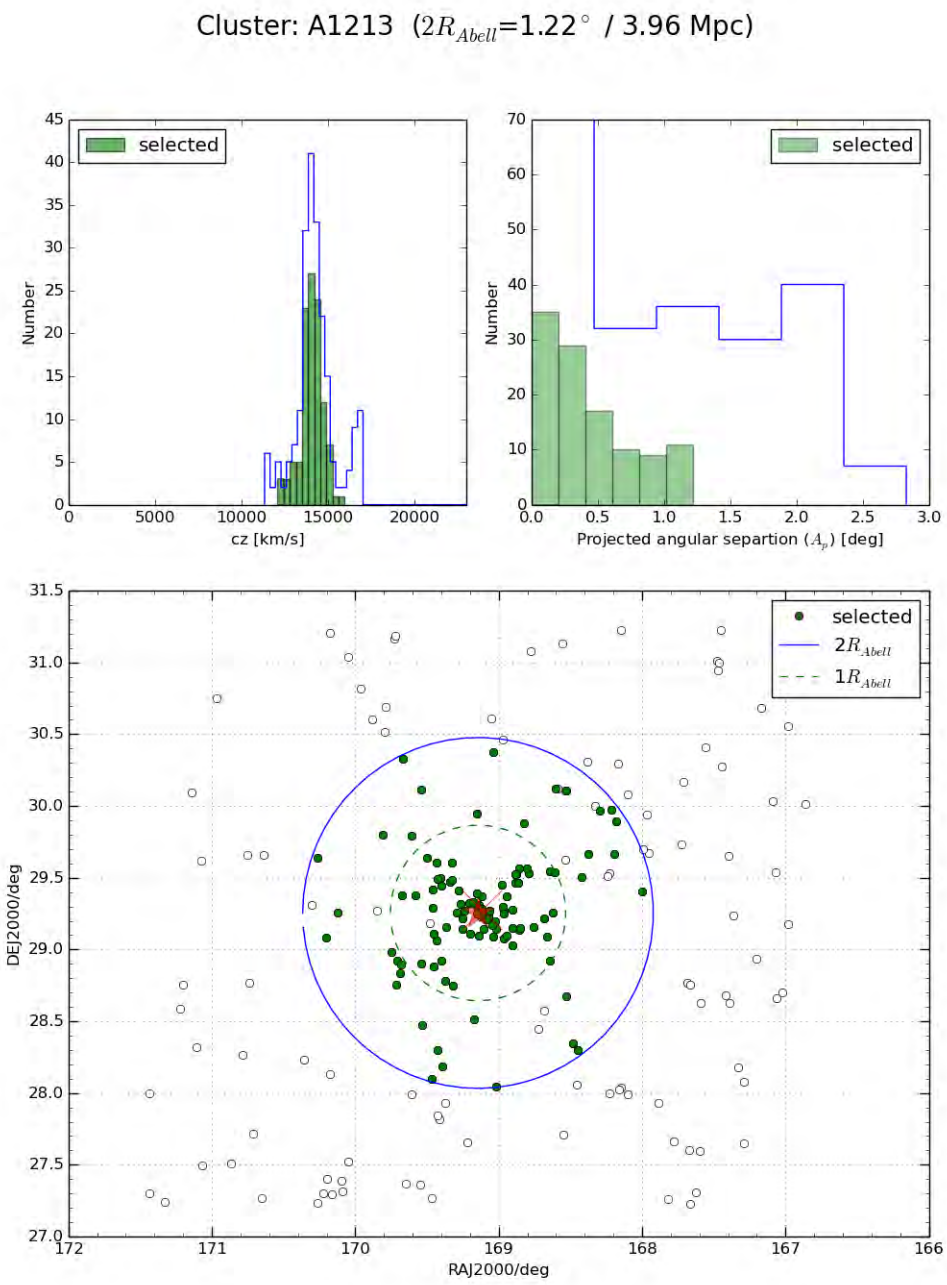

Figure 2.3: The galaxies in the region of the A1213 cluster. Green dots and green histograms represent the galaxies which satisfy the selection criteria and thus were selected as member candidates (see 2.4.2.1). ***Top left****: The radial velocity distribution of the entire galaxy sample (blue unfilled histogram) and the selected member galaxies (green).* ***Top right****: The projected angular separation (great-circle distance) between galaxies and the cluster centre (A_p).* ***Bottom****: The sky distribution of all galaxies in the A1213 region. Green dots are selected galaxies, open circles are excluded galaxies, the red cross is the cluster's centre (X-ray centroid) and the red star is the cluster's BCG. The 2 and 1 Abell radii (centred on the X-ray centroid) are labelled accordingly. The galaxies rejected by the clustering algorithm are discussed in section 2.4.3.*

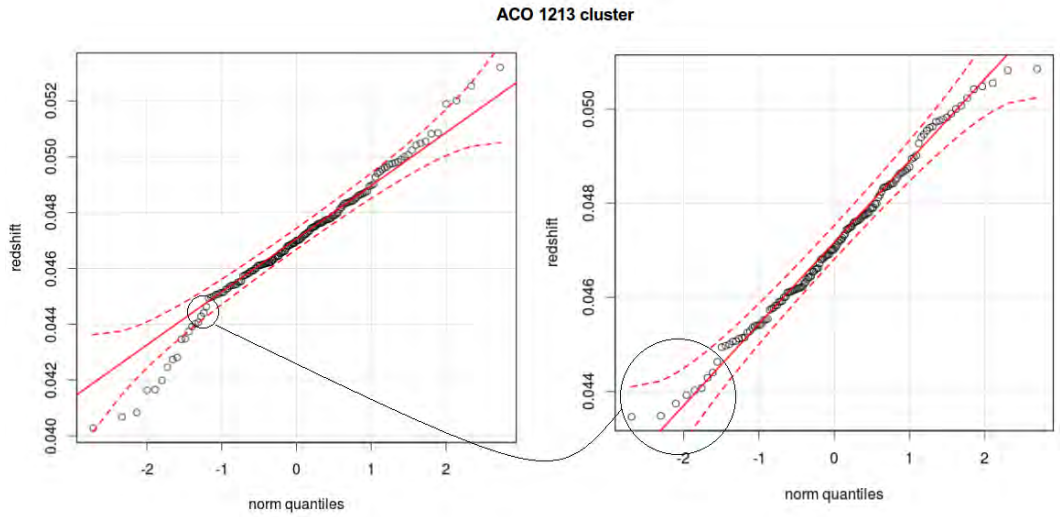

Figure 2.4: QQ plots of the redshift distribution of galaxies in the region of the A1213 cluster (y-axis) compared to a normal distribution (x-axis). The red dashed lines represent the 95 % confidence bands and the open circles are the galaxy redshifts. ***Left****: All of the galaxies that were selected as cluster member candidates. Right: Only galaxies within the 95 % confidence bands, these are identified as cluster members. Galaxies which fall outside the 95 % confidence bands were iteratively removed.*

QQ plot (Figure 2.4). Galaxies which fall outside of the 95 % confidence bands were then removed and the GMM algorithm was applied iteratively until all galaxies satisfied all selection criteria (Figure 2.4). The $\sim 2\sigma$ selection applied above does not necessarily mean that the redshift space (or line-of-sight, LOS, velocity space) distribution is without substructure. The case of A3667 is an example of this: the subclusters found by the GMM algorithm showed bimodality in their LOS velocity distribution (Figure 2.7).

v. **Compare to literature**:

- Compare the cluster members as identified in step (iv) to those in the published literature. This was done by computing the velocity dispersions (equation 1.1) of each cluster and comparing these with those in literature (see Table 2.2).

vi. **Substructure analysis**:

- Use KDE to determine the upper limit on the number of subclusters in each cluster (see Figure 2.5). The GMM algorithm uses the BIC to determine the number of subclusters but it requires an upper limit on this number. We use a limit of 5 subclusters in cases where the KDE analysis is unclear.

- The GMM algorithm was then applied to the sky distribution of each cluster plus a third dimension (*depth*) represented by the redshift distribution of the cluster (RA, Dec, and redshifts of galaxies selected in step (iv)). The number of subclusters were then found for each cluster. See the results of this analysis on A1367 in Figure 2.6.

- Analyse the clustering structure in each cluster via agglomerative clustering (see Table 2.4).

- Analyse the redshift distributions and velocity dispersions of complex clusters (those with subclusters) (see Table 2.3).

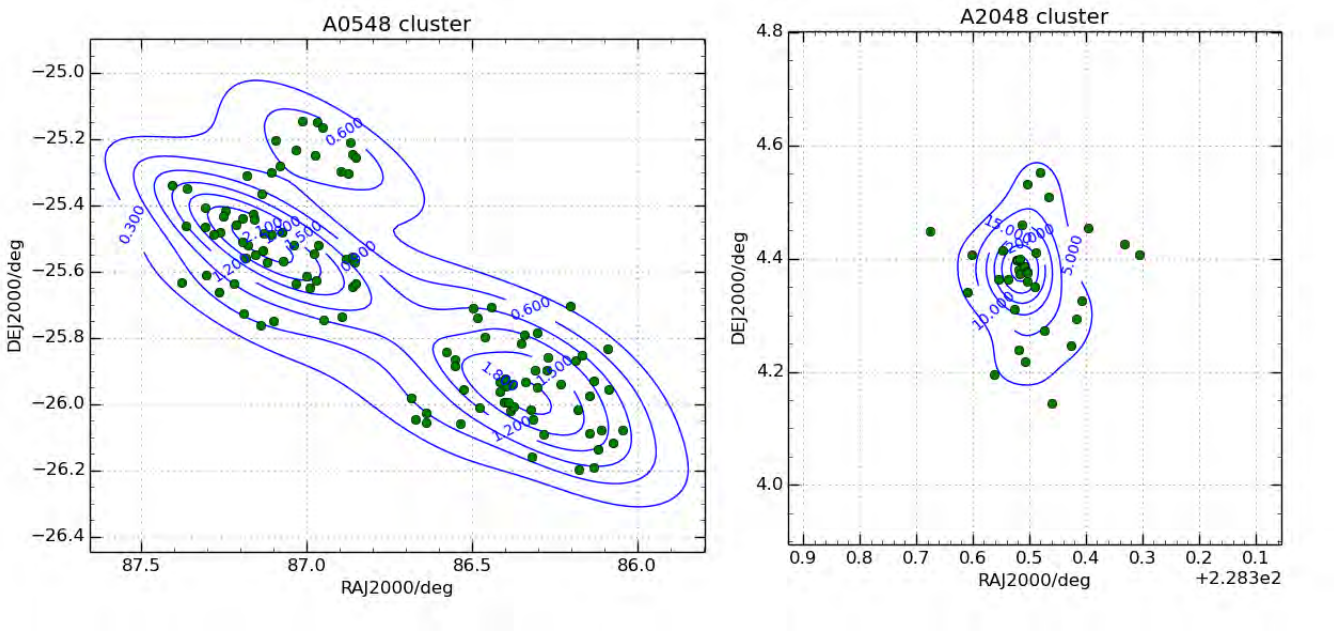

Figure 2.5: KDE approximation of the number of subclusters in clusters A0548 (left) and A2048. A0548 cluster shows significant substructure with at least 3 subclusters that may be in the process of interacting. The case of A0548 is extreme, the average cluster in the sample shows evidence of 2 subclusters at most e.g. in the case of A2048, this cluster has a pronounced over-density centred at the cluster centre with groups of galaxies in the periphery. The iso-density contour levels are indicated on the plot

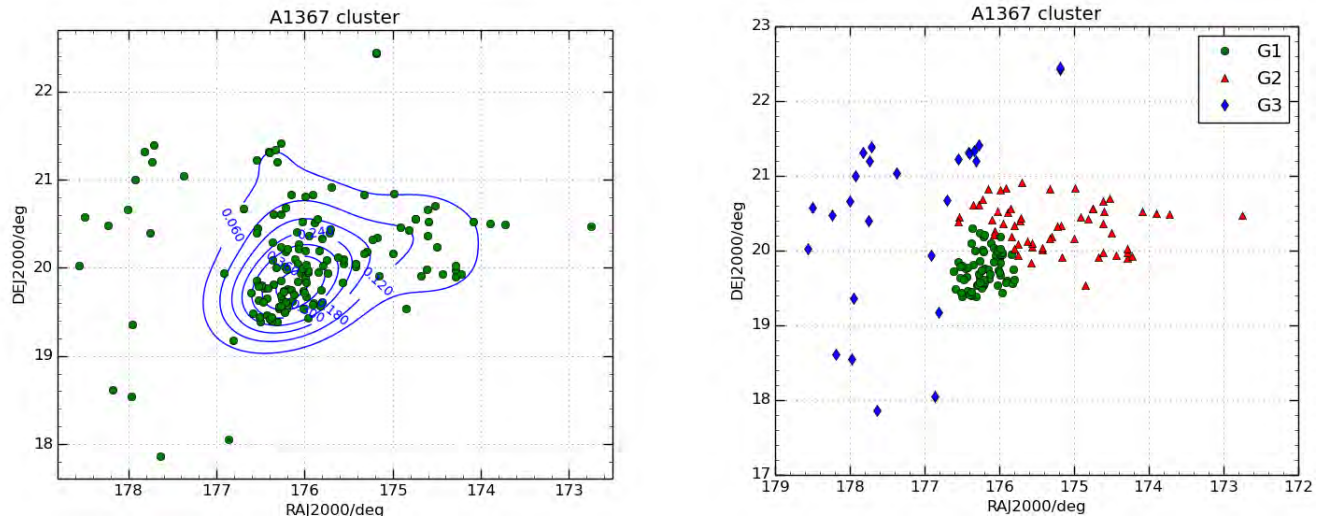

*Figure 2.6: KDE approximation of the number of subclusters for the A1367 cluster (left) and the subclusters found with the GMM algorithm (right). **Right**: Different symbols represent different subclusters (3 subclusters: G1, G2, and G3). This is an example of a case where the maximum number of subclusters (5) was used as an input into the GMM algorithm as the KDE analysis did not clearly indicate this number.*

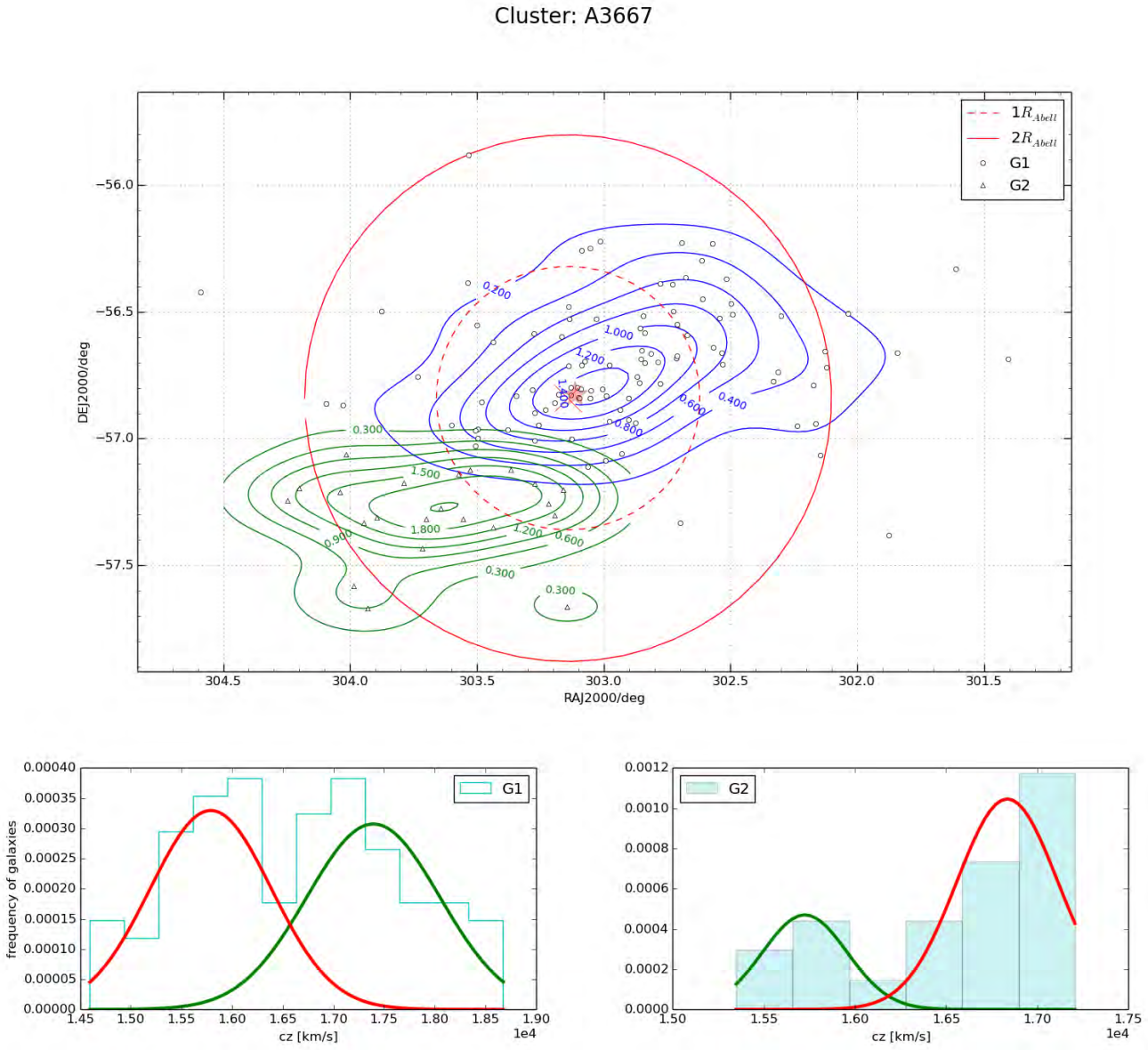

Figure 2.7: Substructure analysis in the A3667 cluster. The on-sky distribution of the cluster galaxies with isodensity contours colour coded according to subcluster. G1 and G2 are the two main subclusters found by the GMM algorithm. ***Top****: The dashed red line circle is the region within an Abell radius (∼ 3.65 Mpc for A3667) and the red solid line circle is the same for a radius of half an Abell radius – both are centred on the X-ray centroid/cluster centre (red cross). The red star is the cluster's BCG.* ***Bottom****: LOS velocity distributions of G1 and G2 with a pair of normal distributions fitted to each to highlight the bimodality in each distribution.*

Table 2.2: Calculated and literature velocity dispersions (σ_v) of each cluster and the peculiar velocities of their BCGs. The velocity dispersions and errors are estimated by using bootstrap methods with 500 re-samplings.

Cluster	σ_v [km/s]	v_{BCG} [km/s]	$\sigma_{v,BI}$ [km/s]	$S_{v,BI}$ [km/s]	σ_{stdev} [km/s]	N_z	$\sigma_{v,lit}$ [km/s]	$N_{z,lit}$	Ref.
A1213	504 ± 24	-97 ± 44	552 ± 24	553	504	144	566	305	20
A1367	696 ± 32	-187 ± 57	680 ± 31	710	673	149	879	121	28
A0013	868 ± 39	-5 ± 145	868 ± 43	953	846	36	886	37	22
A2048	690 ± 30	189 ± 118	643 ± 36	758	685	34	668	25	22
A2061	827 ± 37	208 ± 117	843 ± 43	921	875	54	1020	105	23
A2063	815 ± 36	-30 ± 119	803 ± 37	832	813	46	659	94	24, 25
A2255	1002 ± 46	-1775 ± 84	1029 ± 48	1124	1028	154	1266	42	27
A2256	925 ± 42	194 ± 136	971 ± 45	1011	967	49	1376	116	27
A2319	1111 ± 50	-57 ± 156	1112 ± 51	1174	1115	51	1770	130	26
A3376	780 ± 36	122 ± 82	820 ± 38	862	832	102	862	120	31
A3562	961 ± 42	-82 ± 139	917 ± 45	990	949	46	1048	114	22
A0399	1050 ± 46	-105 ± 135	987 ± 49	1096	1031	58	1186	115	24, 25
A0401	1092 ± 47	266 ± 123	1065 ± 47	1125	1074	73	1130	123	24
A4038	828 ± 38	-402 ± 137	828 ± 39	844	850	36	882	157	27
A0548	808 ± 37	242 ± 79	803 ± 37	858	856	110	842	323	22
A0610	659 ± 29	1932 ± 83	683 ± 33	710	622	60	496	57	21
A0754	863 ± 36	127 ± 72	834 ± 39	875	798	134	931	92	27
A0085	757 ± 33	-166 ± 102	756 ± 36	784	751	53	969	308	22
A3667	892 ± 40	95 ± 82	944 ± 44	955	863	122	1056	550	33
A1656	941 ± 43	-287 ± 52	977 ± 44	976	905	336	1008	499	27
RXJ1720	882 ± 40	-230 ± 47	845 ± 47	1027	857	367	878	26	30

Col. 1: Cluster name. Col. 2: Cluster velocity dispersion calculated using the mean cluster redshift. Col. 3: BCG perculiar velocity. Col. 4: Cluster velocity dispersion calculated using the bi-weight estimator (C_{BI}). Col. 5: Bi-weight scale estimator. Col. 6: Standard deviation of galaxy peculiar velocities. Col. 7: Number of galaxies in the redshift sample of each galaxy cluster. Col. 8: Literature cluster velocity dispersion. Col. 9: Literature cluster size (number of galaxies). Col. 10: Literature dispersion reference codes: (20)Hernádez-Fernádez et al. 2012[113]; (21)Boschin et al. 2008[22]; (22)Mazure et al. 1996[163]; (23)Small et al. 1998[223]; (24)Hill & Oegerle 1993[114]; (25)den Hartog & Katgert 1996[54]; (26)Oegerle et al. 1995[177]; (27)Chen et al. 1998[33]; (28)Moss et al. 1998[168]; (30)Owers et al. 2011[180]; (31)Durret et al. 2012[61]; (33)Owers et al. 2009[179].

Table 2.3: Velocity dispersions and redshifts of complex clusters found with the GMM algorithm. Clusters with zero entries for any column do not have that column's respective subcluster/cluster component.

Cluster	$\sigma_{v,G1}$	$\sigma_{vErr,G1}$	$\overline{z}_{G1}$	N_{G1}	$\sigma_{v,G2}$	$\sigma_{vErr,G2}$	$\overline{z}_{G2}$	N_{G2}	$\sigma_{v,G3}$	$\sigma_{vErr,G3}$	$\overline{z}_{G3}$	N_{G3}
A0610	546	79	0.09752	57	121	64	0.10365	3	–	–	–	–
A1367	762	97	0.02177	65	613	82	0.02277	58	625	123	0.02290	26
A1213	599	76	0.04687	68	680	76	0.04702	86	–	–	–	–
A2048	17	10	0.09807	3	725	141	0.09723	31	–	–	–	–
A0548	691	93	0.04044	59	822	119	0.04285	51	–	–	–	–
A3667	970	102	0.05537	100	544	123	0.05515	22	–	–	–	–
A1656	702	120	0.02203	35	1001	138	0.02355	56	989	74	0.02279	184

Col. 1: Cluster name. Col. 2 & Col. 3: σ_v [km/s] and its error, respectively, for subcluster G1. Col. 4 & Col. 5: G1 average redshift and number of galaxies, respectively. Col. 6 & Col. 7: σ_v [km/s] and its error, respectively, for subcluster G2. Col. 8 & Col. 9: G2 average redshift and number of galaxies, respectively. Col. 10 & Col. 11: σ_v [km/s] and its error, respectively, for subcluster G3. Col. 12 & Col. 13: G3 average redshift and number of galaxies, respectively.

2.4.3 Results

The role of the cluster analysis is to select and characterise cluster members for each cluster and also analyse the substructure that may be present in each of the confirmed populations of cluster members. The resulting cluster members are analysed in the following subsections and later in the following chapters.

Clustering Structures

An analysis of the on-sky and redshift distribution of the galaxy members of each cluster was performed through agglomerative cluster analysis. The clustering structure is measured by the agglomerative coefficient coefficient (AC). AC is defined according to the ratio of the dissimilarity between object/subcluster i and the first subcluster/object that it is merged with (the dissimilarity could be distance for a case of spatial clustering), to the dissimilarity of the merger in the step leading to object/subcluster i. Let this ratio be d_i, then AC is defined as the average of all $(1 - d_i)$. An AC value $\rightarrow 1$ represents strong evidence of substructure while an AC $\rightarrow 0$ represents weak or no evidence of substructure.

Our analysis shows that the galaxy clusters in our sample all display significant substructure, with an average $AC \simeq 0.90$. The clustering structure of the on-sky (2D) galaxy distribution agrees with the 3D galaxy distribution, on average, while the 1D distribution shows more substructures. The 1D analysis may be constrained further by including galaxy motions that are in the plane of the sky as radial motions of galaxies may affect their redshifts.

As AC $\rightarrow 1$, the number of subclusters found increases, as expected (see the right panel of Figure 2.8). The clusters which have 3D subcluster/component numbers > 1 are categorised as complex clusters and further substructure analysis of these clusters is done in section 2.4.3. The cluster `RXJ1720.1+2638` (RXJ1720) in Table 2.4 was used as a control sample and will not be analysed further. `RXJ1720.1+2638` is a cool core cluster, which are thought to be dynamically relaxed (Hudson et al. 2010[116]), located at redshift 0.16 (Giacintucci et al. 2014[94]).

Velocity Dispersions

As discussed in chapter 1, our cluster members are not expected to be distributed normally and as such, a least variance method (other than the arithmetic mean) is required to estimate measures of location in distributions of physical quantities such as the radial velocity distribution. The bi-weight estimators are used in this regard.

The use of the bi-weight location estimator (C_{BI}, see equation 1.7) is compared to that of the arithmetic mean in determining the velocity dispersion as defined in equation 1.2. The velocity dispersion calculated using C_{BI} is denoted as $\sigma_{v,BI}$ and that calculated using the arithmetic mean is denoted as $\sigma_{v,m}$ (or σ_v in Figures 2.9 and 2.10 only). The two dispersions agree well for clusters of all sizes with a linear relationship: $\sigma_{v,BI} = 0.0941\sigma_{v,m} + 50.726$ with scatter 0.051 km/s (see Figure 2.9). The bi-weight estimator method is in slightly better agreement with literature velocity dispersions, where the relation between the velocity dispersions is linear with a scatter of 0.060 km/s, versus the arithmetic mean method which produces a scatter of 0.065 in the same relation (Figure 2.10). The bi-weight estimators are used to approximate location and scale in the analysis of all chapters that follow. The velocity dispersion $\sigma_{v,BI}$ is

Table 2.4: Substructure analysis results. AC is the agglomerative coefficient which measures the clustering structure in each cluster. "3D" refers to the combined distribution of galaxy redshifts, RA and Dec. AC → 1 represents high confidence for substructure.

Cluster	AC_z	AC_{sky}	comps_{sky}	AC_{3D}	comps_{3D}
A1213	0.99	0.94	2	0.94	2
A1367	0.99	0.95	5	0.95	3
A0013	0.96	0.83	2	0.82	1
A2048	0.93	0.82	2	0.81	2
A2061	0.97	0.87	1	0.86	1
A2063	0.97	0.89	2	0.89	1
A2255	0.99	0.94	1	0.93	1
A2256	0.98	0.94	1	0.94	1
A2319	0.98	0.89	1	0.89	1
A3376	0.99	0.90	1	0.90	1
A3562	0.97	0.90	2	0.90	1
A0399	0.98	0.89	2	0.89	1
A0401	0.98	0.89	1	0.89	1
A4038	0.96	0.84	1	0.84	1
A0548	0.99	0.95	2	0.95	2
A0610	0.98	0.89	2	0.89	2
A0754	0.99	0.93	1	0.93	1
A0085	0.96	0.88	2	0.88	1
A3667	0.99	0.93	1	0.93	2
A1656	1.00	0.97	3	0.97	3
RXJ1720	1.00	0.96	5	0.95	5

Col. 1: Cluster name. Col. 2: Agglomerative coefficient (AC) for the redshift distributions. Col. 3 and Col. 4: AC for the RA-dec (sky) distribution of cluster members and the number of components found in the sky distribution, respectively. Col. 5 and Col. 6: AC for the RA-dec-redshift ("3D") distribution of cluster members and the number of components found in this distribution, respectively.

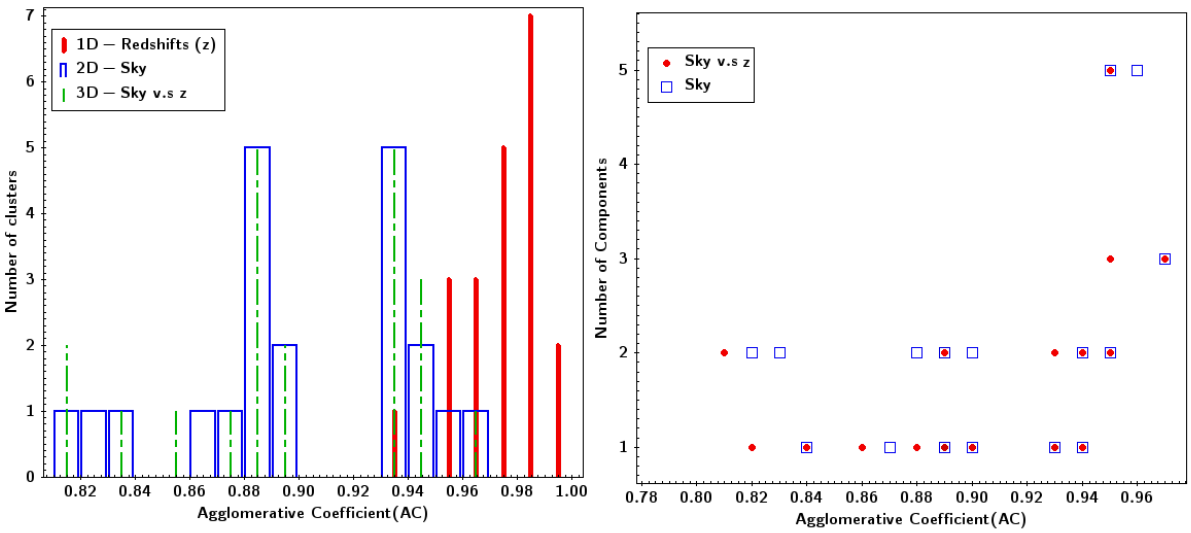

Figure 2.8: Global clustering structure of our cluster sample. ***Left****: the agglomerative clustering coefficient (AC) distribution for each cluster. The cluster analysis was performed on three distributions of redshift (1D), sky (2D), and sky v.s. redshift/spatial depth (3D) for each cluster and these are represented by different histograms as labelled – "3D" refers to the combined distribution of galaxy redshifts, RA and Dec.* ***Right****: The number of subclusters found in 2D and 3D cluster analysis. An AC → 1 implies strong evidence of substructure.*

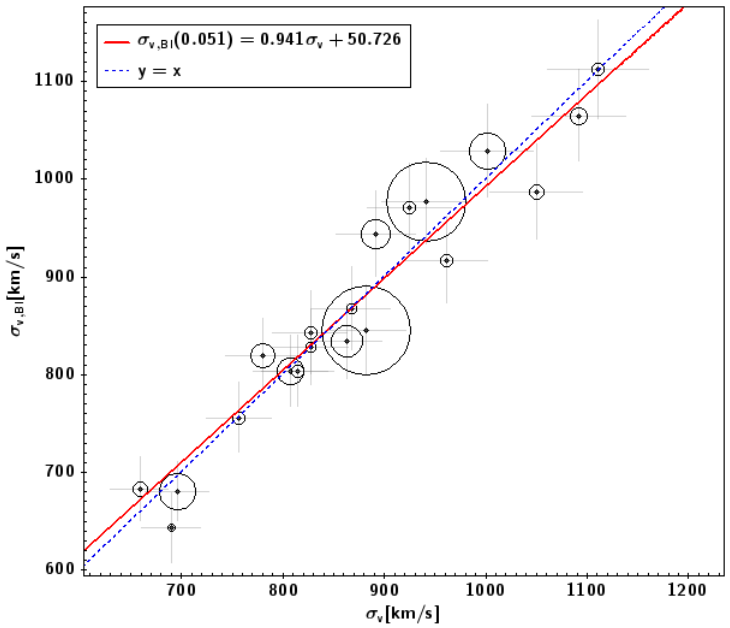

Figure 2.9: The two methods of estimating a cluster representative reference radial velocity for determining velocity dispersions: C_{BI} v.s. the mean. The sizes of circles around each data point indicate the cluster size (number of galaxies), errors are approximated by the standard deviation of the mean in the case of the mean (and that of C_{BI} in the case of the bi-weight location estimator) and both are obtained via bootstrap statistics.

denoted simply as σ_v in the analysis that follows, unless stated otherwise.

The relation between our calculated velocity dispersions and those of the published literature (Table 2.2) was further analysed. Our velocity dispersions are underestimated for the most part (Figure 2.11). Ideally we would like the two to have as little differences as possible but since we use a different member selection method as other authors, differences are expected. Further analysis suggests that our initial radial velocity criteria, where we required that galaxies have radial velocity differences of no more than 2000 km/s relative to the cluster's systematic and BCG radial velocities, may be the cause of these differences. Other authors make use of a larger velocity slice e.g. Hernandez-Fernandez et al. (2012)[113] apply a radial velocity cut of $\sim$ 4497 km/s for galaxies within 2.2 Abell radii (centred on the cluster's centre as given in NED) for the case of A1213 while Moss et al. (1998)[168] use CGCG (Catalogue of Galaxies and of Clusters of Galaxies, Zwicky & Herzog 1963[257]) galaxies in the region of A1367 with radial velocities 4000 - 9000 km/s. We investigated the effect of our velocity cut with an analysis in which we simulated mock galaxy clusters made up of mock galaxies with normally distributed radial velocities. We then sampled the mock velocities at 1σ, 2σ, 3σ and 5σ levels (where σ is the standard deviation of the mock radial velocity distribution) and then calculated velocity dispersions for each sample. We found that as we increased the σ levels, the velocity dispersions also increased to a plateau indicating that the lower σ levels resulted in underestimated velocity dispersions. The numbers of our cluster members are less than, in most cases, those used to calculate the literature velocity dispersions and thus we tend to underestimate the velocity dispersions for the clusters in our sample.

We do not assume that the clusters in our sample are dynamically relaxed nor do we only identify as cluster members, only galaxies falling within the virial region (as done in e.g. Hernandez-Fernandez et al. 2012[113]). We also find that our 2 Abell radii cut-off is significantly larger than R_{200} ($\sim \times 2$) for some of the clusters in our sample. The

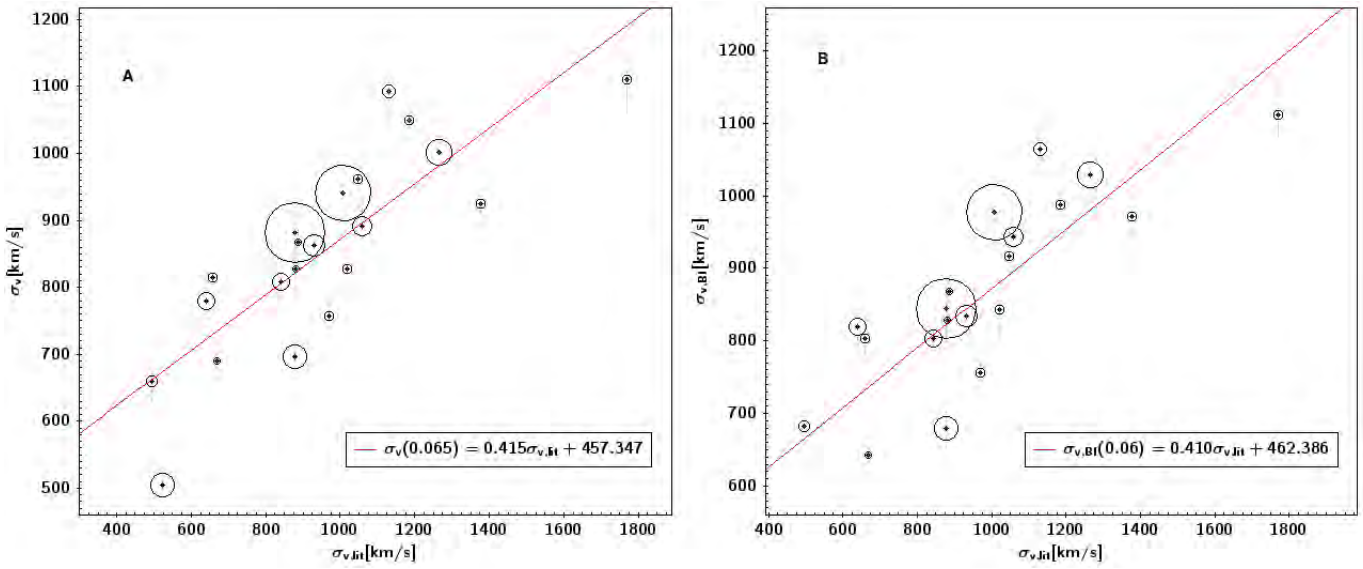

Figure 2.10: Cluster velocity dispersions: C_{BI}-method v.s literature dispersions (figure "B" on the right) and the "mean"-method v.s literature dispersions (figure "A" on the left). The sizes of circles around each data point indicate the cluster size (number of galaxies), errors are approximated as in Figure 2.9.

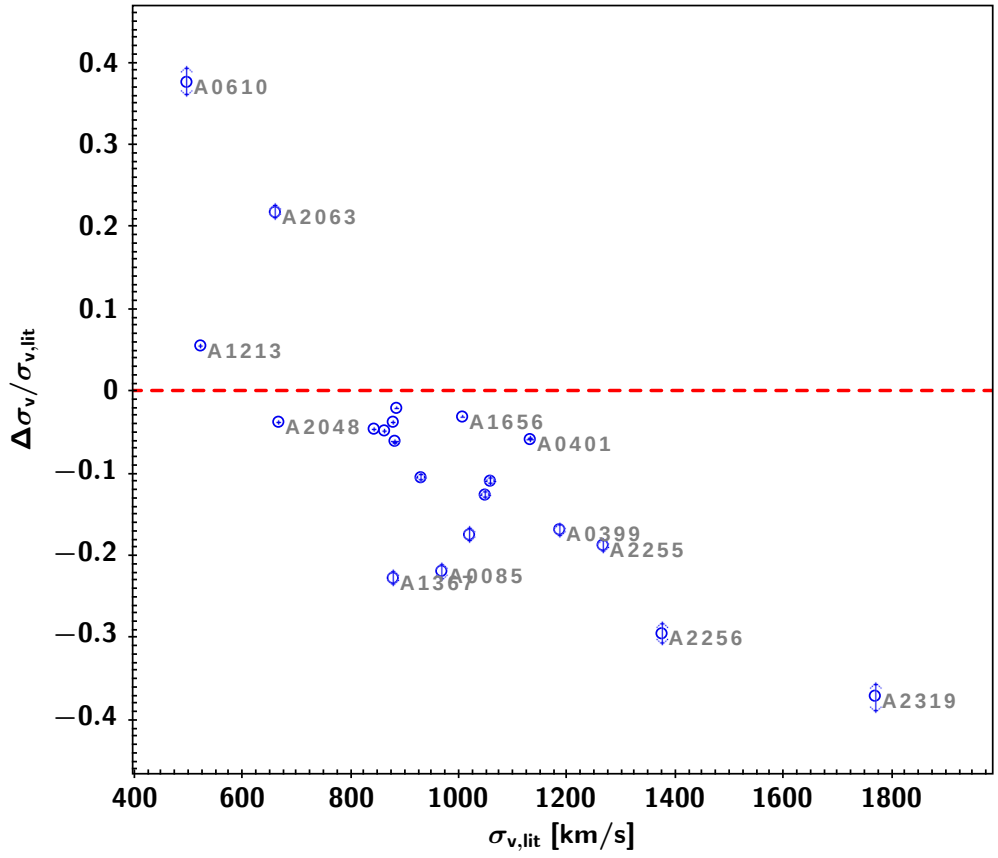

Figure 2.11: Open circles: The differences ($\Delta\sigma_v$/) between calculated velocity dispersions ($\sigma_{v,BI}$) and those from the literature ($\sigma_{v,lit}$) normalised by the literature values and plotted as a function of the literature values, $\sigma_{v,lit}$. Errors plotted are lower bound values approximated by propagating the errors of $\sigma_{v,BI}$.

region within R_{200} is made up largely of the cluster core which is the region most likely to display dynamic equilibrium and thus is well described by methods which utilise the virial theorem for member selection. The velocity dispersions we report are those obtained through bootstrap resampling, with 500 resamplings of redshifts for each cluster. This method of sampling our data *increased* the number densities of galaxies within our 2 Abell radii limits which may also have been the reason of our underestimated velocity dispersions. Velocity dispersions are inversely proportional to the sample size used to calculate them and this, for a given range of velocities, will lead to underestimated dispersions as the sample size increases.

BCG motions

We analyse the perculiar radial velocities of cluster BCGs. As discussed in chapter 1.5.3.1, BCGs are expected to be at the centre of the potential well of their parent clusters and thus have very small peculiar motions unless the cluster has been disturbed and is not dynamically stable. We investigate this expectation of small BCG motions by analysing the distributions of BCG peculiar velocities as a function of cluster mass, indirectly, by probing the dependence of BCG peculiar radial velocity on the cluster's velocity dispersion ($\sigma_{v,BI}$).

The BCGs of clusters A2255 and A0610 have anomalous peculiar velocities in our cluster sample: the A2255 BCG has $v_{pec,BCG} \simeq -1775$ km/s while the A0610 BCG has $v_{pec,BCG} \simeq 1932$ km/s, see Table 2.2 and Figure 2.12. A0610 is one of the complex clusters found by the GMM algorithm and are discussed in section 2.4.3. We find that $\sigma_{v,BI}$ and $v_{pec,BCG}$ are linearly related by $v_{pec,BCG} = -0.634\sigma_{v,BCG} + 448.570$ km/s when the two outliers are excluded from the fit. The mean location for these BCGs is $v_{pec,BCG} = -30$ km/s (obtained via C_{BI}), scale $S_{BI} \sim 157$ km/s with a scatter of 0.711 km/s. A one-sample t-test with the null hypothesis being that the mean $v_{pec,BCG}$ is 0 is rejected at a confidence level of no less than 68%, supporting the notion that our sample is composed of disturbed galaxy clusters.

Complex clusters

The cluster substructures found by our GMM analysis in section 2.4.2.1 are further analysed here. This is done by an in-depth GMM analysis of each cluster's (see Table 2.3) radial velocity and on-sky distribution of member galaxies.

A1367

This cluster has two main subclusters, one North-West (NW) and the other South-East (SE) of the cluster core, and also infalling groups of starburst galaxies (Cortese et al. 2004[44]). The NW subcluster is found to be a cool-core and virialised system with normally distributed radial velocities [44]. There is also a group of galaxies merging with this subcluster and trailing A1367 from the west of the subcluster [44]. Cortese et al. (2004)[44] found that the radial velocity distribution of the NW subcluster peaked at $C_{BI} = 6480 \pm 87$ km/s with scale $S_{BI} = 770 \pm 60$ km/s – with C_{BI} and S_{BI} being the bi-weight location and scale estimators (Beers et al. 1990[16]).

The SE subcluster is non-relaxed and was found to have the largest radial velocity, C_{BI}, and velocity dispersion [44]: $C_{BI} = 6596 \pm 137$ km/s and scale $S_{BI} = 1001 \pm 70$ km/s. Its radial velocity distribution has three main peaks

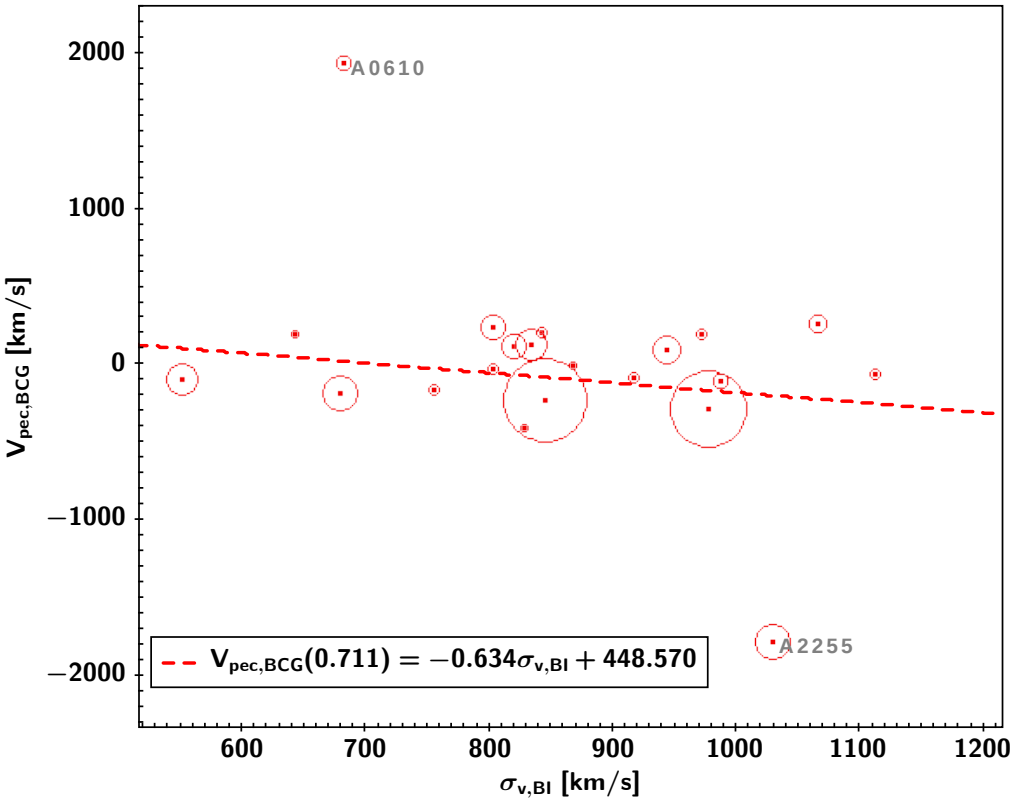

Figure 2.12: Cluster dispersions v.s. BCG peculiar motions. The sizes of circles around each data point indicate the cluster size (number of galaxies), errors are approximated as in Figures 2.9 and 2.10. The two most deviant clusters (A2255 & A0610) are marked in the plot. The circles around each data point indicate the cluster size via number of galaxy members.

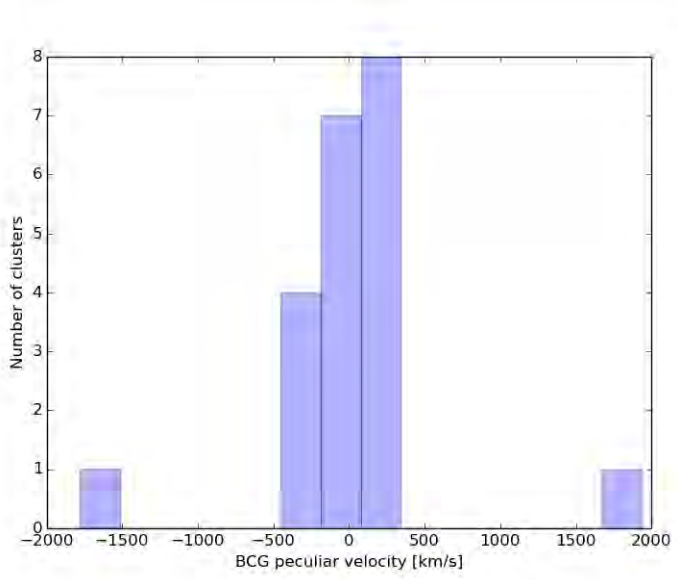

Figure 2.13: The peculiar velocities of BCGs. The two extremes are BCGs of A0610 (at 1932 km/s and on the far right) and A2255 (at -1775 km/s at the far left).

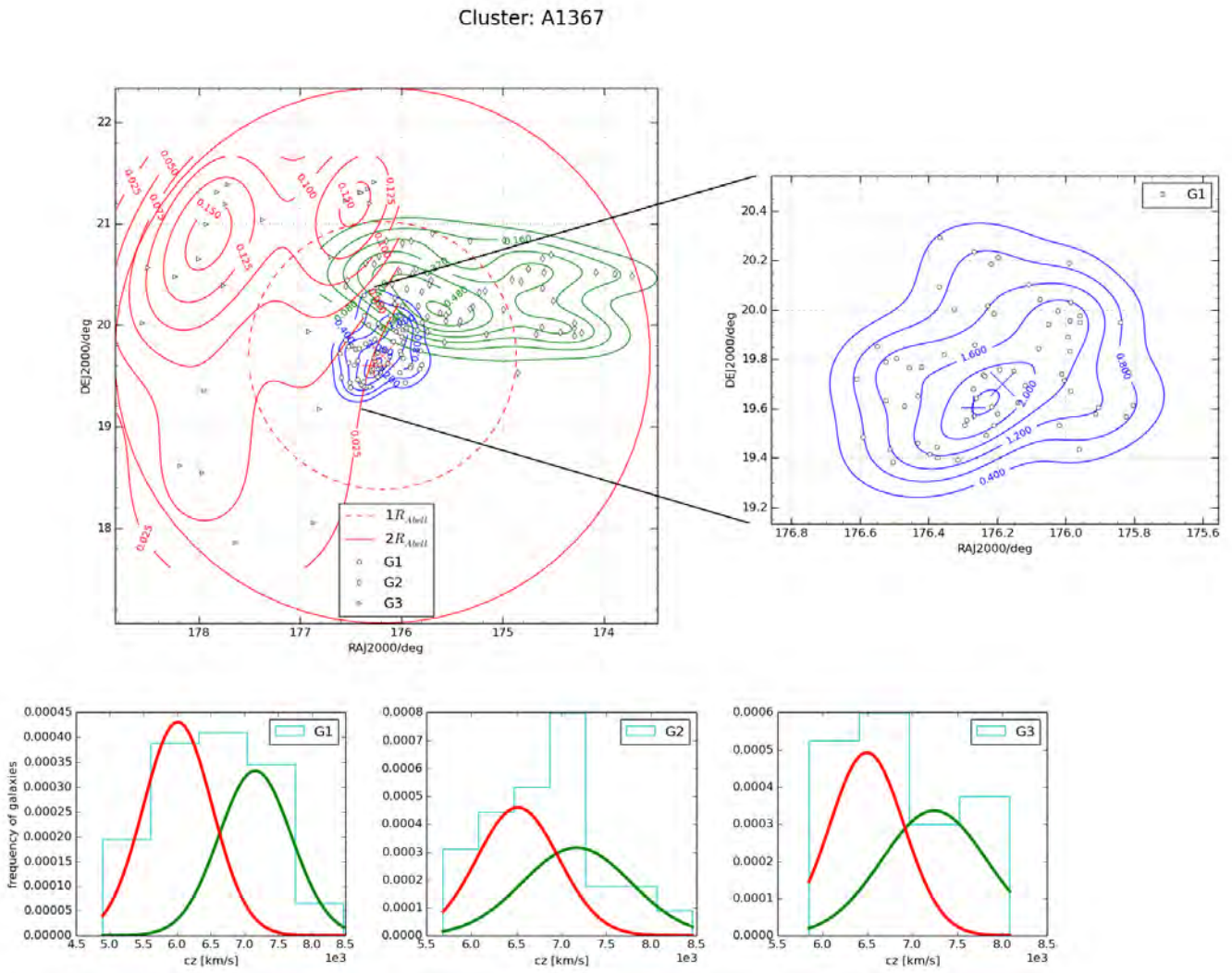

Figure 2.14: Substructure analysis in A1367. ***Top panels****: The on-sky distribution of A1367 galaxies with isodensity contours colour coded according to subcluster. The dashed and solid line red circles represent the 1 and 0.5 Abell radii regions, respectively – both are centred on the X-ray centroid/cluster centre (red/blue cross). The red/blue "+" is the cluster's BCG.* ***Bottom panels****: The radial velocity distributions for each subcluster. Each distribution is fitted with atleast 2 normal distributions (red and green curves).*

which maybe due to three separate groups within the subcluster. Two groups of infalling galaxies are apparent: one is a group of starforming galaxies falling into the subcluster from the near side (Sakai et al. 2002; Gavazzi et al. 2003b) and the other is a low velocity group (in terms of the average radial/line-of-sight velocity) which is falling into the subcluster from the East with respect to the cluster core (Forman et al. 2003[83]).

Our analysis found 3 subclusters: G1, G2, and G3. These have 65, 58, and 26 galaxies, respectively. Their velocity dispersions were found to be 763 ± 97 km/s, 614 ± 82 km/s, and 625 ± 124 km/s, respectively (Table 2.2). The mean locations of the velocity distributions of G1, G2, and G3 were found to be 6535 ± 97 km/s, 6835 ± 82 km/s, and 6865 ± 124 km/s, respectively. The spatial location of G1 corresponds with that of the entire A1367 cluster galaxies of Cortese et al. (2004)[44]. Our less conservative spatial limits from which galaxies, in the field of A1367, were extracted has resulted in more structure in the galaxy distribution. This is expected for a cluster like A1367, which is located in a filamentary wall-like structure connecting the Coma and Virgo clusters. The velocity distribution of each subcluster shows at least two components (Figure 2.14) suggesting that the subclusters are themselves composed of galaxy groups with localised velocities. This is expected for G1 – due to its correspondence with the core of A1367

which is quite complex (e.g Cortese et al. 2004[44]). The same can be said of groups of galaxies, in G2 and G3, which may be falling into the cluster through its interactions with the filamentary structures connecting it with its neighbouring rich clusters Coma and Virgo.

A0610

Boschin et al. (2008)[22] found this poor cluster to have two main cluster components, one of 3 galaxies and the other composed of 54 galaxies. The authors also found that these components have velocity dispersions $\sigma_v \sim 200$ km/s. The cluster's BCG, 2MASS J07591712+2709159 (henceforth BCMI[22]), shows significantly peculiar motion relative to the cluster's systematic radial velocity at a $> 95\%$ confidence level according to the Indicator test of Gebhardt & Beers (1991)[93]. The BCMI peculiar velocity found in this thesis is $\simeq 1932$ km/s (see Table 2.2). The BCG peculiar velocities in our sample have mean location (C_{BI}) $v_{pec,BI} = -30$ km/s and the peculiar velocity of BCGI is far beyond this. This very peculiar motion of BCMI suggests that the cluster has been dynamically disturbed.

A KMM analysis by Boschin et al. (2008)[22] suggests the existence of three cluster components of 3, 34, and 20 galaxies which arise from the 2 main subclusters of 3 and 54 galaxies. The two main subclusters are found to be separated, in radial velocity, by ~ 450 km/s. Our analysis finds the cluster to have 2 main subclusters of 3 and 57 galaxies, these two are found to have a radial velocity separation ~ 1869 km/s suggesting that our subclusters may not necessarily correspond to those of Boschin et al. (2008)[22]. The subcluster, from our analysis, of 3 galaxies has velocity dispersion $\sigma_v = 122 \pm 64$ km/s which is much smaller than the velocity dispersion of the 57 member subcluster which is $\sigma_v = 546 \pm 79$ km/s (see Table 2.3). This discrepancy suggests that the smaller subcluster is a galaxy group falling into the cluster core and merging with the larger, 57 member, component.

Our analysis finds that the 57 member subcluster displays an approximately unimodal normal distribution of radial velocities, at least at the 1σ level, see Figure 2.15. The analysis of Boschin et al. (2008)[22] found the larger of their 2 main subclusters to have a virialised 22 galaxy component. These 22 galaxies, however, may not be truly virialised, but may form only part of a virialised A0610 component, because they were selected (by Boschin et al. 2008[22]) on the basis that they are within the virial radius of A0610. The A0610 relic is located South-East of the cluster core and is not coincident with any significant cluster component found in our analysis and that of Boschin et al. (2008).

A1656 (Coma cluster)

Colless & Dunn (1996)[43] (henceforth CD96) found that the Coma cluster is in the process of several mergers with galaxy groups and will be in such a state indefinitely. They found 2 subclusters through a KMM analysis. The main subcluster in their results is centred on the cD and radio galaxy NGC 4874 (Liu & Xie 1992[153]; Hudson et al. 2001[117]) and has mean radial velocity location $\overline{cz} \simeq 6853$ km/s and velocity dispersion $\sigma_v \simeq 1082$ km/s. The second subcluster is a group centred on the cD radio galaxy NGC 4839 (Liu & Xie 1992[153]) with $\overline{cz} \simeq 7339$ km/s and velocity dispersion $\sigma_v \simeq 329$ km/s.

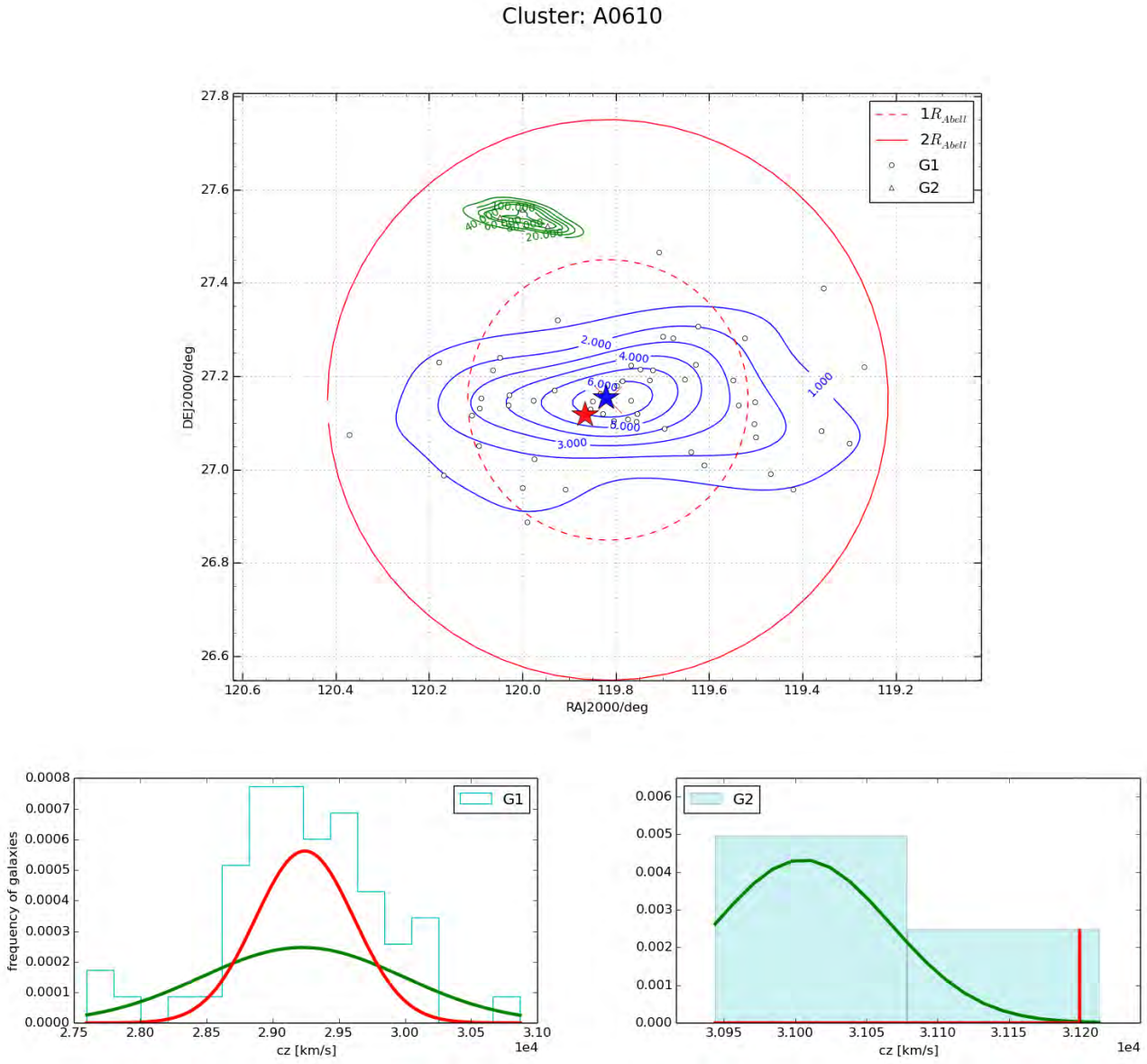

Figure 2.15: Substructure analysis in A0610. G1 and G2 are the two main subclusters found by the GMM algorithm. ***Top****: The dashed red line circle is the region within an Abell radius (∼ 1.85 Mpc for A0610) and the red solid line circle is the same for a radius of half an Abell radius – both are centred on the X-ray centroid/cluster centre (red cross). The red "+" (and faint blue star) is the cluster's BCG, BCMI, and the faint red star (south-east of BCGI) is the second brightest galaxy, BCMII (Boschin et al. 2008[22]). G2 is the small group of galaxies north of the two bright central galaxies.* ***Bottom****: LOS velocity distributions of G1 and G2 with a normal distribution fitted to each to highlight the overall radial velocity distribution in each cluster component.*

CD96 found that the late type galaxy population of A1656/Coma has a velocity dispersion that is $\sim \sqrt{2}$ larger than that of early type galaxies in the cluster and they conclude that late type galaxies are falling into the mainly virialised core region of the cluster. They suggested that the NGC 4839 group is falling into the cluster from the direction of A1367 along the Great Wall (see e.g. Einasto et al. 2011[65] for a recent study on the galaxies of the Great Wall) and that this merger is the source of the Coma radio halo that was first detected by Large et al. (1959)[146] and later confirmed by Wilson (1970)[249]. CD96 also found substructure in the NGC 4874 subcluster where they found 2 main components.

Our analysis found 3 subclusters: G1, G2, and G3. G1 has mean radial velocity location $C_{BI} = 6595 \pm 120$ km/s, velocity dispersion $\sigma_v = 703 \pm 120$ km/s, and a galaxy population of 35 members. G2 has mean radial velocity location $C_{BI} = 7045 \pm 138$ km/s, velocity dispersion $\sigma_v = 1002 \pm 138$ km/s, and a galaxy population of 56 members. The third subcluster, G3, has mean radial velocity location $C_{BI} = 6835 \pm 75$ km/s, velocity dispersion $\sigma_v = 989 \pm 75$ km/s, and a galaxy population of 184 members. G3 is the most spatially compact of the three and is centred on both the X-ray centroid and the BCG NGC 4889 (see Figure 2.16). This subcluster, and also G1 and G2, displays a bimodal radial velocity distribution.

A3667

Owers, Couch, & Nulsen (2009)[179] (henceforth OCN09) found a cluster velocity dispersion $\sigma_v = 1056 \pm 38$ km/s and 2 main subclusters separated by ~ 500 km/s in radial velocity. One subcluster (SE of the centre and associated with the BCG) is centred near the cluster centre and the other near the second dominant cluster galaxy and is located ~ 1 Mpc NW of the cluster's centre. OCN09 also find 2 smaller groups of galaxies centred ~ 1 Mpc SE and west due North. A KMM analysis by OCN09 on the 2 main subclusters showed that, collectively, the 2 were composed of 3 partitions: the main cluster associated with the BCG and with velocity dispersion $\sigma_v = 1073 \pm 64$ km/s and 242 galaxies, the NW subcluster with velocity dispersion $\sigma_v = 1039 \pm 66$ km/s and 164 galaxies, and also a SE cluster component made up of 27 members with velocity dispersion $\sigma_v \sim 209$ km/s.

Our analysis finds 2 main cluster components, G1 and G2, separated by ~ 90 km/s. These 2 both have substructure in their radial velocity distributions – they both show evidence of bimodality in their radial velocities (see Figure 2.7). G1 has velocity dispersion $\sigma_v = 971 \pm 102$ km/s, mean radial velocity location $C_{BI} = 16609 \pm 102$ km/s, and 100 galaxies. G2 has velocity dispersion $\sigma_v = 545 \pm 123$ km/s, mean radial velocity location $C_{BI} = 16519 \pm 123$ km/s, and 22 galaxies. Our G1, which extends to the north-west (blue contours in Figure 2.7), has its galaxy density peak corresponding with the cluster centre and BCG. The velocity dispersion of G1 corresponds with that of the main subcluster of OCN09 suggesting that G1 is a similar partition to that identified as the main subcluster by OCN09 and may be superimposed with the NW subcluster and a part of the south-east subcluster of OCN09. The galaxy density centres of G1 and G2 are separated by ~ 2 Mpc.

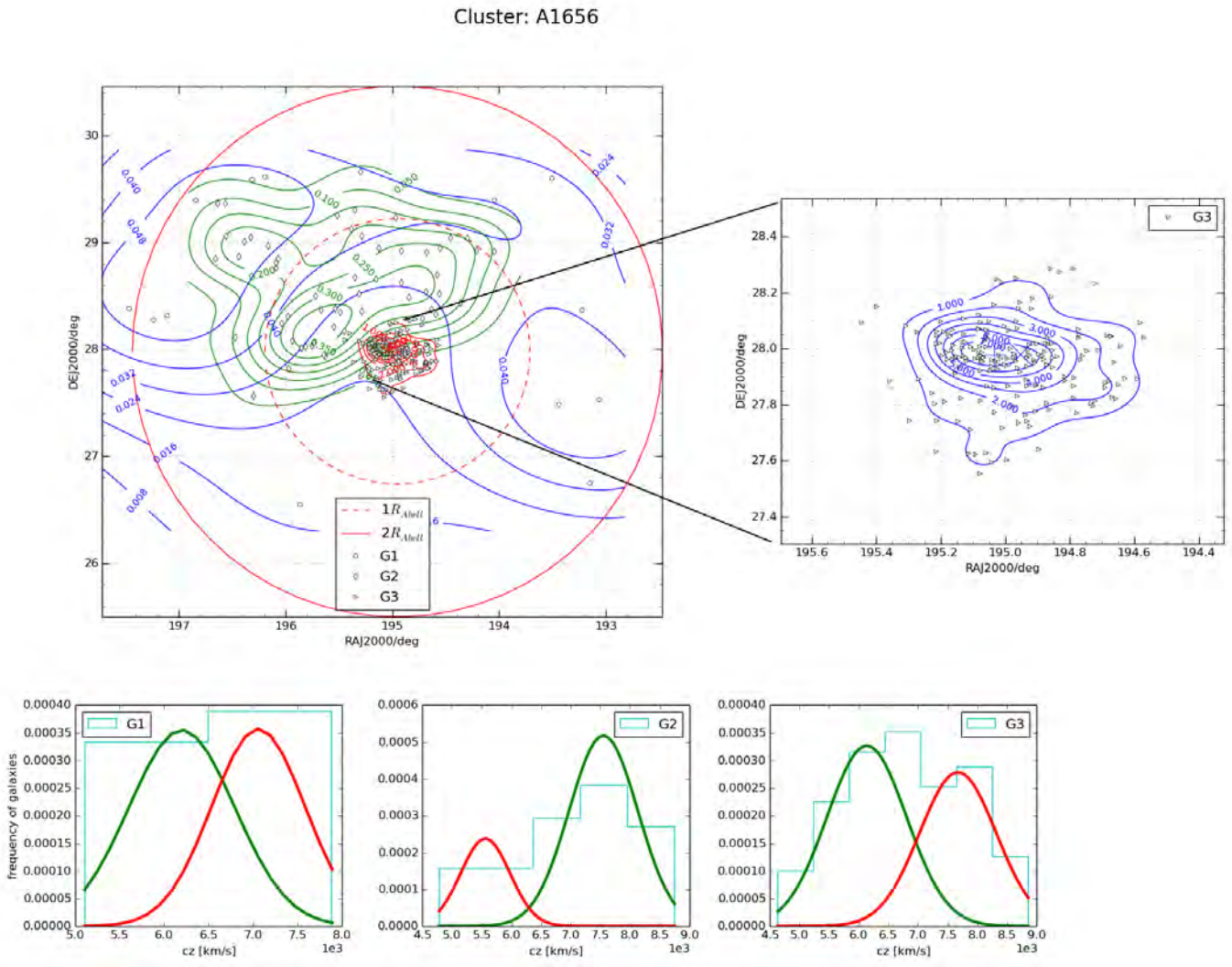

Figure 2.16: Substructure analysis in A1656 (Coma cluster). ***Top panels****: The on-sky distribution of A1656 galaxies with isodensity contours colour coded according to subcluster. The dashed and solid line red circles represent the 1 and 0.5 Abell radii regions, respectively.* ***Bottom panels****: The radial velocity distributions for each subcluster. Each distribution is fitted with atleast 2 normal distributions (red and green curves). The positions of the X-ray centroid/cluster centre (red cross) and the BCG (red "+") are shown in the top panels.*

A0548

A0548 is a rich bimodal cluster with 2 distinct subclusters located NE and SW of the cluster centre (see Figure 2.17 top panel). Flin & Krywult (2006)[81] detected the two main substructures at scales of $\sim$ 100 Mpc. The SW subcluster was found to be non-relaxed, dynamically, with evidence of the existence of $\sim$ 4 components within the subcluster[81]. It corresponds to G2 as identified in our GMM analysis. Our GMM analysis finds this subcluster to have 2 components with the larger of the 2 centred on the SE of the centre of the subcluster while the smaller component is centred near the A0548 BCG. G2 was found to have velocity dispersion $\sigma_v = 823 \pm 119$ km/s, mean radial velocity location $C_{BI} = 12831 \pm 120$ km/s, and 51 galaxies.

The other subcluster found by our analysis, G1, corresponds with the NE subcluster of Flin & Krywult (2006)[81]. G1 was found to have velocity dispersion $\sigma_v = 691 \pm 94$ km/s, mean radial velocity location $C_{BI} = 12112 \pm 94$ km/s, and 59 galaxies. Davis et al. (1995)[49] find a radial velocity scale for the NE subcluster of $S_{BI} \simeq 639$ km/s which is in agreement with the velocity dispersion found in our analysis. Our analysis finds G1 to be made up of 3 components with velocity dispersions $\sigma_v = 857 \pm 239$ km/s (with 13 galaxies and located north due east of the A0548 center), $\sigma_v = 527 \pm 104$ km/s (with 27 galaxies and located north-east of the A0548 center, coincident with the G1 density peak), and $\sigma_v = 501 \pm 118$ km/s (with 19 galaxies and located east of the A0548 center).

A2048

This is a poor BM type II (chapter 1.2) cluster with no dominant galaxy but rather a small group of galaxies (G1 with 3 galaxies) at the centre (Figure 2.18 top panel). This small group at the centre has velocity dispersion $\sigma_v = 18 \pm 11$ km/s and mean radial velocity location $C_{BI} = 29410 \pm 11$ km/s. The peripheral galaxies form the G2 subcluster with velocity dispersion $\sigma_v = 726 \pm 141$ km/s, mean radial velocity location $C_{BI} = 29140 \pm 141$ km/s, and a galaxy population of 31 members. The two subclusters found by our GMM algorithm are separated by $\sim$ 252 km/s in radial velocity. The G1 radial velocities may be unimodal but the this is inconclusive due to small number statistics, while G2 has a bimodal radial velocity distribution (see Figure 2.18 bottom panels) suggesting dynamical instabilities in the clusters outer regions where extended relics are generally found – which is fitting since A2048 hosts an extended relic source, `VLSS J1515.1+0424` (van Weeren et al. 2011)[240].

A1213

This is a very poor cluster with sample size $\sim$ 60 (Hernández-Fernández et al. 2012[113]) and a diameter of $\sim$ 2.7 Mpc (as reported in the NED data base). We sample a larger area (within $\sim$ 1 Abell radius) than this, a diameter of $\sim$ 4.0 Mpc which results in the two components found by the GMM algorithm. The first component, G1, has mean radial velocity location $C_{BI} = 14060 \pm 76$ km/s, velocity dispersion $\sigma_v = 599 \pm 76$ km/s, and a galaxy population of 68 members. The second component, G2, has mean radial velocity location $C_{BI} = 14090 \pm 77$ km/s, velocity dispersion $\sigma_v = 681 \pm 77$ km/s, and a galaxy population of 86 members. The two components are separated by $\sim$ 44 km/s

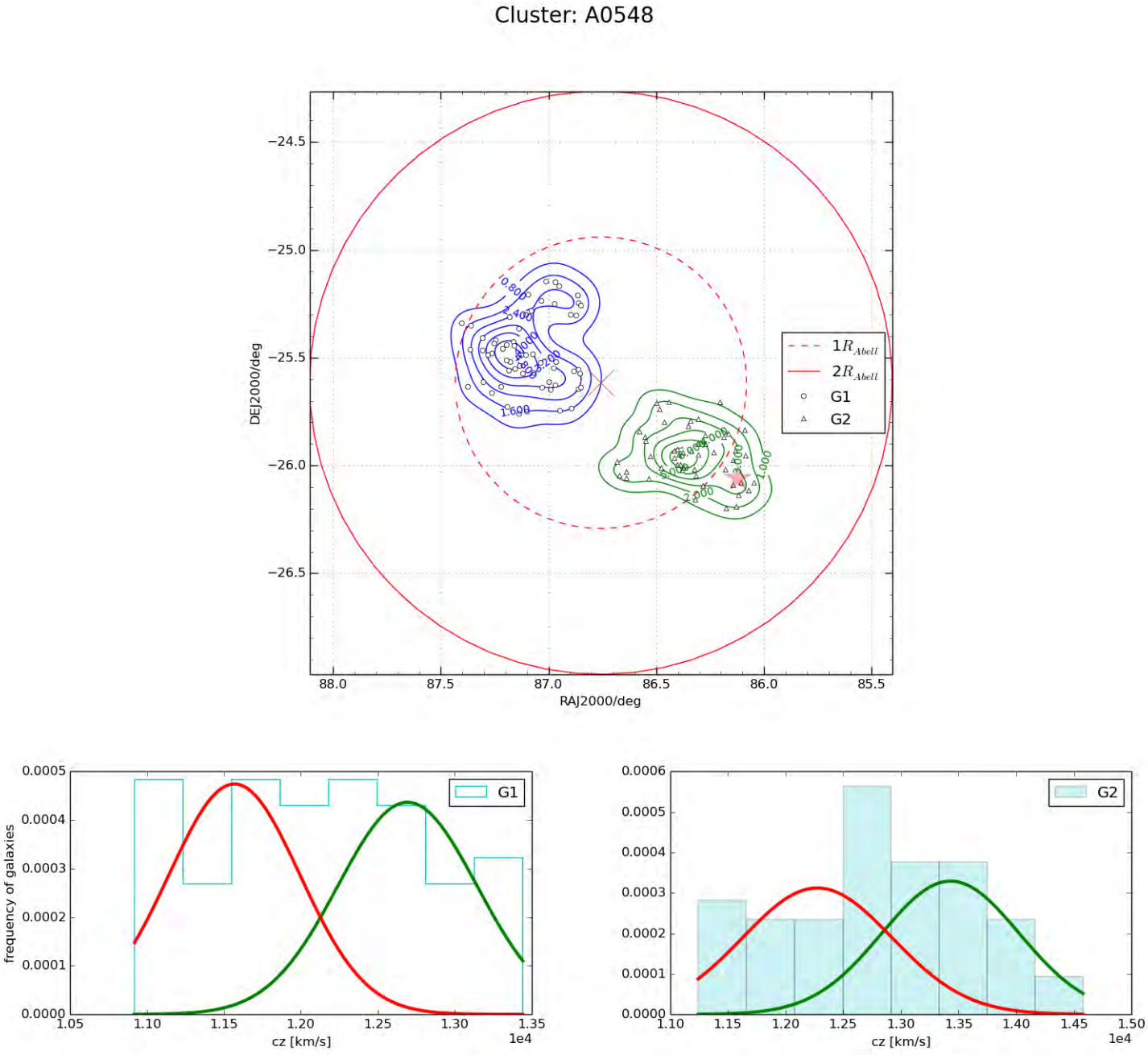

Figure 2.17: Substructure analysis in A0548. ***Top panels****: The on-sky distribution of cluster galaxies with isodensity contours colour coded according to subcluster. The dashed and solid line red circles represent the 1 and 0.5 Abell radii regions, respectively.* ***Bottom panels****: The radial velocity distributions for each subcluster. Each distribution is fitted with atleast 2 normal distributions (red and green curves). The positions of the X-ray centroid/cluster centre (red cross) and the BCG (red "+") are shown in the top panels.*

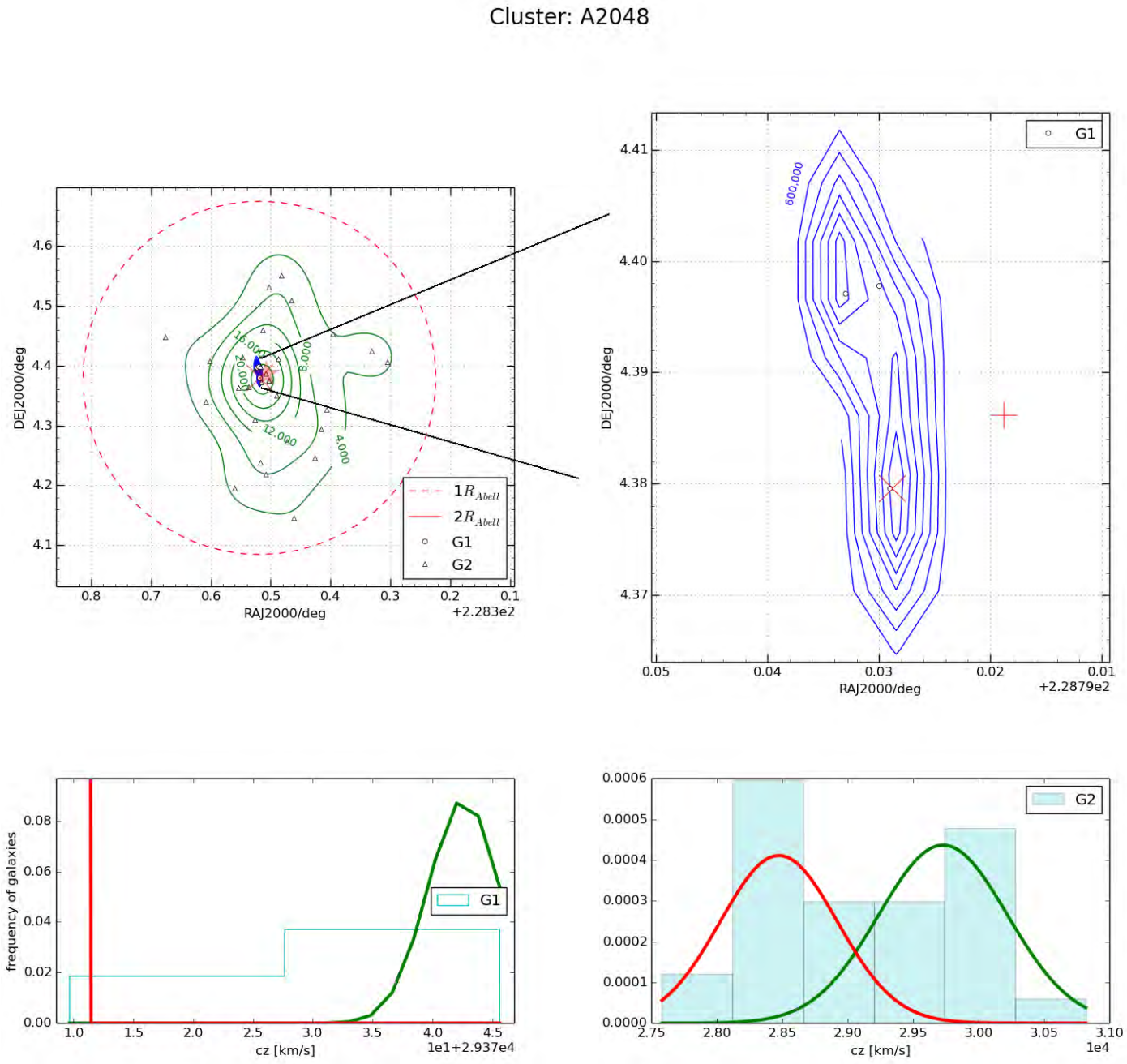

Figure 2.18: Substructure analysis in A2048. ***Top panels****: The on-sky distribution of A2048 galaxies with isodensity contours colour coded according to subcluster. The dashed and solid line red circles represent the 1 and 0.5 Abell radii regions, respectively.* ***Bottom panels****: The radial velocity distributions for each subcluster. Each distribution is fitted with atleast 2 normal distributions (red and green curves). The positions of the X-ray centroid/cluster centre (red cross) and the BCG (red "+") are shown in the top panels.*

in radial velocity. G1 clearly corresponds with the main A1213 cluster core reported on by Hernández-Fernández et al. (2012)[113] while G2 may represent galaxies in the periphery of the core. The G2 galaxies should be of late type according to the morphology density relation (Dressler 1980[56]). These photometric properties of these regions will be analysed in depth in the following chapter.

The lower density G2 population was found to have a unimodal radial velocity distribution while the G1 population was found to have a bimodal distribution (see the bottom panels of Figure 2.19) suggesting that the core region of the cluster is more turbulent than the peripheral region.

Non-member Galaxies

Our analysis uses two points as references: the BCG and the cluster reported (NED and CDS/SIMBAD) centre (X-ray centroid). Galaxies are only classified as cluster members when they satisfy all selection criteria for the two reference points. This has lead to cluster populations that are generally less than those in the literature and thus we expect our velocity dispersions to be lower than those in the literature. The choice of the two reference points was motivated by clusters such as A0548 which have their BCG displaced from the cluster centre. An advantage of using these two reference points is that in cases where the cluster centre and the BCG coincided, the selection is done using two similar reference points; but in cases where the two points differed, no one reference point was biased against the other.

A disadvantage is that the two regions around the two reference points may contain galaxies that are not found in both regions, such as in the case of A0548 (Figure 2.17), and these are then rejected as members. An attempt at lessening this disadvantage was to include these galaxies, if their redshifts were within the range set by $[z_{Xc},\ z_{bcg}]$, in the redshift samples that were to be tested for Gaussianity at 95% confidence (the QQ plot analysis in step (iv) of section 2.4.2.1). The result was the inclusion of some of these *outlying* galaxies.

2.4.4 Conclusion

The cluster membership of galaxies was analysed in depth in this chapter. The method used is based on the Gaussian Mixture Model implemented in the `Mclust` package of the `R` programming language. The results (showing independence with regard to whether a cluster was a radio relic and/or halo host) were two main categories of clusters: those that contained one component of galaxies and those that had at least two subclusters. The categorisation was done through an agglomerative clustering analysis of the clustering structure of each cluster galaxy population. An analysis of the kinematics of each cluster (from both categories) revealed that our galaxy samples for each cluster was in good agreement with published literature. It was found that the relationship between velocity dispersions of our samples and that of the published literature was linear with a scatter of 0.060 km/s (see section 2.4.3). The BCGs of two clusters, A0610 and A2255, were found to be divergent from those of the other clusters in the distribution of BCG peculiar velocities. The BCG of A0610 was found to have a peculiar velocity of $v_{pec,BCG} \simeq 1932$ km/s while that of A2255 was found to have $v_{pec,BCG} \simeq -1775$ km/s. The mean location of the sample BCG peculiar velocities was found to be -30 km/s. The two deviant clusters may have undergone major mergers where their BCGs were displaced

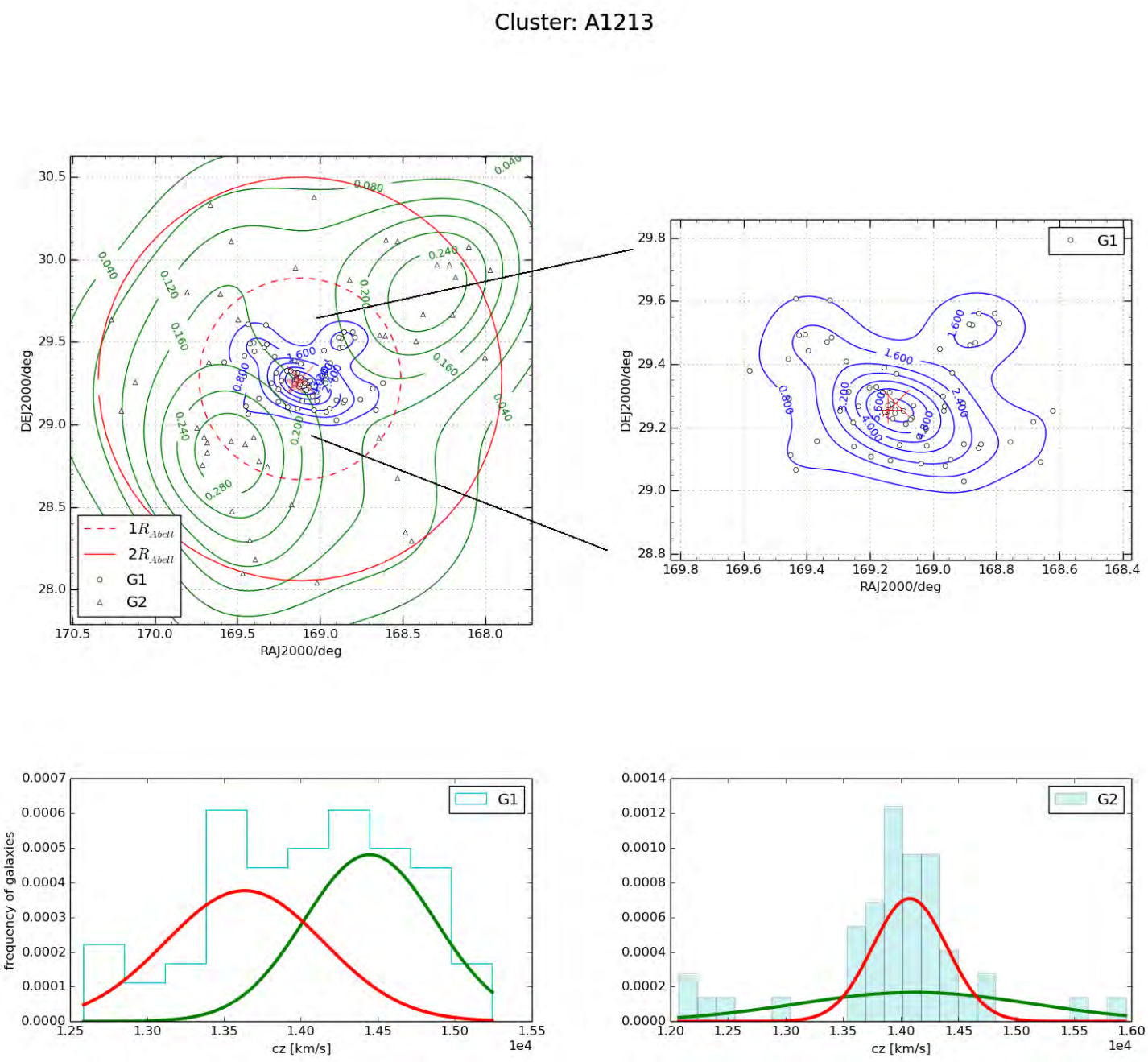

Figure 2.19: Substructure analysis in A1213. ***Top panels****: The on-sky distribution of A1213 galaxies with isodensity contours colour coded according to subcluster. The dashed and solid line red circles represent the 1 and 0.5 Abell radii regions, respectively.* ***Bottom panels****: The radial velocity distributions for each subcluster. Each distribution is fitted with atleast 2 normal distributions (red and green curves). The positions of the X-ray centroid/cluster centre (red cross) and the BCG (red "+") are shown in the top panels.*

from the bottom of the cluster potential well resulting in the very large peculiar motions (Hill & Oegerle 1993[114]).

An analysis on the substructures in the complex clusters revealed that these clusters have multimodal radial velocity distributions which suggests that they have been dynamically disturbed. This is expected from clusters which host radio halos and/or relics (Feretti et al. 2012[78]). It was found also that most of the subclusters in the complex clusters show evidence of internal substructures, for example: the NE subcluster of A0548 has been found to have 3 components whose velocity dispersions are comparable to some of the clusters in our main cluster sample. This is expected from massive rich clusters like A0548, and is observed in the complex clusters which are also rich clusters. The poor complex clusters, like A2048, tend to have a main subcluster and a group of a few galaxies either on the periphery falling into the cluster (e.g. A0610, see Figure 2.15), or in the central region of the cluster (in the case of A2048, see Figure 2.18).

Our substructure analysis suggests that localised regions of radial velocity substructures tend to also be associated with localised galaxy spatial over-densities and thus velocity structure indicates the presence of spatial structure as well (e.g Cortese et al. 2004[44]; Owers, Couch, & Nulsen 2009[179]).

Chapter 3

Multi-colour Analysis

In this chapter a multi-colour analysis is applied to analyse galaxy evolution. Different galaxy populations (blue and red cloud galaxies as well as green valley populations) are analysed.

3.1 K-corrections and Photometric Extinction

For a source observed at redshift zero and in photometric bandpass R (where apparent R-band magnitude is then m_R) but emitted at some redshift z in bandpass Q (with absolute magnitude in this Q-band being M_Q), the k-correction (K_{QR}) is defined by

$$m_R = M_Q + DM + K_{QR}, \tag{3.1}$$

where $DM = 5\log_{10}(D_L) - 5 = m - M$ is the distance modulus and D_L is the luminosity distance divided by 10 parsecs (with apparent magnitude m and absolute magnitude M). The rest frame apparent magnitude will then be given by

$$m_Q = m_R - K_{QR}. \tag{3.2}$$

For k-corrections in this work, we will use two methods, viz. the method of Chilingarian et al. (2010)[34] and Chilingarian & Zolotukhin (2012)[35] (henceforth C1012) that uses an analytical approach which approximates k-corrections as two-dimensional low order polynomials of two parameters: the redshift of the source galaxy and an observed colour of the galaxy. This method is used for ultra-violet (GALEX NUV and FUV), optical and the near infrared 2MASS K_s band photometry. The second method, applied to WISE photometry (Wright et al. 2010[252]), utilises SED template fitting (cf. Cluver et al. 2014[42]). A spectral energy distribution (SED) displays the distribution of emitted energy over wavelength/frequency. Four representative templates were used in the second case: that of an S0, an Sb, elliptical and a late-type galaxy (M51 a.k.a NGC 5194) (Brown et al. 2014[25]). All magnitudes reported on, henceforth, are k-corrected and colours are derived from k-corrected magnitudes.

Another effect that alters observed magnitudes is extinction. This process removes photons from our line of sight

and so tends to dim the observed emission. In the cases of extragalactic sources that are themselves complex galactic systems forming parts of galaxy clusters, extinction is due to the internal ISM of the galaxies (varies with morphology, see e.g. Nagayama et al. 2004[172], Riad et al. 2010[199]), any inter-galactic material between the individual galaxies and the Milky Way and also our own galaxy's internal ISM. Extinction is wavelength dependent being largest in UV-optical photometry and lowest at the longer wavelengths of IR and radio photometry. It also depends on inclinations of galaxies that are emitting the light we observe. This complex effect is not quantitatively accounted for in this work, however, an analysis of the foreground extinction for A3667 galaxy colours is attempted.

The foreground extinction in passband a is approximated by

$$A(a) = R(a)E(B-V), \tag{3.3}$$

where $R(a)$ is the a-band extinction coefficient relative to $E(B-V) = A(V)/R_V$ ($R_V = 3.1$ from the Fitzpatrick 1999[80] reddening law). The colour access/reddening for a given colour $(a-b)$ is then determined approximately by

$$E(a-b) = R(a-b)E(B-V), \tag{3.4}$$

where $R(a-b) = R(a) - R(b)$ is the reddening coefficient in the $(a-b)$ colour relative to $E(B-V)$. Yuan et al. (2013)[254] derived observed model-free reddening coefficients for a range of colours covering observations from the far-UV (GALEX FUV) to the mid-IR (WISE) – with $E(B-V)$ values from Schlegel et al. (1998)[213]. Table 3.1 summarises extinction and colour reddening coefficients from Yuan et al. (2013)[254] extended to some of the colours of A3667 that are analysed in this work. The most reddening occurs in the $NUV - r$ colour adding a systematic error of $\sim 20\%$. The cluster located nearest to the galactic disk was A2319 for which the $NUV - r$ colour had a reddening that would result in a systematic $\sim 40\%$ error. However, GALEX and SDSS data corresponding to the galaxies that we identified as A2319 cluster members was not available and so A3667 (second nearest to the galactic disk) is the worst case scenario with regard to foreground extinction in this work. These corrections are small and not consequential given the ranges of colours analysed and will not significantly affect the colour distributions of galaxies. Other physical phenomena, such as the inclinations of galaxies, can affect the extinction and thus lead one further into erroneous conclusions. These other contributions to the photometric extinction are ignored as well and may be the subject of future work.

Table 3.1: Extinction and colour reddening coefficients of Yuan et al. (2013)[254] extended to colours of A3667 and A2319. $A(V)_{A3667} = 0.130$ *mags,* $A(V)_{A2319} = 0.310$ *and* $E(B-V) = 0.042$ *mags (NED, Schlafly & Finkbeiner 2011[212]).*

Colour$(a-b)$	$R(a-b)$	$E(a-b)_{A3667}$ [mag]	$E(a-b)_{A2319}$ [mag]
$NUV - r$	4.930 ± 0.086	$0.207 \pm 4 \times 10^{-4}$	$0.493 \pm 9 \times 10^{-3}$
$u - r$	2.080 ± 0.050	$0.087 \pm 2 \times 10^{-3}$	$0.208 \pm 5 \times 10^{-3}$
$g - r$	0.990 ± 0.015	$0.042 \pm 6 \times 10^{-4}$	$0.099 \pm 2 \times 10^{-3}$
$W1 - W2$	0.026 ± 0.004	$0.001 \pm 2 \times 10^{-4}$	$0.003 \pm 4 \times 10^{-4}$

Chilingarian et al. (2010)[34] approximate k-corrections for optical and near-infrared observations of galaxies with redshifts $z < 0.5$. Their analytical approach is based on SED fitting of galaxies from SDSS data release (DR) 7 and

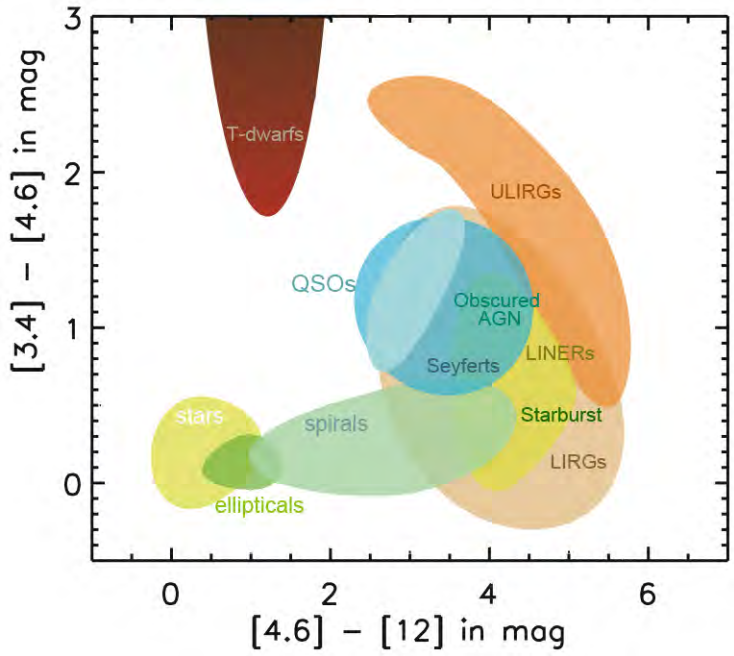

Figure 3.1: The WISE $(W1-W2)-(W2-W3)$ *color-color relation a.k.a WISE bubble plot of Wright et al. 2010[252] and Jarrett et al. 2011[120]. The effective wavelengths are 3.4, 4.6, and 12 microns for* $W1$, $W2$, *and* $W3$ *respectively. The magnitudes are in the Vega photometric system.*

UKIRT infrared Deep Sky Survey DR 5. Chilingarian & Zolotukhin (2012)[35] have extended the analytical approach of Chilingarian et al. (2010)[34] to also include GALEX NUV and FUV photometry.

The k-correction method of C1012 does not include the WISE mid-infrared (MIR) photometric bands and so for this photometry, we used SED template fitting for each galaxy. The observed sources were divided into early-type, S0, Sb, and late-type/starforming galaxies by using the WISE $(W1-W2)-(W2-W3)$ color-color relation (Jarrett et al. 2011[120]) – Figure 3.1. The relation was first used to exclude AGN galaxies by selecting only sources with $(W1-W2) \leq 0.8$ Vega mags (Stern et al. 2012[226]; Cluver et al. 2014[42]). Starforming/late-type galaxies were selected by $(W2-W3) \geq 1.5$ Vega mags, S0 galaxies were identified as those with $(W2-W3) \in [1;1.5)$ Vega mags, early-types were those with $(W2-W3) \in [0.4;1.0)$ Vega mags and $(W2-W3) \in [2.0,3.0]$ Vega mags for Sb galaxies. The different regions of $(W1-W2)-(W2-W3)$ color-color space which are occupied by different galaxy morphologies are displayed in Figure 3.1. The best representative template is then selected according to the colour limits above and then the k-correction is applied. This method was iterated a few times for each galaxy.

3.2 Multi-colour Analysis

Different galaxy morphologies may be found at different locations within a cluster (e.g. morphology-density relation (Dressler 1980[56]). In this section we will analyse the photometrically identified morphologies in each cluster. The clusters are divided into three groups: those that host radio relics, those hosting halos and those hosting both.

3.2.1 UV-Optical relations

The bimodality of galaxy colours is a common characteristic of these objects and Strateva et al. (2001)[227] illustrate this behaviour on a sample of 147920 galaxies from one of the earlier releases of the Sload Digital Sky Survey (SDSS). They illustrate that the optical colour-colour relation between the colours $(g-r)$ and $(u-r)$ is significantly bimodal. They find that there is an optimal $(u-r)$ colour separation, between early-type galaxies (E, S0, and Sa) and late-type galaxies (Sb, Sc, and Irr), of $(u-r) = 2.22$ AB mag. They use this colour separator to define a "blue" sub-sample (late-type galaxies) for which $(u-r) < 2.22$ AB mag and a "red" sub-sample (early-type galaxies) for which $(u-r) \geq 2.22$ AB mag. The authors also illustrate a colour-magnitude relation (CMR) between the g-band magnitude and the $(u-r)$ colour for each of their two main sub-samples, red and blue, which supports their $(u-r)$ colour separator.

Colour-magnitude Relations

The colour $(u-r)$ selection of Strateva et al. (2001)[227] is applied to three cluster sub-samples in this work. The main cluster sample is broken into: (i) a sub-sample of relic host clusters (denoted as "Relic" in corresponding plots), (ii) that of halo hosting clusters (denoted as "Halo" in corresponding plots), (iii) and that of clusters which host a halo and atleast a single relic (denoted as "Halo+Relic(s)" in corresponding plots). The relic clusters are A1367, A0013, A2048, A2061, A2063, A3376 (double relic), A4038, A0548 (double relic), A0610, A0085 and A3667 (double relic). Halo clusters are A1213, A2319, A3562, A0399 and A0401. Halo+Relic(s) clusters are A1656 (Coma), A2255, A2256 and A0754. The photometry of cluster galaxies was investigated in three dimensions where the optical m_r v.s. $(g-r)$ colour-magnitude diagram (CMD) was combined with the $(u-r)$ colour. A least squares linear fit was then applied to the CMD to obtain the CMR of the cluster galaxies in the three sub-samples.

The relic galaxies display an optical CMR: $(g-r) = -0.087m_r + 2.216$ with a scatter $\sigma(g-r) = 0.017$ AB mag (Figure 3.2). The halo clusters are represented by A1213 galaxies as it was the only halo hosting cluster, in the VO[1], that had the photometry required. A1213 galaxies show a larger scatter in their optical CMR ($\sigma(g-r) = 0.024$ AB mag): $(g-r) = -0.050m_r + 1.580$ (Figure 3.3).The clusters which host a halo and a relic(s) are A1656 (Coma), A2255, and A2256. Their CMR was found to be $(g-r) = -0.136m_r + 3.022$ with a scatter of $\sigma(g-r) = 0.016$ AB mag (Figure 3.4).

The bluest (according to $(u-r)$ colour) galaxies are located below and far from the CMR while the reddest galaxies make up the majority of galaxies within 3σ of the CMR, as expected from optical CMDs of galaxies. The low scatter CMR ($\sigma(g-r) \sim 0.02$ mag) agrees with previous findings of $\sigma(g-r) \sim 0.04$ mag (e.g. Strateva et al. (2001)[227]).

Colour-colour Relations

UV-optical colour-colour and colour-colour-magnitude relations were also investigated. In this case we investigated the $(g-r, NUV-r, M_z)$ colour-colour-magnitude and the $(g-r, NUV-r)$ colour-colour diagrams. The $(g-r, NUV-r)$ is plotted with galaxies colour-coded according to M_z to illustrate the colour-colour relations of galaxies as a function of luminosity. The $(g-r, NUV-r)$ colour-colour distributions are analysed with our GMM algorithm to identify

[1]Using the Vizier database: http://vizier.u-strasbg.fr/viz-bin/VizieR

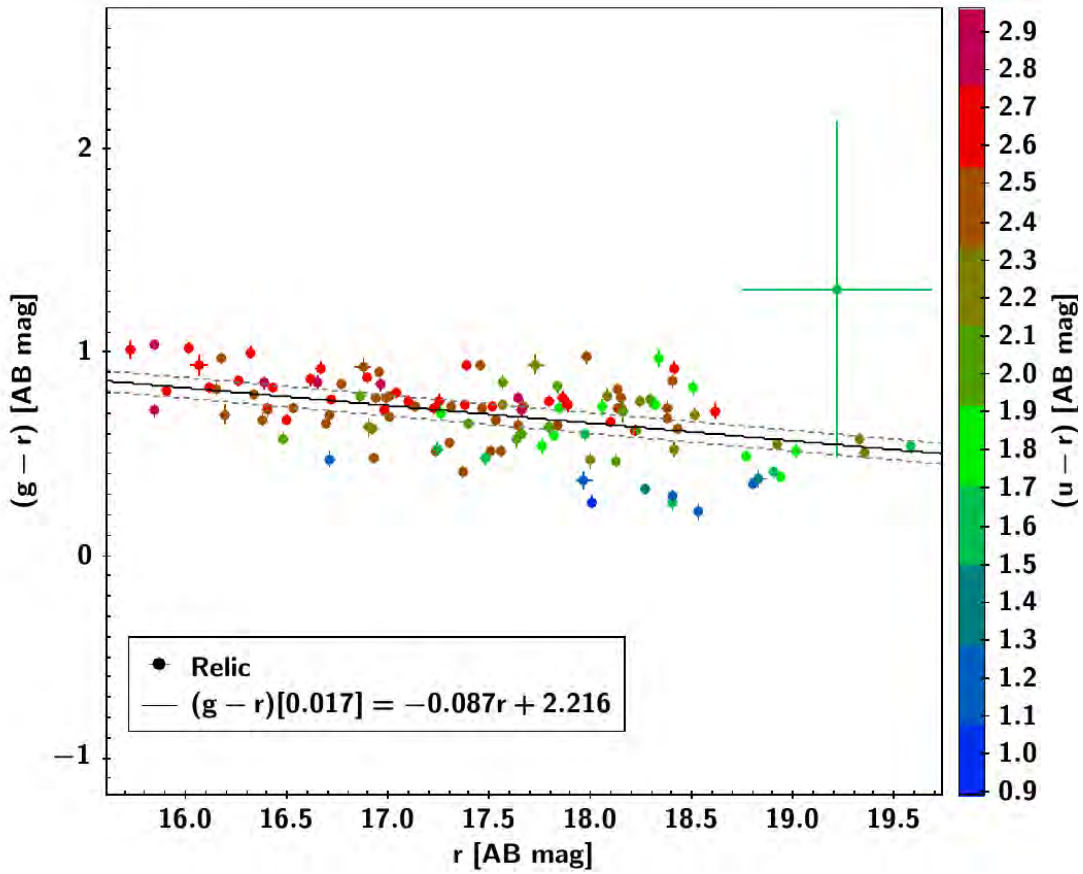

Figure 3.2: The optical m_r v.s. $(g-r)$ CMD colour-coded according to the $(u-r)$ colour for relic cluster galaxies. All colours are derived from k-corrected magnitudes. The black solid line represents the CMR: $(g-r) = -0.087m_r + 2.216$ with a scatter $\sigma(g-r) = 0.017$ AB mag. The two dashed lines represent the 3σ deviations from the CMR.

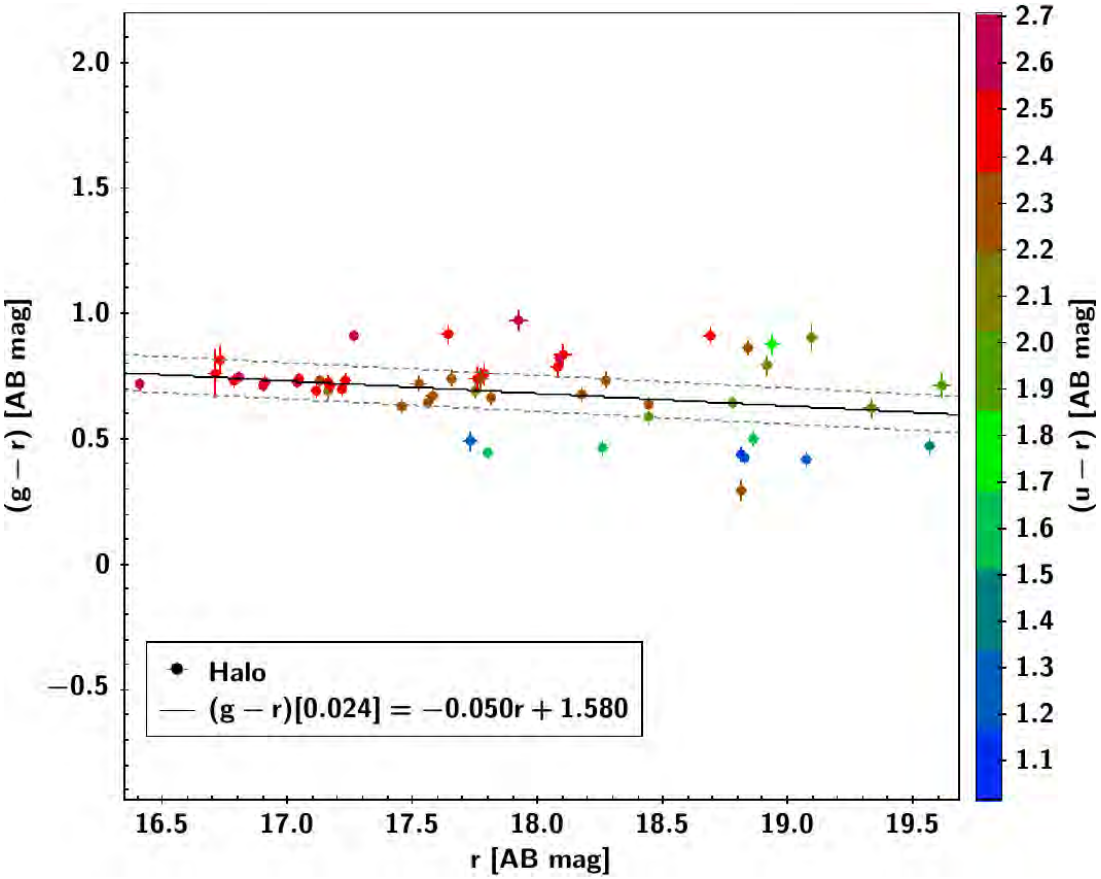

Figure 3.3: The optical m_r v.s. $(g-r)$ CMD colour-coded according to the $(u-r)$ colour for the A1213 halo cluster galaxies. All colours are derived from k-corrected magnitudes. The black solid line represents the CMR: $(g-r) = -0.050m_r + 1.580$ with a scatter $\sigma(g-r) = 0.024$ AB mag. The two dashed lines represent the 3σ deviations from the CMR.

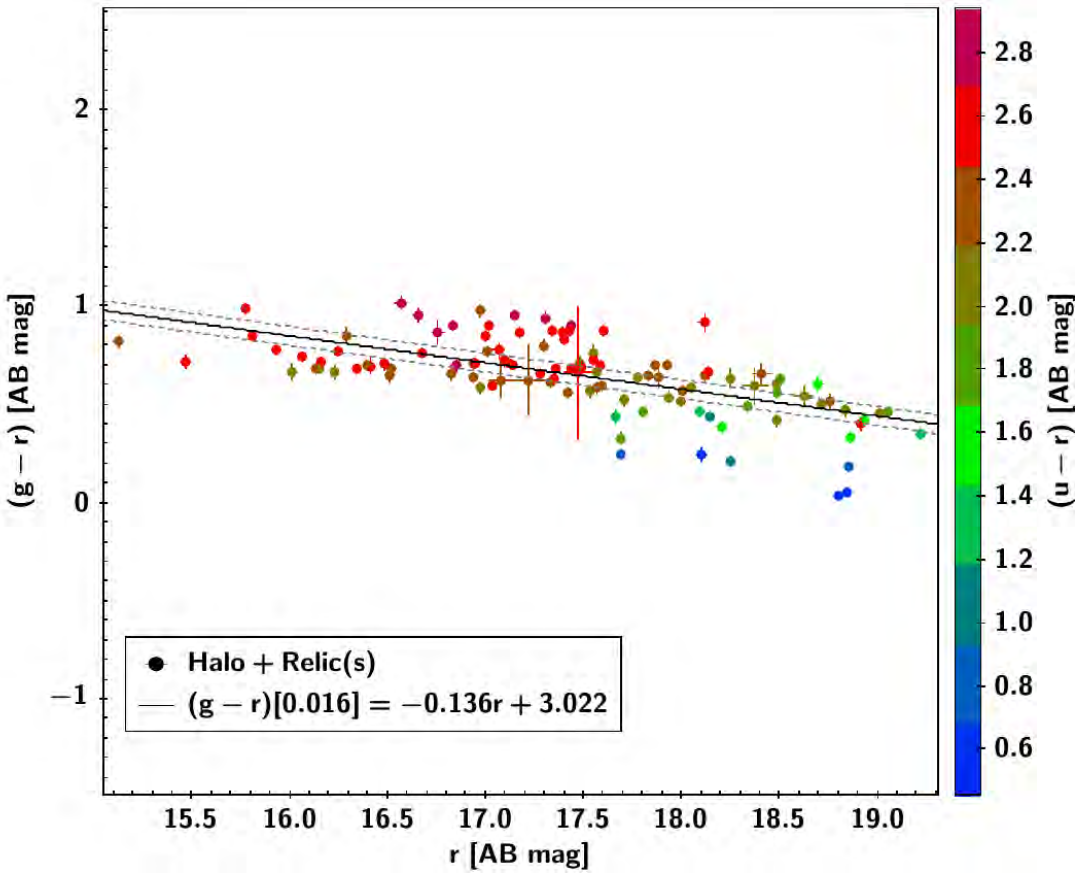

Figure 3.4: The optical m_r v.s. $(g-r)$ CMD colour-coded according to the $(u-r)$ colour of cluster galaxies from clusters which host a halo and atleast a relic. All colours are derived from k-corrected magnitudes. The black solid line represents the CMR: $(g-r) = -0.136m_r + 3.022$ with a scatter $\sigma(g-r) = 0.016$ AB mag. The two dashed lines represent the 3σ deviations from the CMR.

Table 3.2: Galaxy population parameters in $(NUV-r, g-r)$ colour-colour space. The colours are in units of AB magnitudes. A covariance of zero means that the GMM algorithm found no correlations between the two distribution components.

Subsample	component	$\overline{(g-r)}$	$\sigma^2(g-r)$	$\overline{(NUV-r)}$	$\sigma^2(NUV-r)$	$\sigma(NUV-r, g-r)$	Figure
Halo	1	0.728	< 0.001	3.995	0.268	-0.003	3.6
	2	0.679	0.028	1.886	2.818	0.151	
Relic+halo	1	0.683	0.025	3.679	0.867	0.081	3.7
	2	0.369	0.025	-0.372	0.867	0.081	
Relic	1	0.545	0.033	0.934	1.185	0.	3.5
	2	0.750	0.018	3.529	0.642	0.	

Col. 1: Cluster subsample according to whether a relic, halo or both are present in the cluster. Col. 2: GMM identified subsample colour-colour component (group of galaxies). Col. 3: mean $(g-r)$ colour. Col. 4: variance of $(g-r)$ colour. Col. 5: mean $(NUV-r)$ colour. Col. 6: variance of $(NUV-r)$ colour. Col. 7: $(NUV-r, g-r)$ colour-colour covariance. Col. 4: Figures illustrating the distributions.

present galaxy populations in colour-colour space, see Table 3.2 for a summary of the results.

The relic galaxy population (Figure 3.5) displays two distinct populations. There is a red cloud population, component 2 (see Table 3.2), with $\sigma(g-r) \sim 0.13$ mag, $\sigma(NUV-r) \sim 0.80$ mag, and no correlation between the two colours. A blue cloud population also exists, component 1, with $\sigma(g-r) \sim 0.18$ mag, $\sigma(NUV-r) \sim 1.09$ mag, and also no correlation between the two colours. There is a region of galaxies, reminiscent of the green valley, with colours intermediate between the red and blue clouds – the green valley region has been shown to be complex and made up of two galaxy populations on different evolutionary paths (Schawinski et al. 2014[211]). The green valley galaxies are displayed as large grey-black points on Figure 3.5 A. The colour-colour-magnitude diagram (CCMD) displays a clump of M_z bright galaxies (blue points in Figure 3.5 B) which are located in the vicinity of the red cloud, component 1. Mixed with these are galaxies of intermediate M_z brightness (in shades of green) which extends to to the green valley region and toward lower M_z brightness (and redder $(g-r)$ colours). Very few M_z bright galaxies occupy the region in the vicinity of the blue cloud component, while M_z faint ($M_z \gtrsim -18$ mag) and red cloud galaxies do make up a non-negligible fraction of the red cloud population. Chilingarian & Zolotukhin (2012)[35] found a narrower colour-colour-magnitude relation in the UV-optical $(NUV-r, g-r, M_z)$ diagram of galaxies, where they found that $\sigma(g-r) \sim 0.03-0.07$ mag for galaxies with $M_z \lesssim -17.5$ mag.

Clusters with both a halo and relic(s) have galaxies which also display bimodal UV-optical colours with the red and blue clouds showing similar distributions. In this case we found that $\sigma(g-r) \sim 0.16$ mag, $\sigma(NUV-r) \sim 0.93$ mag, and a positive color-colour correlation of 0.55. The correlation is computed from the covariances and variances of the colours via:

$$correlation = \frac{\sigma_{XY}}{\sigma_X \sigma_Y}, \tag{3.5}$$

for random variables X and Y, which are the colours $(NUV-r)$ and $(g-r)$ in our colour-colour analysis. The green valley, plotted in the same manner as in the case of relic cluster galaxies, is also present (see Figure 3.7).

Figure 3.7 B displays the blue cloud, red cloud, and green valley regions clearer that in the case of relic galaxies. The green valley is populated by both M_z faint and M_z bright galaxies which supports the findings of Schawinski et al. (2014)[211] who found that the green valley is composed of both late (M_z faint galaxies – whose dominant stellar

population is young massive stars) and early-type galaxies (M_z bright galaxies – whose dominant stellar population is old stars).

The halo cluster's galaxies have a narrow $(g-r)$ distribution ($\sigma(g-r) \sim 0.01$ mag) which is also M_z bright ($M_z \lesssim -20.4$ mag). These galaxies make up component 1 with $\sigma(NUV-r) \sim 0.52$ mag, and a negative color-colour correlation of -0.41. A bluer and broader component displays a positive colour-colour correlation of 0.54 with $\sigma(g-r) \sim 0.17$ mag and $\sigma(NUV-r) \sim 1.68$ mag. A large fraction of the red cloud in this cluster has large classification uncertainties and may be made up of green valley galaxies, see Figure 3.6.

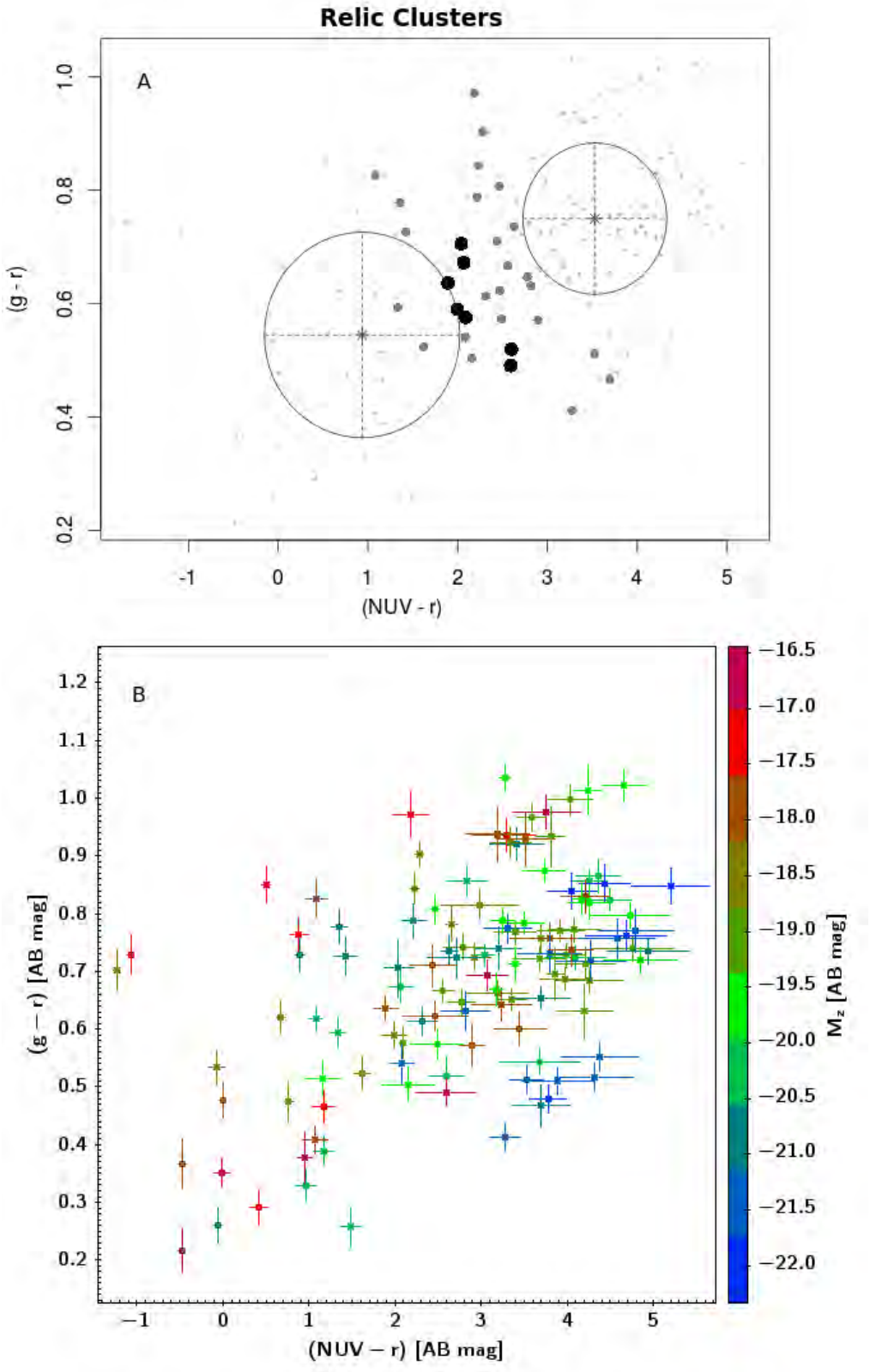

Figure 3.5: The UV-optical colour-colour (A/top panel) and CCMD (B/bottom panel) of relic cluster galaxies. ***Top panel****: Each component found by our GMM algorithm is indicated by an ellipse centred on the colour means ($\overline{(g-r)}$ and $\overline{(NUV-r)}$) with ellipse axes representing the covariances of each component. The size and grey-scale depth of each galaxy/point represents its classification uncertainty – the darker the point the more uncertain its classification as part of any component. Green valley galaxies are the large grey-black points in between the two ellipses.* ***Bottom panel****: The UV-optical CCMD where the $(g-r), (NUV-r)$ colour-colour relations are colour coded according to the z-band luminosity M_z.*

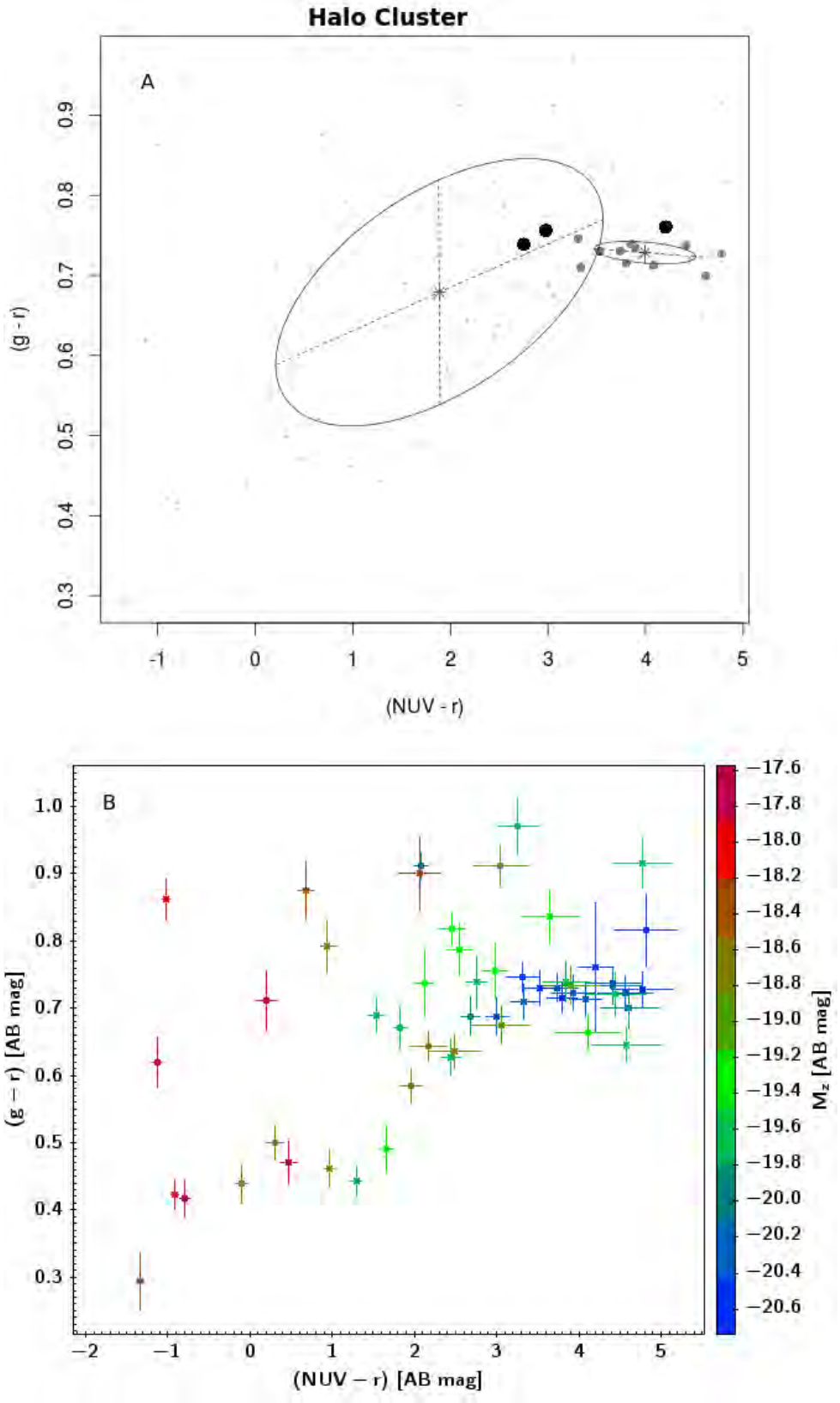

Figure 3.6: The UV-optical colour-colour (A/top panel) and CCMD (B/bottom panel) of the A1213 halo cluster galaxies. ***Top panel****: Each component found by our GMM algorithm is indicated by an ellipse centred on the colour means (* $\overline{(g-r)}$ *and* $\overline{(NUV-r)}$*) with ellipse axes representing the covariances of each component. The size and grey-scale depth of each galaxy/point represents its classification uncertainty – the darker the point the more uncertain its classification as part of any component.* ***Bottom panel****: The UV-optical CCMD where the* $(g-r), (NUV-r)$ *colour-colour relations are colour coded according to the z-band luminosity* M_z*.*

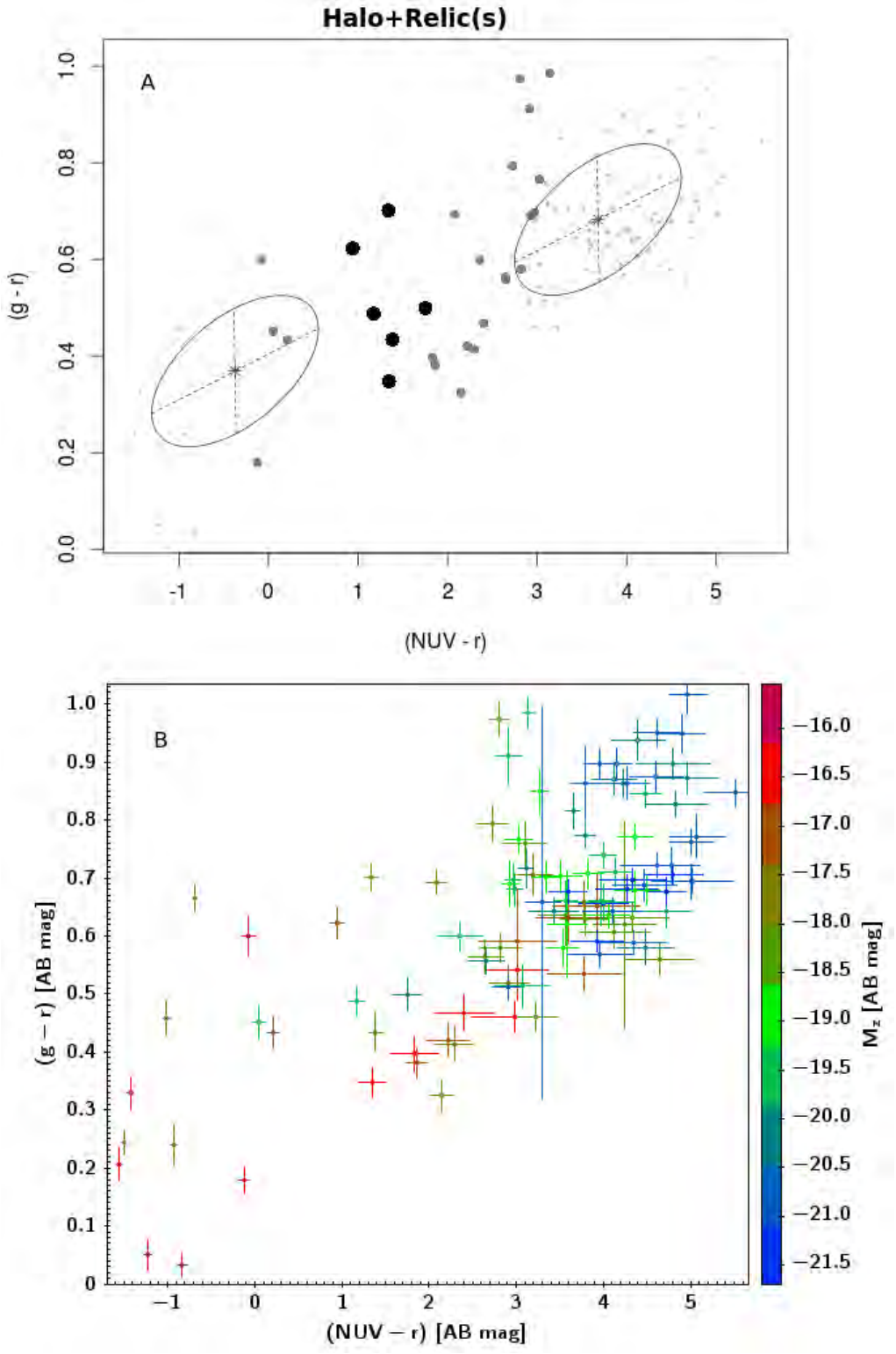

Figure 3.7: The UV-optical colour-colour (A/top panel) and CCMD (B/bottom panel) of cluster galaxies from clusters hosting a halo and relic(s). ***Top panel****: Each component found by our GMM algorithm is indicated by an ellipse centred on the colour means ($\overline{(g-r)}$ and $\overline{(NUV-r)}$) with ellipse axes representing the covariances of each component. The size and grey-scale depth of each galaxy/point represents its classification uncertainty – the darker the point the more uncertain its classification as part of any component. Green valley galaxies are the large grey-black points in between the two ellipses.* ***Bottom panel****: The UV-optical CCMD where the $(g-r), (NUV-r)$ colour-colour relations are colour coded according to the z-band luminosity M_z.*

Colours and morphologies

Chilingarian & Zolotukhin (2012)[35] found that the $(NUV - r)$ colour is linearly related to galaxy morphology via:

$$Type \simeq 6.6 - 1.1(NUV - r), \tag{3.6}$$

where $Type$ corresponds to the Hubble type viz.: < 0 for ellipticals, 1 for S0, 2 for Sa, 3 for Sb and > 4 for Sc and Irr morphologies. This colour-morphology relation is analysed as a function of galaxy location and $(u - r)$ colour for relic, halo, and halo+relic(s) hosting clusters.

Galaxies from clusters that host a halo and relic(s) have a compact red ($u-r \geqslant 2.22$ mag) population which largely corresponds to early-type spiral galaxies found within a projected radius of ~ 1.5 Mpc around cluster centres (Figure 3.8). A2256 galaxies display an approximately unimodal morphological distribution of early-type spirals located within the ~ 1.5 Mpc projected radius. The Coma cluster, on the other hand, displays a large population of peripheral[2] galaxies (within projected radii $\gtrsim 3.0$ Mpc) and central galaxies (within a projected radius of $\lesssim 1.0$ Mpc) with very blue ($u-r \lesssim 1.0$ mag) colours and late-type spiral morphologies. This blue galaxy population is unexpected from the morphology density relation (Dressler 1980[56]) – where the bluest galaxies are found at cluster peripheries while the reddest galaxies are located in central regions. This blue population will be investigated further in the sections that follow.

The halo cluster has a large fraction of red galaxies located within a projected radius of ~ 1.0 Mpc. These show a mixture of early to late-type spiral morphologies. A small proportion of red galaxies is located at large projected radii ($\gtrsim 4.0$ Mpc – the green to blue points located on the right of $u - r = 2.22$ mag in Figure 3.9). These galaxies are also found to span a large range of spiral morphologies from S0 to Sc and Irr galaxies according to the $(NUV - r)$ colour-morphology relation of Chilingarian & Zolotukhin (2012)[35] (equation 3.6). The blue region ($u - r < 2.22$ mag) is also populated by galaxies located in the cluster periphery ($\gtrsim 4.0$ Mpc) and central regions ($\lesssim 1.0$ Mpc) while also showing late-type morphologies.

[2]Peripheral regions, in this work, are those beyond an Abell radius which for Coma is ~ 2.1 Mpc.

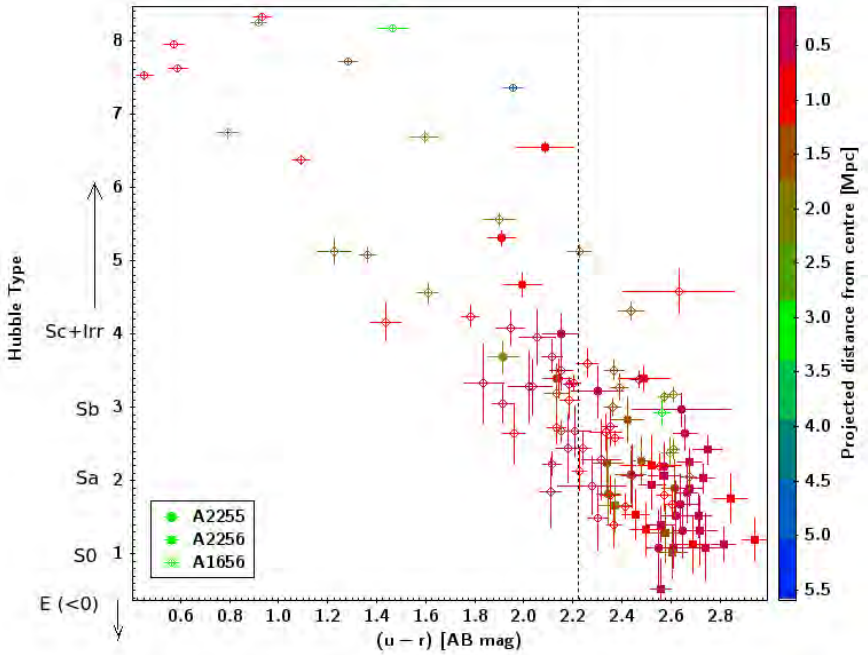

Figure 3.8: A comparison of the colour-morphology relations of Strateva et al. (2001)[227] and Chilingarian & Zolotukhin (2012)[35] for galaxies in clusters hosting a halo and at least one relic. Three clusters hosting a halo and relic are plotted with different symbols. The vertical dashed line represents the $(u-r)_{AB} = 2.22$ mag colour separation of Strateva et al. (2001)[227].

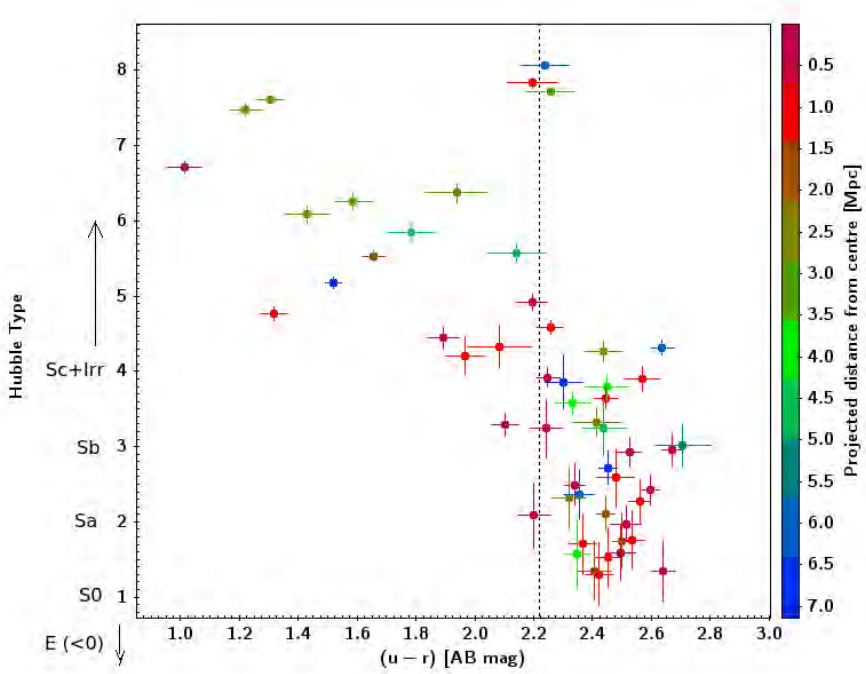

Figure 3.9: A comparison of the colour-morphology relations of Strateva et al. (2001)[227] and Chilingarian & Zolotukhin (2012)[35] for the halo cluster, A1213, galaxies. Three clusters hosting a halo and relic are plotted with different symbols. The vertical dashed line represents the $(u-r)_{AB} = 2.22$ mag colour separation of Strateva et al. (2001)[227].

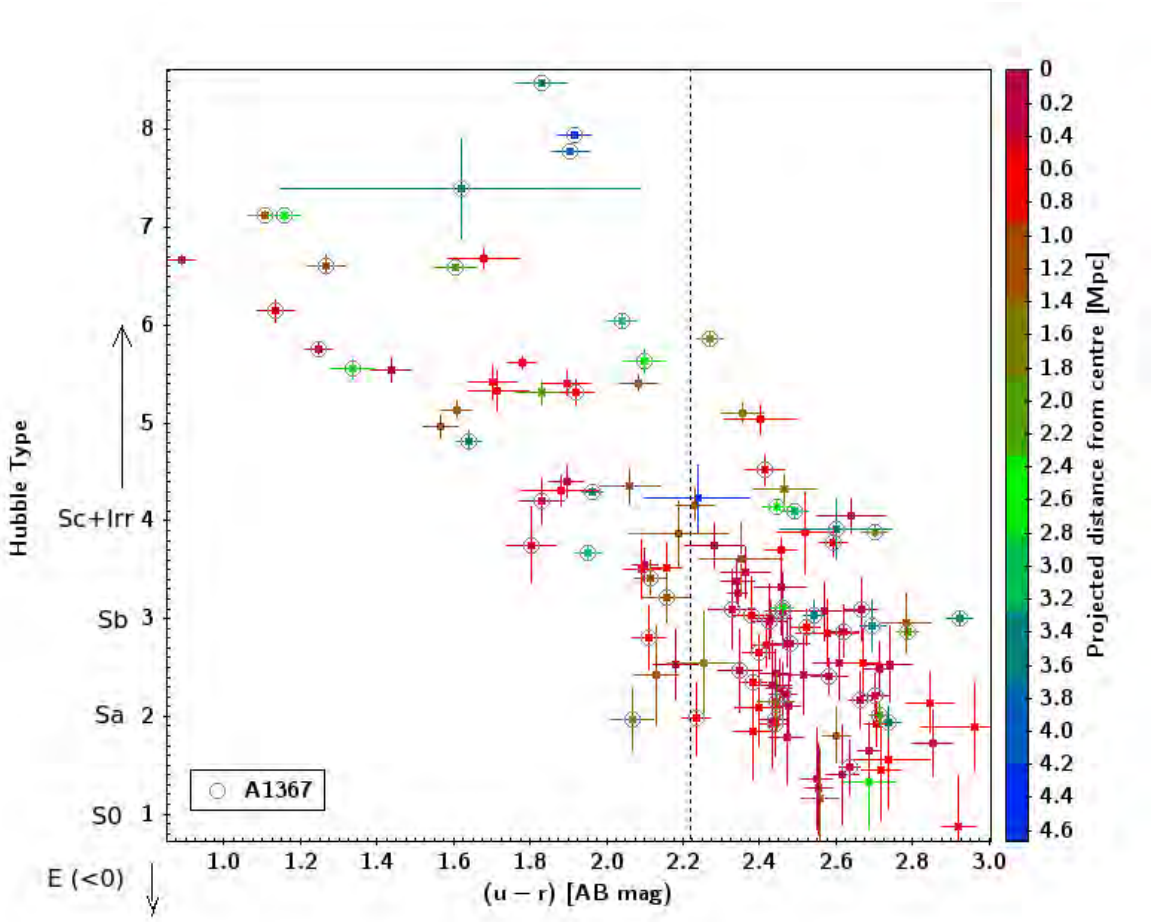

Figure 3.10: Colour-morphology relations of Strateva et al. (2001)[227] and Chilingarian & Zolotukhin (2012)[35] with galaxy location for relic cluster galaxies. The vertical dashed line represents the $(u-r)_{AB} = 2.22$ mag colour separation of Strateva et al. (2001)[227].

The relic galaxies show a large population of red galaxies in cluster central regions (projected radii $\lesssim 1.0$ Mpc) with early to late-type spiral morphologies. The region occupied by these galaxies also contains peripheral galaxies (projected radii $\gtrsim 2.5$ Mpc). A population of central and peripheral galaxies with very late-type morphologies and a broad blue $(u-r)$ colour distribution also exists. A1367 galaxies (open circles in Figure 3.10) make up a large fraction of these galaxies. This suggests that the dynamical properties of the cluster (e.g. Cortese et al. 2004[44]) may also lead to peculiarities in the cluster's galaxy evolution, not only from galaxy evolution in relaxed clusters but also from the evolution of galaxies in other relic clusters.

3.2.2 Relations in the Infrared

The infrared colour-morphology relations of galaxies as functions of galaxy location in a cluster are analysed in this section. The cluster sample is again divided into three main subsamples: relic, halo, and halo+relic(s) clusters. The infrared samples are further divided into resolved and unresolved sources. Unresolved sources are likely to be dwarf galaxies or AGN host galaxies (emission dominated by the galaxy nucleus). Resolved sources are photometrically more complex – their light emanates from both the central regions and also from diffuse regions which extend to the peripheries of galaxies.

A large fraction of cluster galaxies in the halo subsample have S0 to late-type WISE colours as can be seen in Figure 3.11. The early-type galaxy population (galaxies with $(W2-W3) < 1.0$ colours) in our halo clusters was found to be located near cluster centres, within projected radii $\lesssim 1.0$ Mpc. A very small fraction of these galaxies were, however, found to be at very large projected radii ($\gtrsim 4.0$ Mpc) placing them at the peripheries of clusters.

Galaxies with S0 colours were found to also mainly reside near cluster centres but also with a small fraction of peripheral galaxies. The locations of the late-type populations were found to have the largest variations. Galaxies in this population, that were located nearest the centres of clusters also displayed the largest spread in $(W2-W3)$ colours – spanning the entire colour range. Late-type galaxies found at projected radii in the range $\sim (2.5; 4.5)$ Mpc formed a more compact distribution of colours with a smaller fraction of these morphologies located at larger projected radii ($\gtrsim 5.5$ Mpc). The colour distributions of both resolved and unresolved galaxies were found to be similar but with resolved sources dominating the early-type colour regions. One resolved source, located near the central region (within projected radius $\lesssim 0.5$ Mpc), displaying AGN-like colours – above the $(W1-W2) = 0.8$ mag threshold separating AGN from non-AGN systems (Jarrett et al. 2011[120]; Stern et al. 2012[226]).

Resolved and unresolved relic cluster galaxies showed similar late-type galaxy colours. The early-type colour region was found to be dominated by resolved sources in a fashion similar to the case of halo cluster galaxies (Figures 3.12 and 3.11). Galaxies, in relic clusters, with early-type colours occupy a larger range of locations – ranging from projected distances of ~ 0.2 to ~ 3.2 Mpc from cluster centres. The galaxies in the S0 colour region, as specified in the above section, show a smaller spread in location with projected distances of ~ 0.2 to ~ 2.6 Mpc from cluster centres. Galaxies with late-type colours displayed the largest spread in colours, as in the case of halo cluster galaxies,

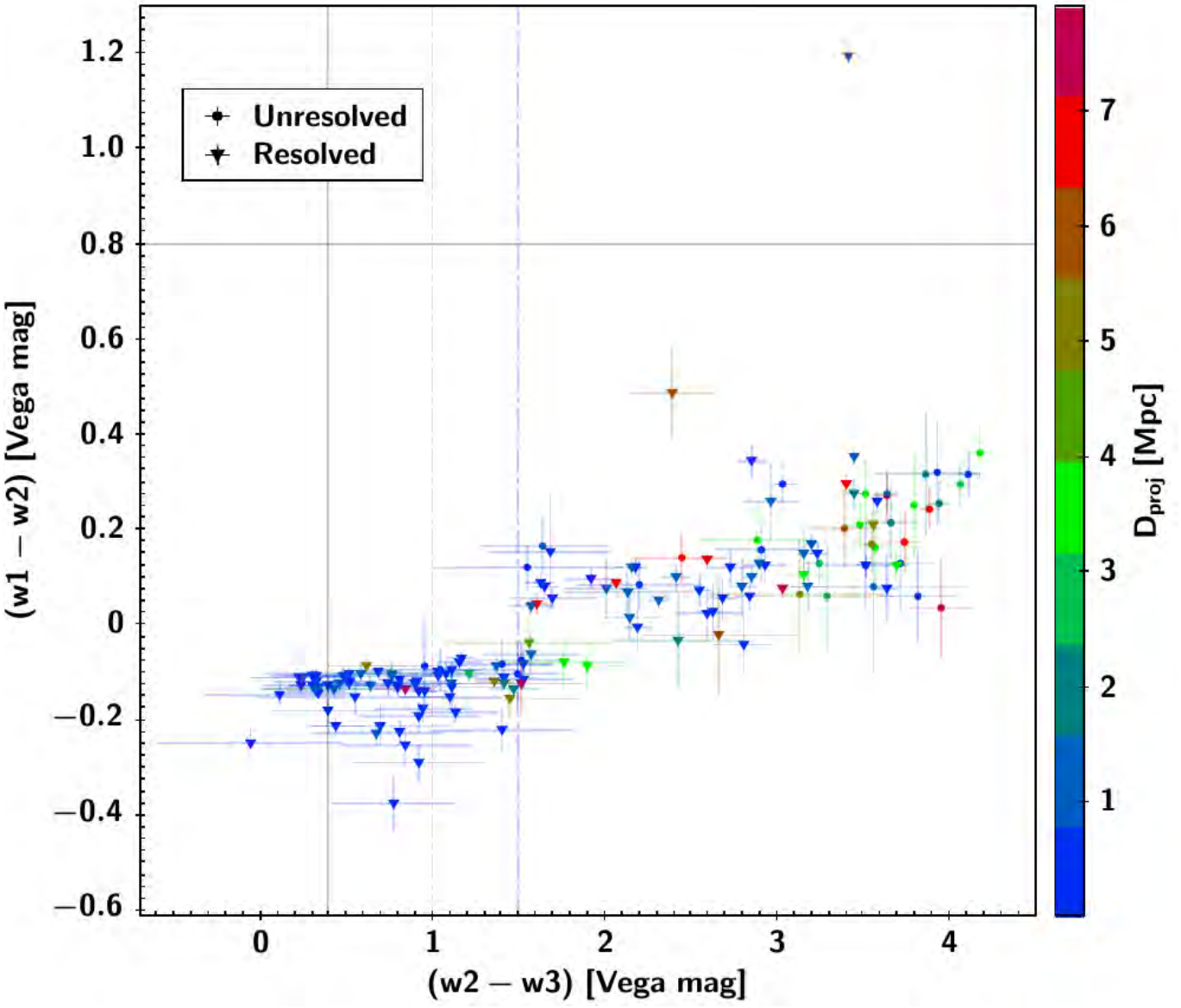

Figure 3.11: WISE $(W1-W2, W2-W3)$ *colour-colour plot of halo cluster galaxies. The vertical lines represent the* $(W2-W3)$ *colour-morphology thresh holds as inferred from Figure 3.1 viz.: early types (bounded within solid black and red dot dashed lines), S0 galaxies (bounded within red and blue dot dashed lines), and late types in the region from, and to the right, of the blue dot dashed line. The solid black line is the* $(W1-W2) = 0.8$ *mag threshold for non-AGN galaxies (Stern et al. 2012[226]).*

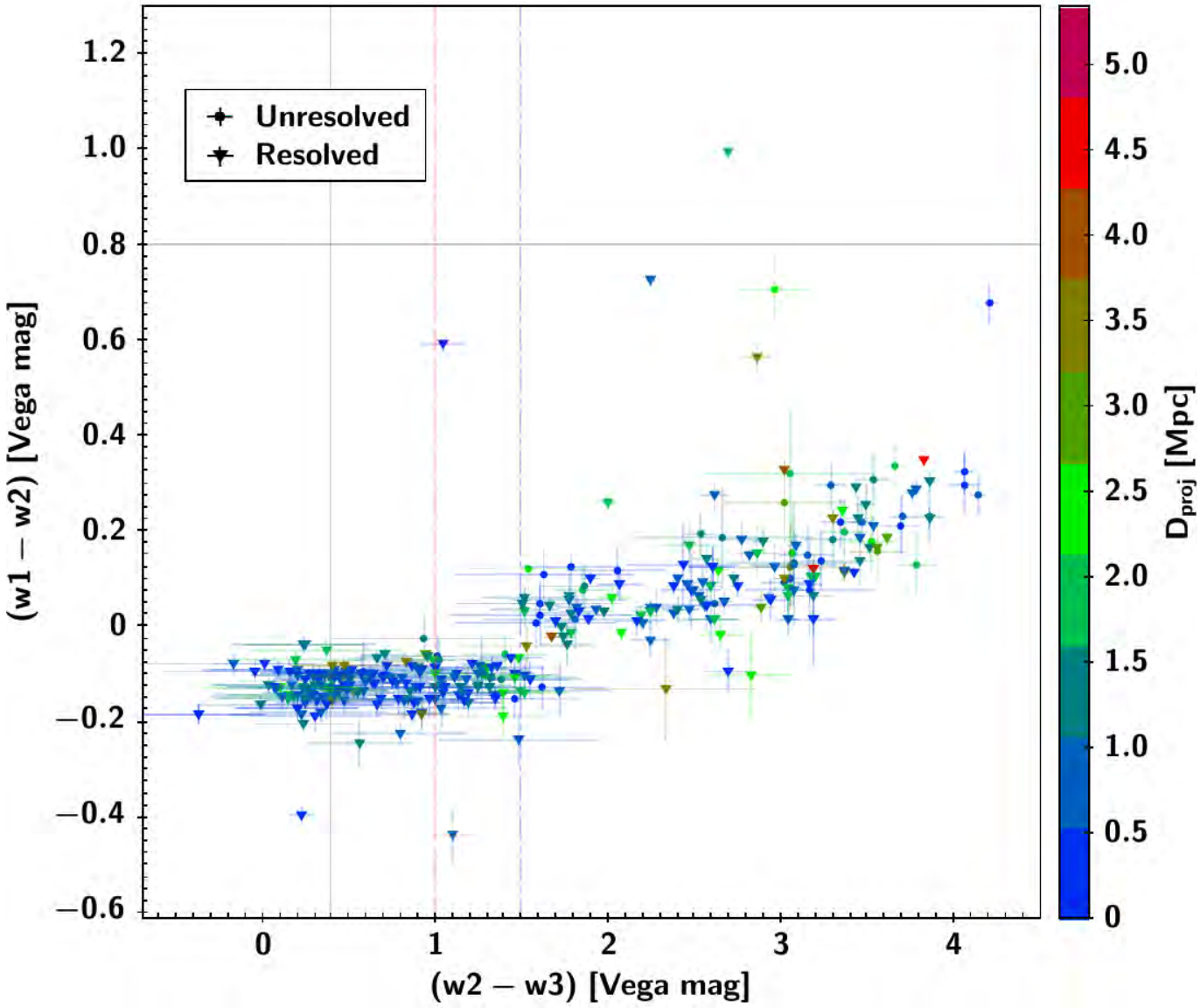

Figure 3.12: WISE $(W1-W2, W2-W3)$ *colour-colour plot of relic cluster galaxies. The vertical lines represent the* $(W2-W3)$ *colour-morphology thresh holds as inferred from Figure 3.1 viz.: early types (bounded within solid black and red dot dashed lines), S0 galaxies (bounded within red and blue dot dashed lines), and late types in the region from, and to the right, of the blue dot dashed line. The solid black line is the* $(W1-W2) = 0.8$ *mag threshold for non-AGN galaxies (Stern et al. 2012[226]).*

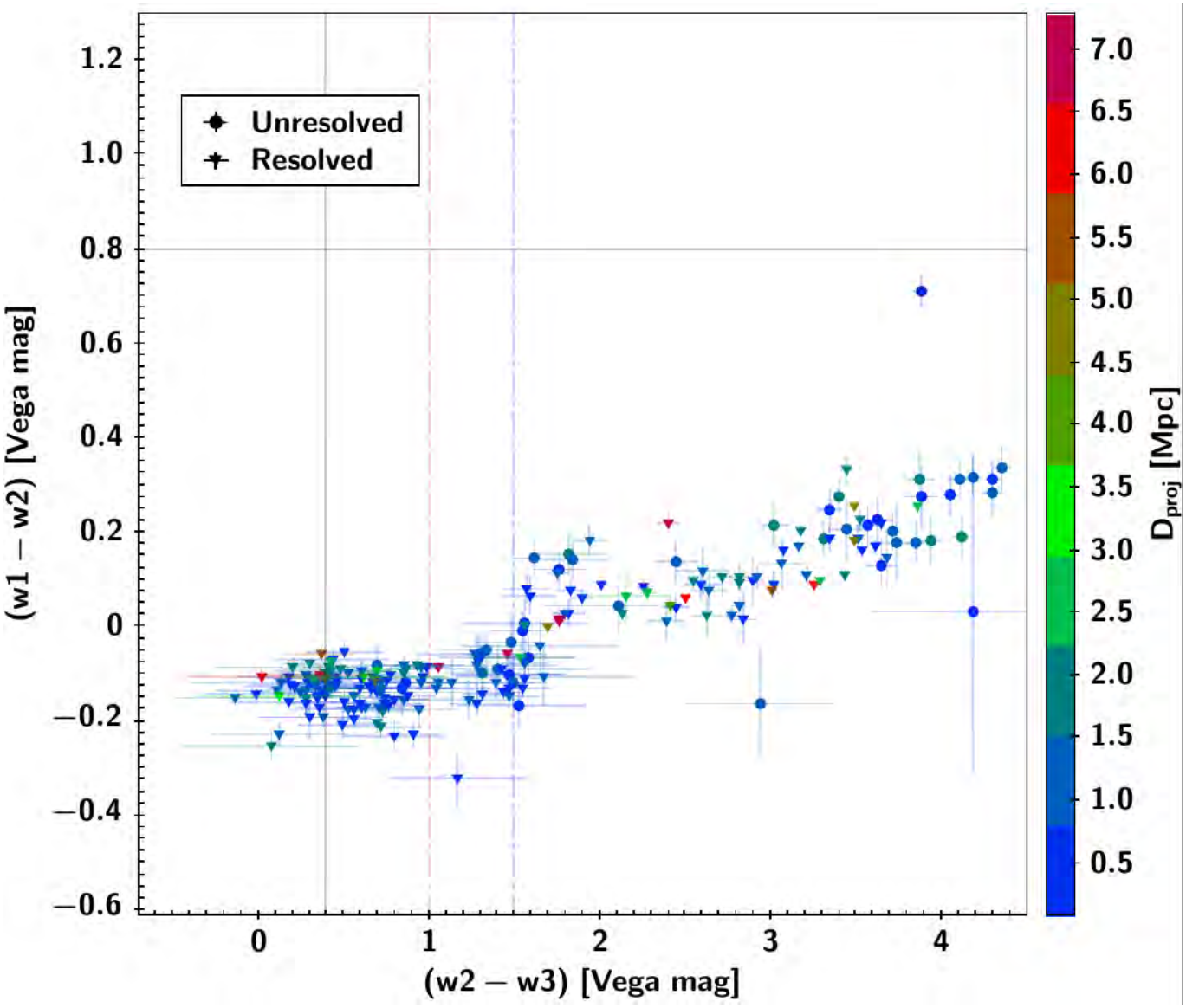

Figure 3.13: WISE $(W1-W2, W2-W3)$ *colour-colour plot of halo+relic(s) cluster galaxies. The vertical lines represent the* $(W2-W3)$ *colour-morphology thresh holds as inferred from Figure 3.1 viz.: early types (bounded within solid black and red dot dashed lines), S0 galaxies (bounded within red and blue dot dashed lines), and late types in the region from, and to the right, of the blue dot dashed line.*

but these galaxies showed locations similar to those of the early-type galaxies. A very small fraction of these late-type galaxies was found to reside at large projected distances of $\gtrsim 4.0$ Mpc. A larger fraction (green points in Figure 3.12) was found to be located at projected distances ~ 2 Mpc, while the majority ($\sim 60\%$) of the late-type galaxies was found to reside within $\lesssim 1.8$ Mpc projected radii. One galaxy, located at projected distance ~ 2 Mpc, showed AGN colour behaviour.

The case of clusters hosting both a halo and relic(s) differs from the previous two. Galaxies in these clusters were found largely within projected radii of $\lesssim 2$ Mpc (blue points in Figure 3.13). Those with late-type colours displayed a larger spread in colours, similar to the two previous cluster subsamples. These late-type galaxies have a small population located in cluster peripheries (red points which have projected distances ~ 6 Mpc) just like in the case of relic clusters, but these clusters have a smaller population of late-types with projected distances ~ 2 Mpc (points in green). The galaxies with S0 and earlier colours also have small fractions of galaxies located beyond projected radii of ~ 2.5 Mpc. Our colour analysis on this cluster subsample did not reveal any galaxies with AGN-like colours.

3.3 Conclusion

K-corrections were applied to GALEX near-UV and far-UV, optical SDSS, near infrared 2MASS K_s, and WISE infrared photometry of relic and/or halo cluster galaxies. Two methods were used to this effect: the method of C1012[34][35] (applied to UV, optical and near infrared photometry) which is an analytical approach that approximates the k-corrections as low order polynomial functions of the redshift of the source and an observed colour of the source, and also the method of template SED fitting to observations – applied to WISE photometry. Three representative SEDs were used in the second k-correction: an early-type (elliptical galaxy), an S0 type, and a late-type (M51) template. Each galaxy was iteratively fitted with an SED selected by WISE $(W1-W2)$ and $(W2-W3)$ colour-colour-morphology relations of Jarrett et al. (2011)[120].

UV-optical and IR colour-magnitude relations (CMR), colour-colour relations, colour-colour-magnitude relations, and colour-morphology relations of the galaxy sample were then analysed. The optical m_r v.s. $(g-r)$ CMR was approximated by a linear least-squares fit for relic, halo, and halo+relic(s) cluster galaxies. The CMR was found to show the expected red sequence and blue cloud as is universally expected for non-AGN/"normal" galaxies (e.g. Strateva et al. 2001[227]). The CMRs of each of the three subsamples were found to have scatter $\sigma(g-r) \sim 0.02$ AB mag, in agreement with other optical CMRs which show a scatter of ~ 0.04 mag (e.g. Visvanathan & Sandage 1977[248]; Haines et al. 2006[110]). The optical CMRs of halo cluster galaxies may differ from that found in this work due to the low number statistics of our analysis on the representative halo cluster, A1213 – a poor cluster and the only halo hosting cluster in our sample to have the optical photometry used in this work.

A UV-optical $(NUV-r, g-r)$ colour-colour analysis was also performed on galaxies in the three cluster subsamples. Galaxy colour bimodality and the so called "green valley" were recovered for relic and halo+relic(s) cluster galaxies. The case of the halo clusters is ambiguous due to lack of data for galaxies in these systems for the cluster sample in this work. A1213 galaxies displayed a UV-optical colour-colour relation akin to the blue cloud but no unambiguous red cloud population was seen in our analysis.

A UV-optical colour-colour-magnitude analysis suggests a strong correlation between the $(NUV-r, g-r)$ colour-colour distribution and optical galaxy luminosity in the SDSS z band. Red cloud objects were found to have primarily bright z band luminosities, with the reverse being true for blue cloud objects. A considerable number of sources also showed colours and luminosities intermediate between the blue and red clouds. These objects encroached on both the limits of these two clouds (red and blue cloud limits as suggested by the classification/variance ellipses illustrated in Figures 3.5, 3.6, and 3.7). This observation supports the findings of Schawinski et al. (2014)[211] that the green valley is actually composed of two different galaxy populations. This green valley population may actually be more enhanced in halo and relic cluster galaxies.

The locations and morphologies of galaxies were analysed by using the $(NUV-r)$-morphology relation of Chilingarian & Zolotukhin (2012)[35] and the starformation-$(u-r)$ relation of Starteva et al. (2001)[227]. The $(u-r) = 2.22$

mag colour separator of Strateva et al. (2001) suggests that the least starforming (so called "red and dead" galaxies) are found at cluster centres, and that they also show much smaller variation in optical colours than their more actively starforming counterparts. These passive galaxies also correspond to the earliest morphologies, in support of the galaxy morphology-density relation (Dressler et a. 1980[56]). The Coma cluster and A1367, however, have been found to have significant galaxy populations with very blue $(u - r)$ colours, i.e. active starformers, but which also show morphologies later than Sc while still being located near cluster centres. These may be galaxies with enhanced starformation due to ram-pressure, at a phase before star formation is halted (by ram pressure stripping, strangulation or harassment), as they fall into massive cluster centres such as those found in rich clusters like Coma and A1367.

The resolved and unresolved galaxies showed similar WISE IR colours. These two subsambples were analysed in $(W1 - W2) - (W2 - W3)$ colour-colour space. Galaxies found within small projected radii, with S0 and earlier type colours (Figure 3.1), showed the least variation in terms of IR colours and projected distances from cluster centres. Small fractions of these galaxies were, however, to the contrary with regard to projected distances. These were found in cluster peripheries while they displayed early type colours. The galaxies classified as spirals and later types showed the largest spread in IR colours and projected distances from cluster centres. These galaxies spanned the central and peripheral regions approximately equally in the halo cluster. In the cases of relic and also halo+relic(s) clusters, these galaxies were confined to locations within projected radii of no more than ~ 3 Mpc – as opposed to $\gtrsim 3.5$ Mpc in the case of the halo cluster galaxies. An analysis on the star formation histories and their connections to the kinematics and positions of these galaxies will be performed in the next chapter.

Chapter 4

Star Fomation

In this chapter we study the evolution of galaxies by investigating their star formation rates. The star formation rate (current star formation activity) and galaxy stellar mass (star formation history) can be used to probe the rate at which galaxies convert their inter-stellar medium (ISM) into stars. This process evolves galaxies with time and is a critical metric for galaxy evolution (Jarrett et al. 2013[121]). The metric is the so-called specific star formation (sSFR) which is a ratio of the star formation rate to the stellar mass, thus a measurement of of the past-to-present star formation history.

4.1 Obscured Star Formation

The star formation rate (SFR) is roughly proportional to the galaxy infrared luminosity and we probe this physical property by approximating SFR lower bounds through the use of WISE $W3$ (12 micron) photometry – sensitive to ISM, molecular (polycyclic aromatic hydrocarbons (PAH)) and dust emission. A large proportion of the longer wavelength galaxy photometry from WISE originates from re-radiated stellar UV light that has been absorbed by dust. WISE $W4$ (22 micron) photometry is more sensitive to the dust continuum (Jarrett et al. 2013[121]) but this band has a much lower sensitivity compared to $W3$ and so only $W3$ photometry will be used to approximate the obscured present-day star formation instead. The UV radiation is emitted by massive young stars that are obscured from sight by the ISM and so galaxy SFR approximated using luminosities in longer WISE bands is representative of the obscured present-day star formation. A full multi-wavelength analysis would be the most complete but analysing only the $W3$-IR derived SFR may qualitatively expose underlying trends in galaxy SFR. Jarrett et al. (2013) found that the $W3$ emission of galaxies is related to the SFR in the following manner:

$$SFR_{W3}(\pm 0.28) = 4.91(\pm 0.39) \times 10^{-10} \nu_{W3} L_{W3}, \tag{4.1}$$

where ν_{W3} is the $W3$ effective central frequency and L_{W3} is the spectral luminosity density in the $W3$ band. SFR has units $M_{\odot}$/yr. The spectral luminosity is given by the flux density (f_{ν}) and luminosity distance (D_L) through

$$L_{\nu} = 4\pi D_L^2 f_{\nu}. \tag{4.2}$$

The luminosity densities, $\nu_{W3}L_{W3}$, are normalised by the bolometric solar luminosity $L_{\odot} = 3.839 \times 10^{26}$ Watts in this work – similar to the manner of Jarrett et al. (2013)[121]). All fluxes and luminosities are derived from k-corrected magnitudes. Magnitude errors are propagated to give errors of order 10% in $W3$ flux densities.

Total stellar masses are estimated from the WISE short wavelength bands, $W1$ and $W2$, by using the mass-to-light relation of Cluver et al. (2014)[42]. The stellar backbone of galaxies is made up of old stars (post star formation) which dominate WISE short wavelength galaxy emission and so can be considered sufficient to approximate the global galaxy stellar mass (Jarrett et al. 2013[121]). Cluver et al. (2014) found that the mass-to-light relation in both resolved and unresolved galaxies (with $z < 0.15$) can be represented by

$$\log\left(\frac{M_{\star}}{L_{W1}}\right) = -1.96(W1 - W2) - 0.03, \tag{4.3}$$

where $(W1 - W2)$ is the rest frame IR colour, $M_{\star}$ is the stellar mass, and L_{W1} is the $W1$ in-band luminosity. The in-band luminosity is the galaxy luminosity measured in a photometric band, relative to the solar luminosity in the same band. It is given by

$$L_{W1} = 10^{-0.4(W1_{abs} - W1_{\odot})}, \tag{4.4}$$

here $W1_{abs}$ is the galaxy absolute $W1$ magnitude and $W1_{\odot} = 3.24$ Vega mags is the solar equivalent.

The sSFR is then given by the ratio

$$sSFR_{W3} = \frac{SFR_{W3}}{M_{\star}}, \tag{4.5}$$

in units of $M_{\odot}$/yr per unit stellar mass (yr^{-1}). Passively evolving galaxies tend to have $sSFR \lesssim 10^{-11}$ yr^{-1} while actively evolving galaxies tend to have $sSFR \gtrsim 10^{-10}$ yr^{-1} at low redshifts (Jarrett et al. 2013[121]). A caveat of the above SFR and stellar mass relations is that they do not apply to AGN host galaxies thus any galaxies which displayed AGN-like IR colours are expected to have anomalous IR-SFR and stellar mass estimates.

4.1.1 Star Formation-morphology Relations

The general trend in the relation between WISE colours and sSFR followed that suggested by the colour-colour-morphology relation given in the WISE bubble plot ($(W1 - W2)$ v.s. $(W2 - W3)$ colour-colour diagram; Figure 4.1). Galaxies with early-type colours were found to have the lowest sSFR; $\sim 1 \times 10^{-13}$ yr^{-1}. Galaxies with S0-type colours displayed intermediate sSFR values; $\sim 1 \times 10^{-12}$ yr^{-1}, and galaxies with spiral-type colours were found to have the highest sSFR; $\sim 1 \times 10^{-11}$ to 1×10^{-9} yr^{-1} (Figures 4.1, 4.2 and 4.3). Relic and halo+relic(s) cluster galaxies, when excluding those with AGN-like colours, have been found to have the same range of sSFR 2×10^{-13} to 1×10^{-9} yr^{-1} while halo clusters showed a smaller range: sSFR $\lesssim 2 \times 10^{-10}$ to 5×10^{-9} yr^{-1}. Both relic and halo+relic(s) clusters have galaxies displaying IR colours in the region of starbursts $(W2 - W3) \sim 3.5 - 4.0$ mag and $(W1 - W2) \sim 0.1 - 0.7$ mag.

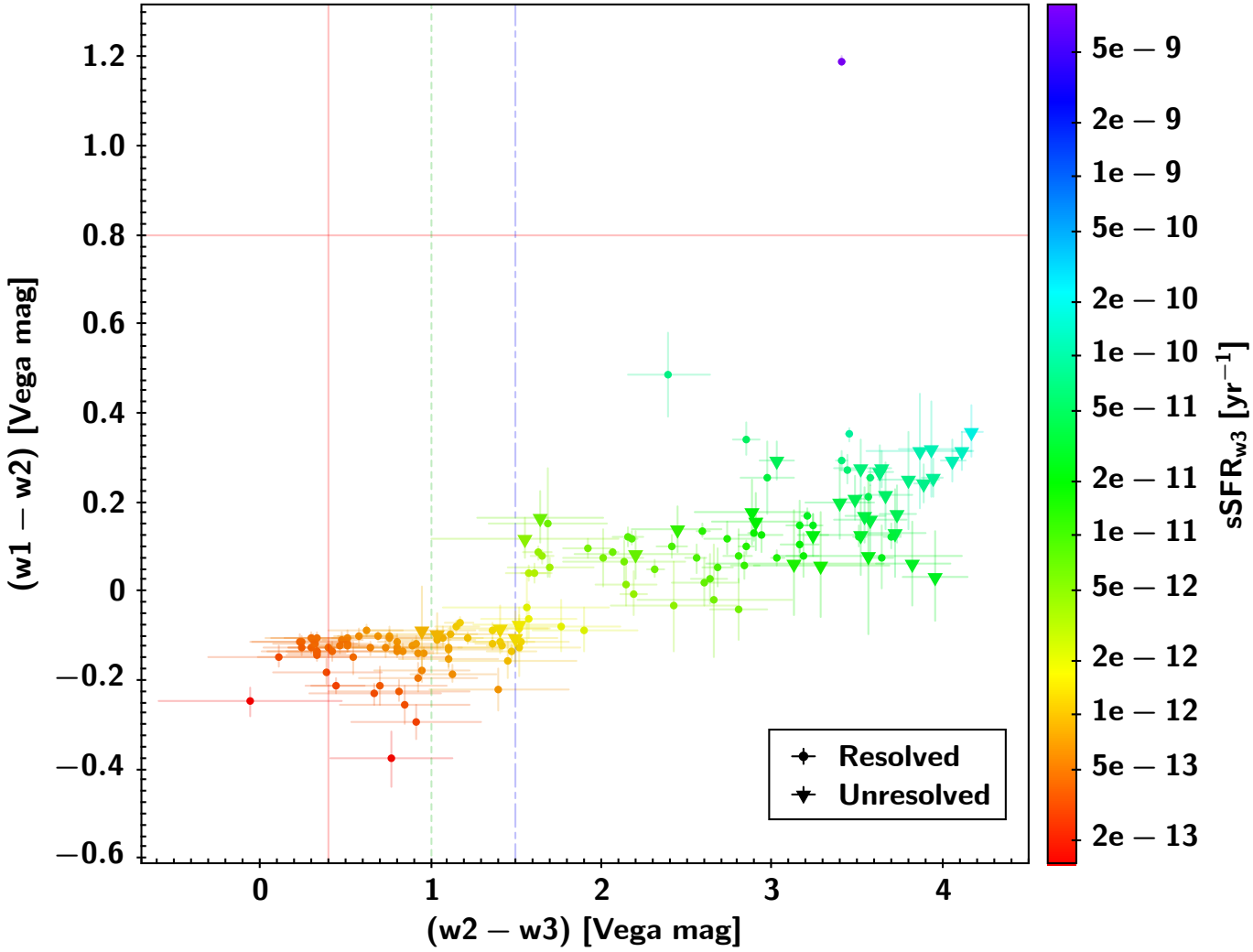

Figure 4.1: W3 IR specific star formation as a function of IR colours in halo clusters. The vertical dot dashed lines represent the $(W2 - W3)$ colour-morphology thresh holds as inferred from Figure 4.1 viz.: early types $(W2 - W3 < 1.0)$, S0 galaxies (bounded within green and blue dot dashed lines), and late types in the region from, and to the right, of the blue dot dashed line. The solid horizontal red line is the $(W1 - W2) = 0.8$ mag threshold for non-AGN galaxies (Stern et al. 2012[226]). Both resolved and unresolved sources are within projected distances < 8.0 Mpc from cluster centres.

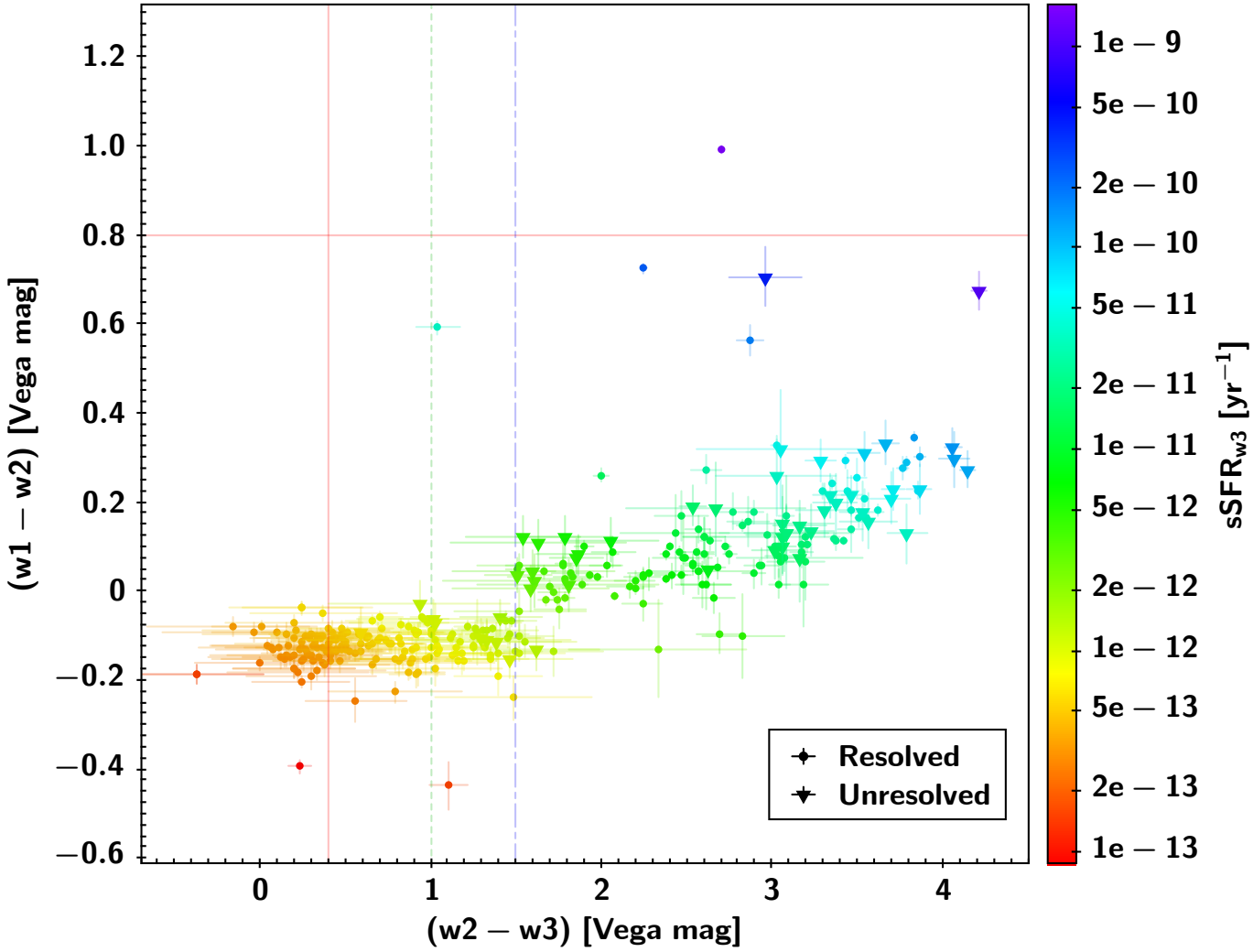

Figure 4.2: W3 IR specific star formation as a function of IR colours in relic clusters. The vertical dot dashed lines represent the $(W2-W3)$ colour-morphology thresh holds as inferred from Figure 4.1 viz.: early types $(W2-W3<1.0)$, S0 galaxies (bounded within green and blue dot dashed lines), and late types in the region from, and to the right, of the blue dot dashed line. The solid horizontal red line is the $(W1-W2)=0.8$ mag threshold for non-AGN galaxies (Stern et al. 2012[226]). Unresolved and resolved sources are within projected distances <3.4 and <5.4 Mpc, respectively, from cluster centres.

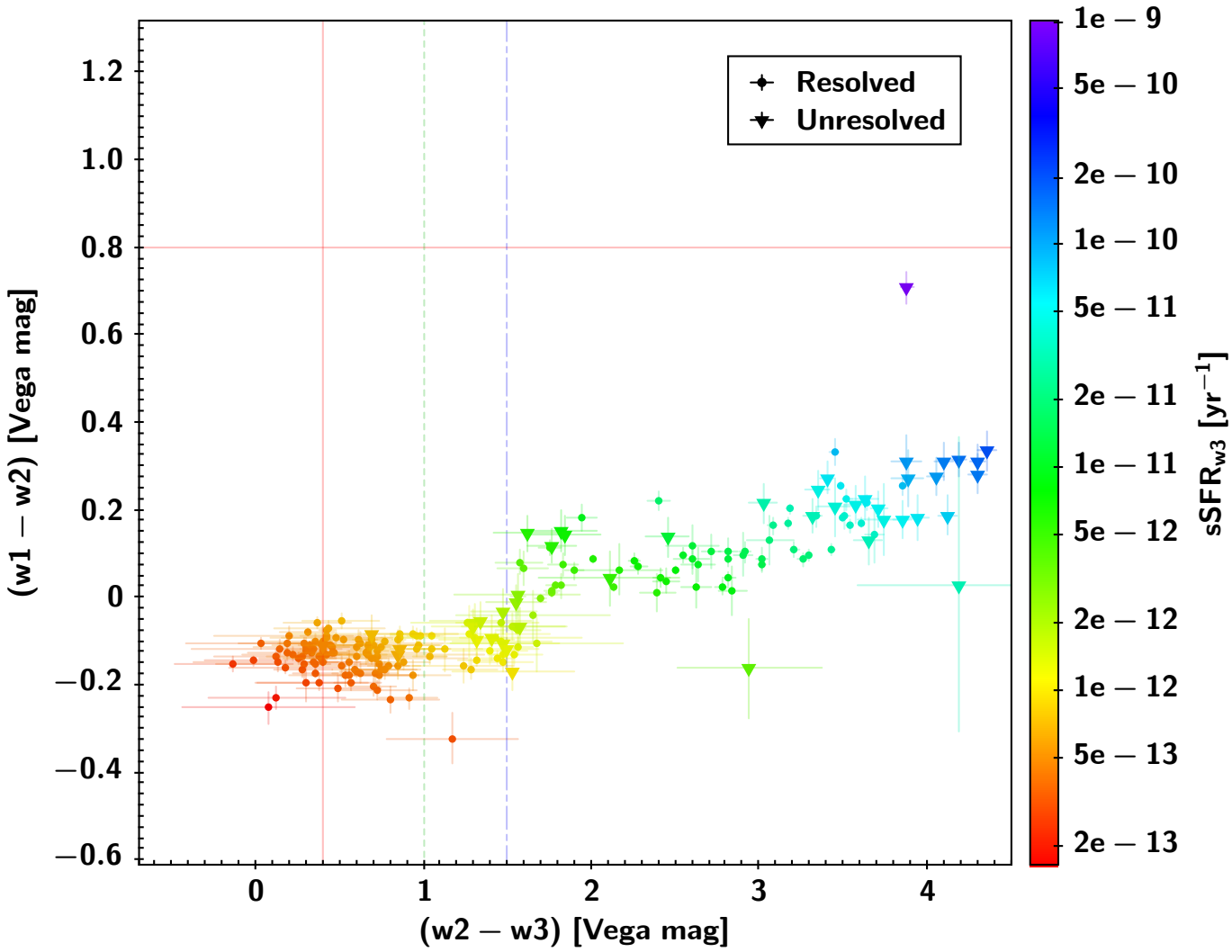

Figure 4.3: W3 IR specific star formation as a function of IR colours in halo+relic(s) clusters. The vertical dot dashed lines represent the $(W2-W3)$ colour-morphology thresh holds as inferred from Figure 4.1 viz.: early types $(W2-W3<1.0)$, S0 galaxies (bounded within green and blue dot dashed lines), and late types in the region from, and to the right, of the blue dot dashed line. The solid horizontal red line is the $(W1-W2)=0.8$ mag threshold for non-AGN galaxies (Stern et al. 2012[226]). Unresolved and resolved sources are within projected distances <2.3 and <7.3 Mpc, respectively, from cluster centres.

4.1.1.1 Outliers

The first set of outliers are AGN galaxies. In these cases the light detected is dominated by the central source and so does not carry information about the evolutionary state of the host galaxy. The SFR and sSFR calibrations used in this work do not apply to these sources. A resolved galaxy from the relic sub-sample displayed AGN-like IR colours: $(W1-W2) = 0.99 \pm 0.01$ and $(W2-W3) = 2.70 \pm 0.01$ Vega mag. This placed the galaxy in the colour region of quasi-stellar objects (QSOs), seyfert galaxies and luminous IR galaxies (LIRGs) (Figure 4.1). This galaxy is `2MASX J20150927-5710320` and it belongs to the cluster A3667. The galaxy is separated from the cluster centre by a projected distance $D_{proj} \simeq 1.8$ Mpc and radial velocity ~ 544 km/s. It is morphologically classified as an ED galaxy (Johnston-Hollit et al. 2008[125]). Our analysis found an IR sSFR $\sim 1 \times 10^{-9}$ yr^{-1}, among the highest in the relic cluster subsample, and a stellar mass $M_\star \sim 2 \times 10^9$ M$_\odot$. Another similar galaxy (`2MASX J11173714+2929447`) was found in the halo cluster subsample. This galaxy displayed IR colours similar to AGN hosts: $(W1-W2) = 1.19 \pm 0.01$ and $(W2-W3) = 3.41 \pm 0.01$ Vega mag. This placed the galaxy in the colour region of QSOs and seyfert galaxies. This galaxy is part of A1213 and is separated from the cluster centre by a projected distance $D_{proj} \simeq 1.1$ Mpc and radial velocity ~ 550 km/s. An IR sSFR $\sim 9 \times 10^{-9}$ yr^{-1} and a stellar mass $M_\star \sim 2 \times 10^8$ M$_\odot$ were found for this object. Both galaxies show obscured star formation rates and stellar masses that are uncharacteristic of their reported morphological types (giant ellipticals) – in direct contradiction with the majority of the galaxies in our three subsamples, asserting that the SFR and stellar mass relations used in this work do not apply to these objects. This evidence suggest that the two are truly AGN host galaxies where their light is dominated by the galaxy nucleus.

The AGN candidates found in this work, using galaxies with available WISE photometry, make up $\sim 0.3\%$ of entire galaxy sample. These AGN candidates form part of the halo cluster A1213 and the double relic source A3667 and neither of them are BCGs. The A3667 AGN candidate is located near the second brightest galaxy in the cluster and the A1213 AGN candidate is located within half an Abell radius of the cluster. Stern et al. (2012)[226] report ~ 62 AGN per square degree from their sample of 130 WISE extragalactic sources in the S-COSMOS field. These sources have redshifts $z \lesssim 3$ and $W2 \leq 15$ Vega mag. The SDSS quasar selection algorithm gives 13 quasars per square degree down to $i = 19.1$ AB mag for sources with $z \lesssim 3$ (Richards et al. 2002[200]). Given our selection criteria, we select galaxies within 1.22° around A1213 giving an area of ~ 4.7 square degrees and thus ~ 0.2 AGN per square degree. A similar analysis of the 2 Abell radii A3667 region (sample radius of $\sim 1.04^\circ$) gives ~ 0.3 AGN per square degree. The A1213 AGN candidate has $W2 \simeq 15.6$ Vega mag while the A3667 AGN candidate has $W2 \simeq 15.5$ Vega mag. Our fraction of AGN candidates is much less than the much deeper Stern et al. (2012)[226] approximation due to our much more conservative redshift limit of $z < 0.1$. We do not expect AGN to dominate our sample but such a small fraction we found may be the subject of future work.

Another set of outliers ($\sim 16\%$) are galaxies that were found to show IR colours which are similar to those of stars (Figures 4.1, 4.2 and 4.3, and also Figure 6.4 in Appendix C). These are the low sSFR galaxies with $(W2-W3) < 0.4$ Vega mag. A further analysis was performed on these (from all three subsamples) to investigate where they are located in their parent clusters in relation to their stellar masses (a metric for galaxy size) and star formation (Figure 4.4). Peculiar velocities are used to probe the radial separation between the galaxies and their parent cluster centres while projected distances (D_{proj}) are used to probe the on-sky/tangential separation. Each galaxy is represented by a data

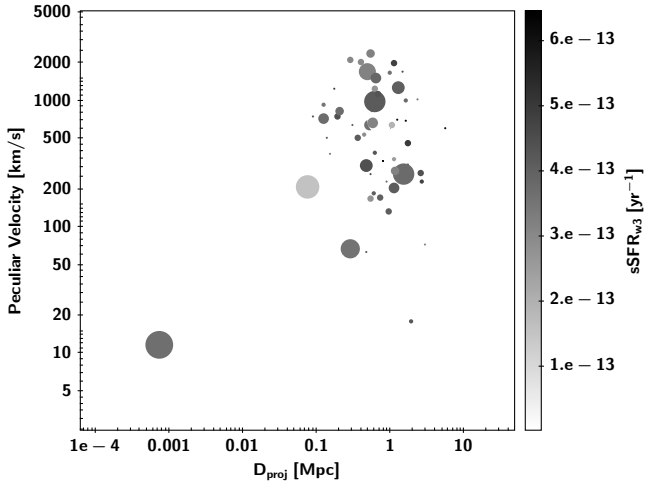

Figure 4.4: ***Left panel****: W3 IR specific star formation as a function of location and stellar mass for galaxies with IR colours similar to stars ($W2-W3<0.4$ Vega mag). Peculiar velocities are illustrated with respect to projected distances (D_{proj}), W3 derived sSFR (grey scale) and stellar mass (directly proportional to the size of data points).* ***Right panel****: The distribution of stellar masses of the entire sample of galaxies (red line histogram) and that of the non-AGN outlier subsample (those with colours $W2-W3<0.4$ Vega mag – shaded histogram).*

point that is colour-coded according to $W3$ derived sSFR and the data point size is directly proportional to galaxy stellar mass. Over $\sim 80\%$ of these galaxies are found within $D_{proj} \sim 1$ Mpc with peculiar velocities ranging from ~ 100 to ~ 2000 km/s which may indicate that their parent clusters are dynamically disturbed. This suggests that these galaxies are unlikely to have been falsely classified as cluster members according to the algorithm used in this work. A majority of these outliers (over $\sim 90\%$ of them) displays obscured $sSFR \sim 1 \times 10^{-13}$ yr^{-1} while the smaller fraction ($\lesssim 10\%$ of them) displays much lower star formation ($sSFR \sim 1 \times 10^{-15}$ yr^{-1}). This smaller fraction is made up of galaxies with significant stellar masses while the larger population has very few galaxies with stellar masses larger than that of the galaxy, from the smaller fraction, with the smallest stellar mass. Overall, the outlying galaxies are massive, with stellar masses $M_\star \sim 1 \times 10^{11}$ M$_\odot$ and the lowest sSFR among the entire galaxy sample, indicating that these may be massive E/S0 galaxies (e.g. Kannappan et al. 2009[130]).

Stellar contamination of galaxy light may have also played a role in the odd colours of the non-AGN outlier subsample. The WISE beam is large, so foreground stars in our own galaxy can land in the beam.

4.1.2 Evolution of Star Formation

The sSFR and its evolution with stellar mass is investigated in this section. These two physical galaxy properties are analysed according to: locations (projected distances) of cluster galaxies with respect to their parent cluster centre and also as functions of their parent cluster's redshift.

Figure 4.5 illustrates the $W3$ derived galaxy sSFR as a function of stellar mass and projected distance for each of our 3 cluster subsamples. A trend is apparent: galaxies of lower stellar masses are forming more stars per unit stellar mass than the most massive galaxies. This trend is consistent with field galaxies (those not gravitationally bound to any galaxy cluster) and is known as the "galaxy main sequence" (Noeske et al. 2011[174]). There also seems to be two populations of galaxies in sSFR-M$_\star$ space as displayed in the resolved galaxy sample: one that follows the general trend mentioned above, and another with sSFR values around ~ -13 dex – the lowest sSFR values. The lower sSFR

galaxies are found to reside within projected radii of $\lesssim 2$ Mpc with a majority within projected radii of $\lesssim 1$ Mpc (right panels if Figure 4.5). The fraction of galaxies which follows the general trend (steeper sSFR-M$_\star$ slope) are found at all projected distances with no clear relationship between sSFR and projected distance. This relation is displayed in Figures; 6.6, 6.7, 6.8, and 6.9 (in the appendix), which display the sSFR-location distributions for each cluster – the size of each point indicate its projected distance from its parent cluster centre and colours indicate redshift. A small fraction (10 galaxies making up $\lesssim 4\%$) of resolved relic cluster galaxies is found to follow the steeper sSFR-M$_\star$ relation well beyond the sSFR ~ -13 dex group. Galaxies in this fraction have sSFR values down to ~ -15 dex and are located within projected radii $\lesssim 1$ Mpc. Seven of these galaxies are also part of the outlier group with $(W2-W3) < 0.4$ Vega mag discussed above.

Figure 4.6 shows the sSFR-M$_\star$ relations with respect to cluster redshifts. Another clear trend is apparent in these distributions: clusters at higher redshifts tend to have steeper sSFR-M$_\star$ relations and so at a given stellar mass, galaxies at higher redshifts display higher sSFR values and hence more star formation activity. The low sSFR group (sSFR ~ -13 dex) is apparent at all redshifts, while the small fraction of galaxies with the lowest sSFR (sSFR ~ -15 dex) is found to form part of the cluster A0013 ($z \simeq 0.0943$), suggesting that this X-ray bright cluster ($L_X \sim 1.3 \times 10^{44}$ ergs/s – Böhringer et al. 2004[20]) is populated largely by massive early type galaxies that are passively evolving.

4.2 Conclusion

Galaxy star formation rates (SFR) were investigated in this chapter by probing the obscured SFR in cluster galaxies. The IR (WISE $W3$) derived star formation rate (Jarrett et al. 2013[121]), which represents molecular ISM obscured star formation, was used to probe the general trends of galaxy evolution in our galaxy sample. The majority of our cluster galaxies have $W3$ derived sSFR values that agree with the IR colour-morphology relations illustrated in the $(W1-W2; W2-W3)$ colour-colour diagram of Wright et al. 2010[252], Jarrett et al. (2011)[120] and Cluver et al. (2014)[42]: galaxies with early type colours have the lowest sSFR, those with early type spiral/S0 (regions of overlap between spiral and early type morphologies – Figure 4.1) colours have intermediate sSFR, and galaxies with spiral type colours display the highest sSFR.

There was a small fraction of galaxies with IR colours similar to those of AGN galaxies (QSOs, LIRGs and seyferts). AGN galaxy hosts tend to be mostly found in the green valley and are a possible cause of a transition phase in galaxy evolution from active evolution to quiescence (Pović et al. 2012[192]; Cluver et al. 2013[41]). AGN galaxies have been found to have morphologies ranging from early-type to late-types (Gabor et al. 2008[88]) and are expected to be present in galaxy cluster regions (e.g. Martini et al. 2007[161]). Another set of outliers, with IR colours that are similar to those of stars, was a considerable fraction of galaxies which displayed the lowest obscured sSFR values. These galaxies were found to also have high stellar masses ($M_\star \sim 1 \times 10^{11}$ M$_\odot$), peculiar velocities ~ 100 to ~ 2000 km/s and located within projected radii ~ 1 Mpc, suggesting that they may be passively evolving early type galaxies (E/S0 galaxies) as opposed to misclassified objects.

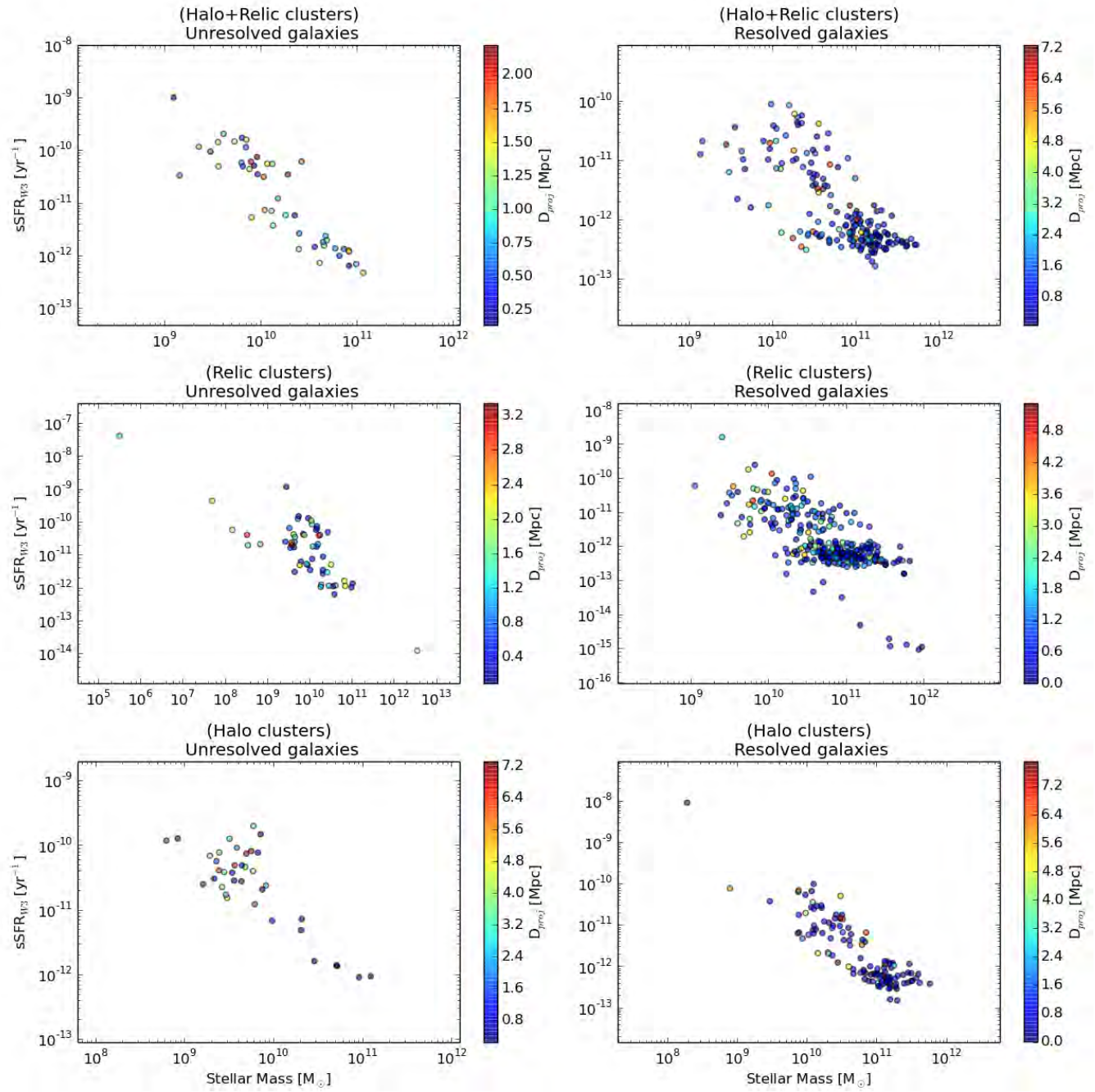

Figure 4.5: W3 IR specific star formation of unresolved (left) and resolved (right) galaxies as a function of galaxy stellar mass and location within the parent cluster. The galaxies are colour coded according to their projected distance (D_{proj}) from their parent cluster's centre.

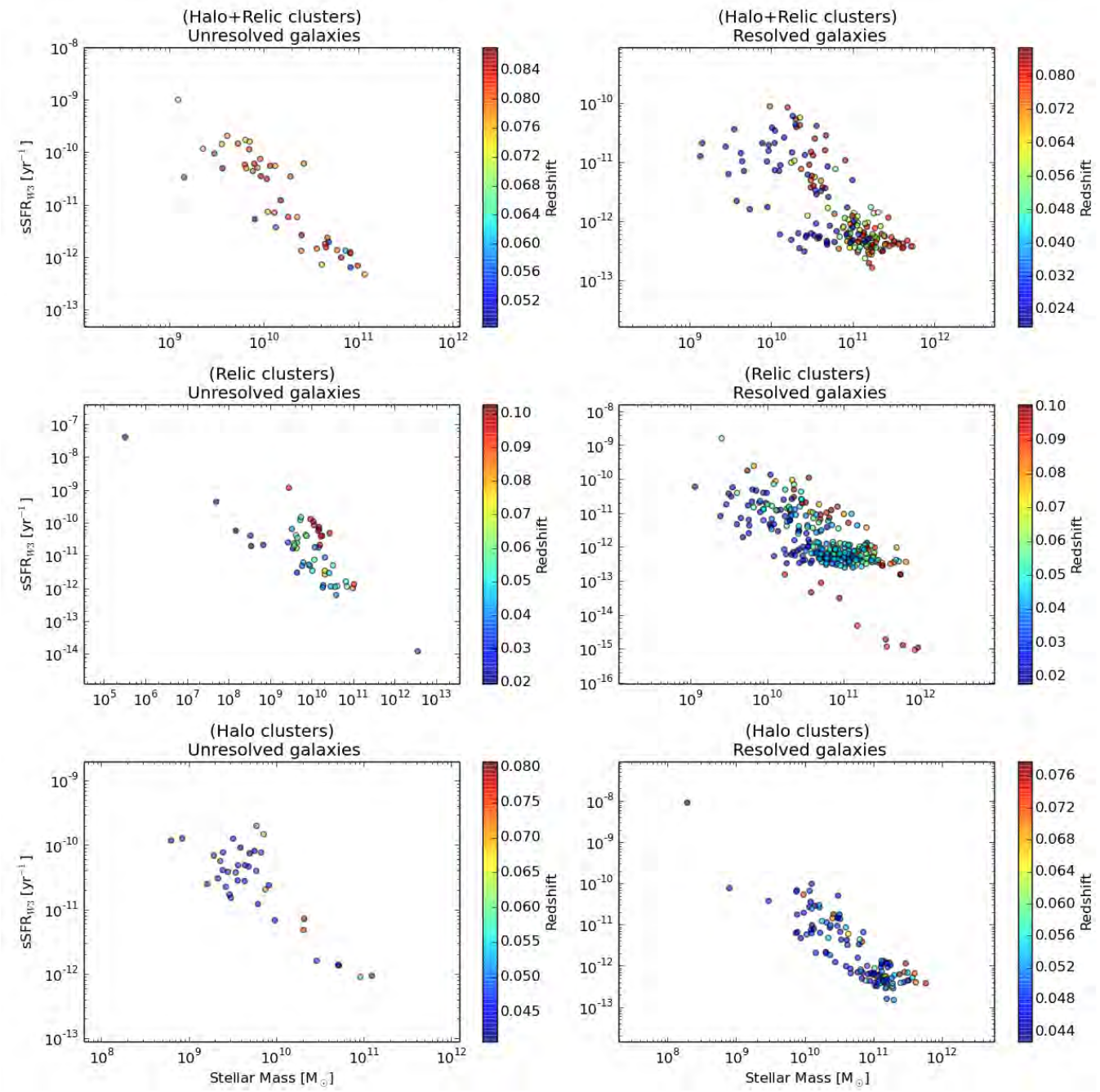

Figure 4.6: W3 IR specific star formation of unresolved (left) and resolved (right) galaxies as a function of galaxy stellar mass and redshift (colour coding) of the parent cluster.

The SFR of galaxies as a function of location within a cluster (on-sky separation) and also as a function of cluster redshift (cosmic evolution) were also investigated. Unresolved galaxies, most likely to be compact/dwarf/AGN galaxies, showed a decrease in sSFR with stellar mass. These galaxies displayed no significant relations between the sSFR and location in the parent cluster, however, the majority of low SFR galaxies were located near their parent cluster centres (within projected radii $\lesssim 0.6$). A more robust analysis of sSFR-location relations, which includes a radial depth (using redshifts), is illustrated in Figures 6.6, 6.7, 6.8, and 6.9 in the appendix. Our analysis also suggests that star formation rates were higher in the past (higher redshift) for a given stellar mass – in agreement with the notion of "cosmic downsizing" (e.g. Fontanot et al. 2009[82] and references therein).

Chapter 5

Summary and Conclusions

The aim of this thesis was two-fold: (i) to develop an algorithm for characterisation of galaxy cluster members in galaxy clusters that have a radio halo and/or radio relics; (ii) to understand the evolution of galaxy cluster members (galaxies) in these galaxy clusters. This chapter serves to summarise the work done, conclusions arrived at and suggestions for future work.

5.1 Discussion and Conclusions

Galaxy clusters are broadly grouped according to their physical properties such as the number densities of their member galaxies (richness – Abell 1958[1]; Zwicky 1961[258]) and the population of their central brightest galaxies (BCGs – Bautz & Morgan 1970[15]). Current formation paradigms are based on hierarchical structure formation under gravity in the early universe (Kravtsov & Borgani 2012[144]). The affects of gravity are important still, for the evolution of galaxy clusters on scales of galaxy-galaxy interactions and also on larger scales where cluster-cluster mergers occur and are thought to lead to radio relics and radio halos (Buote 2001[30]; Giovannini & Feretti 2002[97]; Ferrari et al. 2008[79]; Feretti et al. 2012[78]). The environment in which galaxies are found affects their evolution (e.g. Porter et al. 2008[191]) and we endeavour to probe galaxy evolution in relic and halo cluster environments.

Galaxy clusters that host radio relics and halos are a minority among galaxy clusters in general, with ~ 27 halo clusters, ~ 14 clusters with both a halo and/or relic(s) and ~ 25 relic clusters confirmed as of this report (Feretti et al. 2012[78]). The sample is slowly growing as new halos and relics are being discovered (e.g. Bonafede et al. 2012[21]; de Gasperin et al. 2014[51]; Lindner et al. 2014[152]). The sample used in this work consists of 20 galaxy clusters extracted from the halo and relic cluster collection of Feretti et al . (2012). Only clusters up to redshift $z \leqslant 0.1$ are selected for completeness. The sample consists of 5 halo clusters, 4 clusters with both a halo and/or relic(s) and 11 clusters that host radio relics. The virtual observatory (NED and SIMBAD) was then used to mine for galaxies contained within 5 Mpc of the cluster central coordinates as given in Feretti et al. (2012). SIMBAD uses a hierarchical clustering method to populate galaxy clusters and so galaxies that were identified as cluster members by SIMBAD and also satisfied our criteria, were selected as part of our sample of membership candidates for each of our sample clusters. Our cluster analysis algorithm was tested on a simulated sample of randomly generated and normally

distributed (unimodal) points in the region of each galaxy cluster, i.e. the mean RA, Dec and redshifts of each cluster were used to generate a mock cluster of similar parameters but with a unimodal normal distribution of *galaxy* positions.

Each galaxy in our mined sample has to be confidently characterised as a gravitationally bound member of a cluster before any further analysis. This was done in two main steps outlined as follows: (i) selecting only galaxies that were found within 2 Abell radii of each cluster and with radial velocities that were within 2000 km/s of the systematic radial velocity of the cluster (ii) selecting galaxies from step (i) that formed a normal distribution, within 95% ($\sim 2\sigma$) confidence, in radial velocity space. In the Abell catalog of rich clusters, the Abell radius is defined as a typical "radius" of a cluster in which at least 50 galaxies are found around the centre of the cluster (Abell 1958[1]). We extend this radius by doubling it so as to include galaxies residing in or falling in from cluster peripheries, e.g. the case of A1367 where a group of star forming galaxies are falling into the cluster from its periphery (Cortese et al. 2004[44]). Our choice of a radial velocity range, of $\pm$2000 km/s around the systematic radial/recessional velocity of galaxy clusters, is motivated by the findings of Merritt (1988)[166] for the case of the Coma cluster (A1656). A1656 has a velocity dispersion $\sigma_v \simeq 1008$ km/s (Chen et al. 1998[33]), making a width of 2000 km/s equivalent to $\sim 2\sigma$ in the radial velocity distribution for this cluster. Merritt (1988)[166] found that the observed radial velocity distribution and theoretical models for the Coma cluster (dynamic and rich cluster) galaxies displayed this "width" of 2000 km/s. The galaxies which satisfied the above criteria (steps (i) and (ii)) were then classified as cluster members i.e. galaxies gravitationally bound to the cluster.

Radio relic and halo sources are found in dynamic clusters that are often far from being virialised and so substructure in these clusters is expected. To probe this, we employed a Gaussian mixture model (GMM) algorithm, based on the `Mclust` and `cluster` packages of the `R` programming language, to characterise substructures in each galaxy cluster. Our GMM algorithm analysed the spatial and recessional velocity distributions of the galaxy clusters and used the Bayesian information criterion (BIC) to find substructures.

We compare our cluster members to the literature by computing velocity dispersions (σ_v) of each of our galaxy clusters and comparing this parameter to those in the literature. We use the bi-weight location and scale estimators in our analysis. The estimators have the advantage that they provide minimum variance estimations of location and scale in cases of non-Gaussian distributions (Tukey 1958[233]; Beers et al. 1990[16]). The estimators approach the mean and standard deviation for increasingly normal distributions. Different authors constrain cluster members differently and thus determine physical parameters, such as velocity dispersions, in various ways – e.g. Boschin et al. (2008)[22] use the adaptive-kernel method to characterise cluster membership (see e.g. Fadda et al. 1996[70]) and determine σ_v for A0610 and two other clusters by using the bi-weight location estimator. Owers et al. (2009)[179] also do the same for A3667 while the approach of Hernández-Fernández et al. (2012)[113] (on several clusters including the halo cluster A1213) combines visual inspections with a robust iterative analysis of spatial and radial velocity distributions. We have found that the velocity dispersions of our galaxy cluster samples agree with those in the literature in a linear manner: $\sigma_v = 0.410\sigma_{vlit} + 462.386$ km/s with a scatter of 0.060 km/s. However, our calculated velocity dispersions are underestimated for most clusters due to our radial velocity cut in the initial steps of our cluster member selection..

This validates our cluster member selection.

Agglomerative cluster analysis was also performed to quantitatively analyse levels of substructure in the galaxy populations in each cluster. We use the agglomerative coefficient (AC $\in [0.0; 1.0]$) to quantify substructure – AC $\rightarrow 1.0$ signifies increasingly significant substructure. We have found that the clusters in our sample all show significant substructure, with AC > 0.8 and increasing numbers of subclusters as AC $\rightarrow 1.0$. This is in agreement with what has been observed for relic and halo clusters: these systems tend to be dynamically disturbed (e.g. Ferreti et al. 2012[78]).

The BCGs of galaxy clusters are usually used as spatial reference points as they tend to be located at the bottom of gravitational potential wells of virialised clusters. Significant deviations from the mean radial velocity ($c\bar{z}$) of the parent cluster would suggest that the BCG has had a gravitational "tug" i.e. that the cluster has been dynamically disturbed (Hill & Oegerle 1993[114]). An analysis on the peculiar velocities of the BCGs of clusters in our sample reveals that 90% of cluster BCGs form a unimodal peculiar velocity distribution centred at $\overline{v}_{pec} \simeq -30$ km/s with a weak dependence on cluster mass (directly proportional to σ_v). The remaining 10% of BCGs, two BCGs (one belonging to the poor relic cluster A0610 and the other to A2255 – a rich cluster hosting a halo and relic), displayed large peculiar velocities (> 1700 km/s) suggesting a significant dynamical disturbance in the clusters. Boschin et al. (2008)[22] have found that A0610 is composed of up to three subclusters and also has two bright massive ellipticals (the BCG and a second brightest cluster member) associated with different A0610 subclusters. A2255 has also been found to be a spatially complex system (e.g. Yuan et al. 2003[255]; Sakelliou & Ponman 2006[206]; Pizzo et al. 2011[188]; Shim et al. 2011[217]). Our analysis of the clustering structure of all clusters in our sample, and our analysis of the kinematics of clusters that were found to be composed of subclusters (complex clusters) further supports and agrees with observations that relic and halo clusters are considerably disturbed (non-virialised).

With cluster and subcluster members selected for each galaxy cluster, we then moved to analyse galaxy evolution in our sample of clusters. Our multi-wavelength analysis employed ultra-violet GALEX, optical SDSS, and mid-IR WISE photometry. In this analysis we first apply k-corrections by using two methods because neither of the two methods could be extended to both ends the wavelength range probed (UV to mid-IR). Starting on the short wavelength side, we used the k-correction method of Chilingarian et al. (2010)[34] and Chilingarian & Zolotukhin (2012)[35] which provides k-corrections for UV, optical and near-IR (2MASS). The authors analytically approximated k-corrections as low order polynomial functions of redshift and an observed colour. The second method used was employed for k-corrections on WISE photometry. In this case SED fitting was performed for each galaxy using three main galaxy templates (early type, S0-type and late type templates). The WISE $(W1 - W2)$ v.s $(W2 - W3)$ colour-colour-morphology relation of Wright et al. (2010)[252] and Jarrett et al. (2011)[120] was used to iteratively select which template to fit which galaxy. This SED fitting method is a simplified version of that illustrated in Cluver et al. (2014)[42].

An analysis of the optical r versus $(g - r)$ CMD was performed to probe the optical colour-magnitude relations of galaxies in relic, halo and halo+relic(s) clusters. The red sequence and blue cloud were recovered for the galaxy distributions and a linear least-squares fit to the data resulted in scatter $\sigma(g - r) \sim 0.02$ AB mag

($\sigma(g-r) = 0.017$, $\sigma(g-r) = 0.024$, $\sigma(g-r) = 0.016$ AB mag for relic, halo and halo+relic(s) cluster galaxies, respectively). Several authors (e.g. Visvanathan & Sandage 1977[248]; Strateva et al. 2001[227]; Haines et al. 2006[110]) have found that normal/non-AGN galaxies have optical CMRs with scatter $\sigma(g-r) \sim 0.04$ AB mag, in agreement with the result found in this work. Our galaxy sample was much smaller (< 1000 galaxies) than the sample sizes used in the other works which may explain the factor of two difference in the CMR scatter. We also did not apply any foreground galactic extinction corrections and so the red sequence and blue cloud we found may have been enhanced or diminished accordingly. Foreground galactic extinction, although important, is small (of order ~ 0.1 mag for UV wavelengths, decreasing to less than ~ 0.02 mag for the SDSS z-band and to less than ~ 0.007 mag for the 2MASS K-band – Schlafly & Finkbeiner 2011[212]).

The UV-optical colour-colour distributions of galaxies was also analysed by using the colours $(NUV-r)$ and $(g-r)$. Relic cluster galaxies and those from clusters with both a halo and/or relic(s) showed the red and blue clouds along with the green valley. These populations were separated by applying the GMM algorithm on the colour-colour distributions. The halo cluster subsample of galaxies, from only one cluster A1213 (poor cluster), did not unambiguously show all three populations as in the cases of the relic and halo+relic(s) clusters. Galaxies with GALEX UV and SDSS optical photometry in the halo cluster subsample formed a very small sample of 53 galaxies and so our analysis on this subsample suffered most from small number statistics and is most likely not representative of halo cluster galaxies in general. A1213 is also peculiar in that its radio halo does not follow the X-ray-radio luminosity relation: the cluster has an X-ray luminosity that is lower than the trend given its radio halo power (Giovannini et al. 2009[95]; Feretti et al. 2012[78]), casting more doubt into whether its galaxies can be used to represent the halo cluster galaxy subsample. No conclusions can therefore be reached for halo cluster galaxies in this particular UV-optical colour-colour analysis.

Chilingarian & Zolotukhin (2012)[35] illustrated a universal UV-optical colour-colour-magnitude relation of galaxies. This relation is investigated for our sample of galaxies by analysing the $(NUV-r, g-r, M_z)$ colour-colour-magnitude diagram. Both the red and blue clouds were found with the red cloud objects found to have the brightest z-band luminosities. This supports the notion that the stellar populations of passively evolving galaxies are dominated by solar type stars (e.g. Nikolic 2005[7]). The green valley objects displayed colours that were similar to both red and blue cloud galaxies. Schawinski et al. (2014)[211] have shown that green valley galaxies are actually two different populations, that are on different evolutionary paths, rather than one transitional population of galaxies evolving from active star formation to a quiescent state.

Chilingarian & Zolotukhin (2012)[35] also found that there is a relation between the $(NUV-r)$ colour and galaxy morphology. Combining this relation with the $(u-r) = 2.22$ AB mag colour separator of Strateva et al. (2001)[227], we found that rich dynamic clusters such as Coma and A1367 tend to have galaxies with blue $(u-r)$ colours (actively star forming) and morphologies later than Sc but while being located at small projected distances from cluster centres. This may be a projection effect, but if not, it may be explained by a scenario where the galaxies are falling into the cluster core with their star formation rate enhanced in the process.

Wright et al. (2010)[252] and Jarrett et al. (2011)[120] have illustrated a clear connection between mid-IR WISE colours ($W1-W2, W2-W3$) and morphology, AGN (and radio) nature, and the star formation of galaxies. This relation is also investigated in this work. Resolved (complex photometry) galaxies and unresolved (compact sources that may be dwarf or AGN galaxies) are separated for clarity. The mid-IR colour-colour distribution was analysed with the addition of projected galaxy to cluster centre separation (D_{proj}). The analysis, though not robust, showed that galaxies with the earliest morphologies were located within small projected radii while later morphologies were located at larger projected distances. There were interlopers in both early type (ellipticals) and late type (spirals) colour-colour regions, where galaxies located at very large projected distances ($D_{proj} \gtrsim 3$ Mpc) were evident. These are most probably real peripheral galaxies which are falling into the cluster cores.

We further analyse the mid-IR colour-colour distributions by introducing the $W3$ derived, molecular ISM obscured specific star formation rate ($sSFR_{W3}$) (Jarrett et al. 2013[121]; Cluver et al. 2014[42]). The stellar masses are approximated using the mass-to-light relation for both resolved and unresolved sources shown by Cluver et al. 2014[42]. Galaxies from all three cluster subsamples (relic, halo, and halo+relic(s) clusters) with early type colours have the lowest sSFR ($\lesssim 1 \times 10^{-12}$ yr^{-1}), those with early type spiral/S0 colours (regions between spiral and early type morphology colours that overlap – Figure 4.1) have intermediate sSFR ($\sim 1 \times 10^{-11}$ yr^{-1}), and galaxies with spiral type colours display the highest sSFR ($\gtrsim 1 \times 10^{-11}$ yr^{-1}). This suggests that the mid-IR properties of galaxies found in clusters with diffuse radio emission, tend to be similar to those of galaxies in general. A tiny fraction of galaxies ($\lesssim 0.03\%$) was found to have mid-IR AGN colours. AGN galaxies are expected among galaxy cluster populations (e.g. Martini et al. 2007[161]; Pimbblet et al. 2013[184]). Another set of outliers was a small fraction ($\sim 16\%$) of galaxies found to have mid-IR colours that were similar to stars. These galaxies were found to have the lowest obscured star formation (sSFR $\sim 1 \times 10^{-13}$ yr^{-1} to $\sim 1 \times 10^{-15}$ yr^{-1}). Their stellar masses ($M_\star \sim 1 \times 10^{11}$ $M_\odot$) were among the largest in the sample, suggesting that these are passively evolving early type galaxies.

We also analyse the star formation rates and stellar masses of galaxies as functions of location in clusters (projected galaxy to cluster centre separation, D_{proj}) and also as functions of galaxy redshift. It was found that on a radial separation basis (redshift and D_{proj} – see figures in Appendix), the majority of low star formation galaxies is found within projected radii $\leqslant 0.6$ Mpc but there was no clear connection between location (redshift and D_{proj}) and star formation. This suggests that clusters in our sample may have a component of passively evolving, centrally located early type galaxies and another component of galaxies (with star formation halted or enhanced) located through out the cluster volume. The distribution of the second component of galaxies may be due to merger activities in the clusters.

Analysing the star formation rates and stellar masses of galaxies as functions of cluster redshifts showed that star formation is higher for higher redshift cluster galaxies given a certain stellar mass. Our analysis focusses on the nearby universe and so minimal cosmic galaxy SFR evolution is expected, but our results are in accord with the notion of "cosmic downsizing" where galaxies at high redshift have been found to have higher star formation rates than those of similar stellar masses at low redshifts (e.g. Fontanot et al. 2009[82]). We cannot, however, conclusively make this assumption of accordance since our sample may have biases and thus requires further understanding with regard to

limitations and completeness.

5.2 Future Work

Our multi-colour analysis was limited in three main aspects: (i) the redshift range of our cluster sample, (ii) corrections for photometric extinction (iii) and the wavelength range of our photometric analysis. An increase in both (i) and (iii) of these aspects would greatly affect the statistical robustness of the multi-colour analysis and thus lead to more solid conclusions on larger scales. Photometric extinction corrections will be vital for larger samples. Foreground extinction correction may be applied through the methods of Yuan et al. (2013)[254]. Internal extinction corrections are more illusive as one often does not have enough information regarding the physical characteristics of extragalactic sources. These corrections are usually based on models (e.g. Cho & Park 2009[36]).

Another area of improvement would be the expansion of the star formation analysis to include contributions from short (UV) and long (IR) wavelengths so as to analyse the total star formation rate that is composed of both obscured (IR derived) and unobscured (UV derived) components (e.g. Elbaz et al. 2007[66]; Buat et al. 2011[29]; Jarrett et al. 2013[121]). The dependence of galaxy star formation on environment may also also be investigated by computing the local densities of galaxies in cluster environments and analysing their relations to star formation (e.g. Brough et al. (2013)[24] where star formation is studied with respect to fifth nearest neighbour surface densities). Star formation analysis may also be enriched by including spectroscopic analysis where galaxy chemical abundances and ages may be probed as functions of environment (e.g. Bernardi et al. 2006[17]; Clemens et al. 2006[40]).

The techniques and tools developed here will be of value to future deep multi-wavelength surveys such as: the radio survey MighTEE (MeerKAT International GigaHertz Tiered Extragalactic Exploration survey) with the MeerKAT, ASKAP-EMU (the Evolutionary Map of the Universe, EMU, survey with the Australian Square Kilometre Array Pathfinder, ASKAP), X-ray survey with eROSITA (Extended Roentgen Survey with an Imaging Telescope Array), and optical/IR surveys with VISTA (Visible and Infrared Survey Telescope for Astronomy).

Chapter 6

Appendices

Appendix A

The results of the clustering algorithm (section 2.4.2.1) applied to the mock cluster sample are presented in this section.

The case of the A3667 mock cluster is presented.

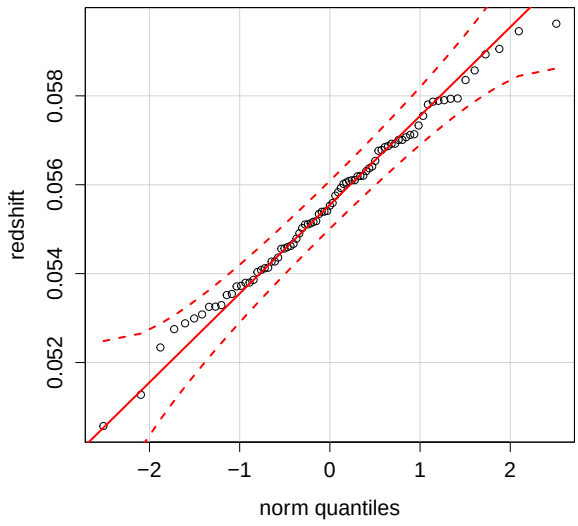

Figure 6.2: QQ plot analysis on the mock redshifts of the A3667 mock cluster. All mock galaxies fall within the 95% confidence bands as expected.

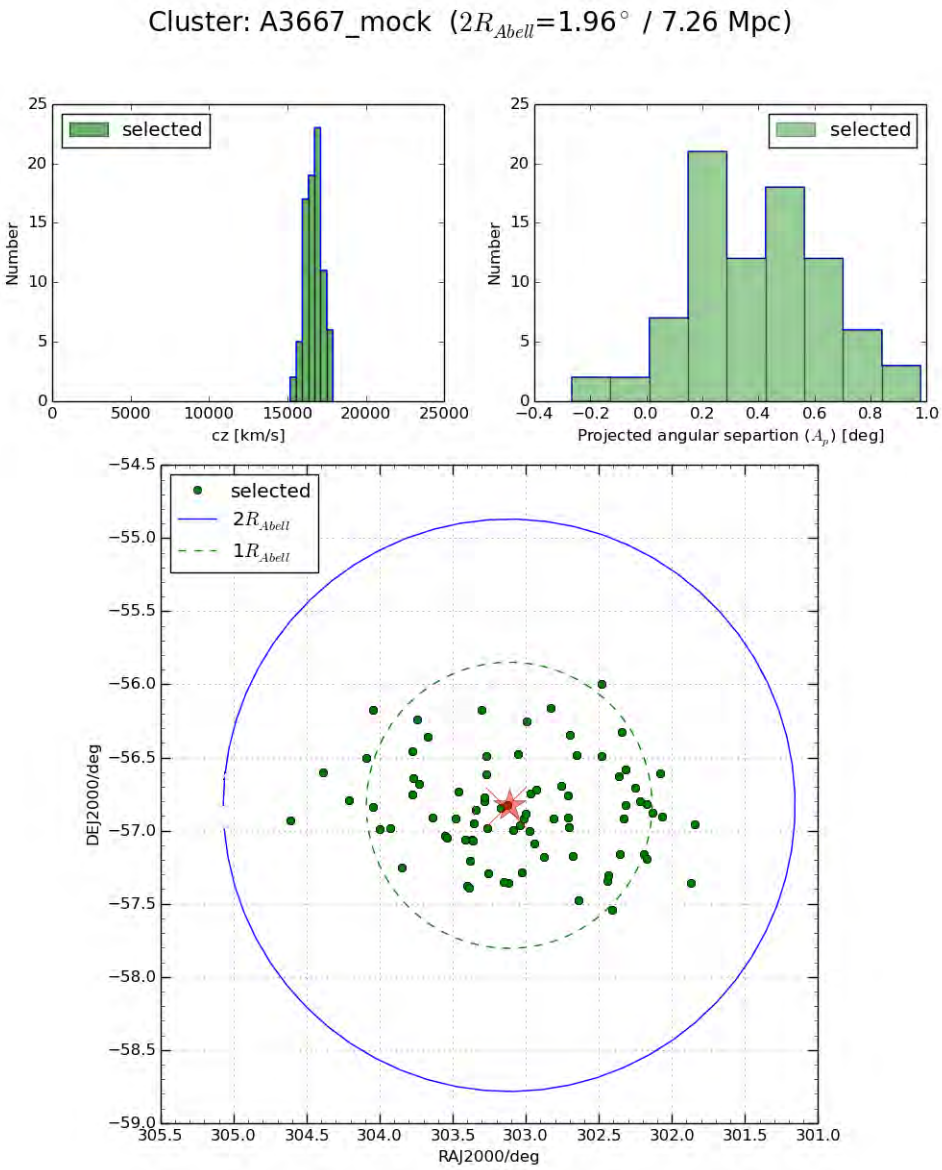

Figure 6.1: Clustering analysis applied to a mock cluster of A3667. Green dots and green histograms represent the galaxies which satisfy the selection criteria and thus were selected as member candidates (see 2.4.2.1). Top left: The radial velocity distribution of the entire galaxy sample (blue unfilled histogram) and the selected member galaxies. Top right: The projected angular separation between galaxies and the cluster centre (A_p). Bottom: The sky distribution of all mock galaxies in the A3667 mock sample. Green dots are selected galaxies, open circles are excluded galaxies, the red cross is the mock centre (X-ray centroid) and the red star is the mock BCG. The 2 and 1 Abell radii (centred on the X-ray centroid) are labelled accordingly.

Appendix B

This section displays the UV-optical colour-colour-magnitude relations in each of the clusters in our sample.

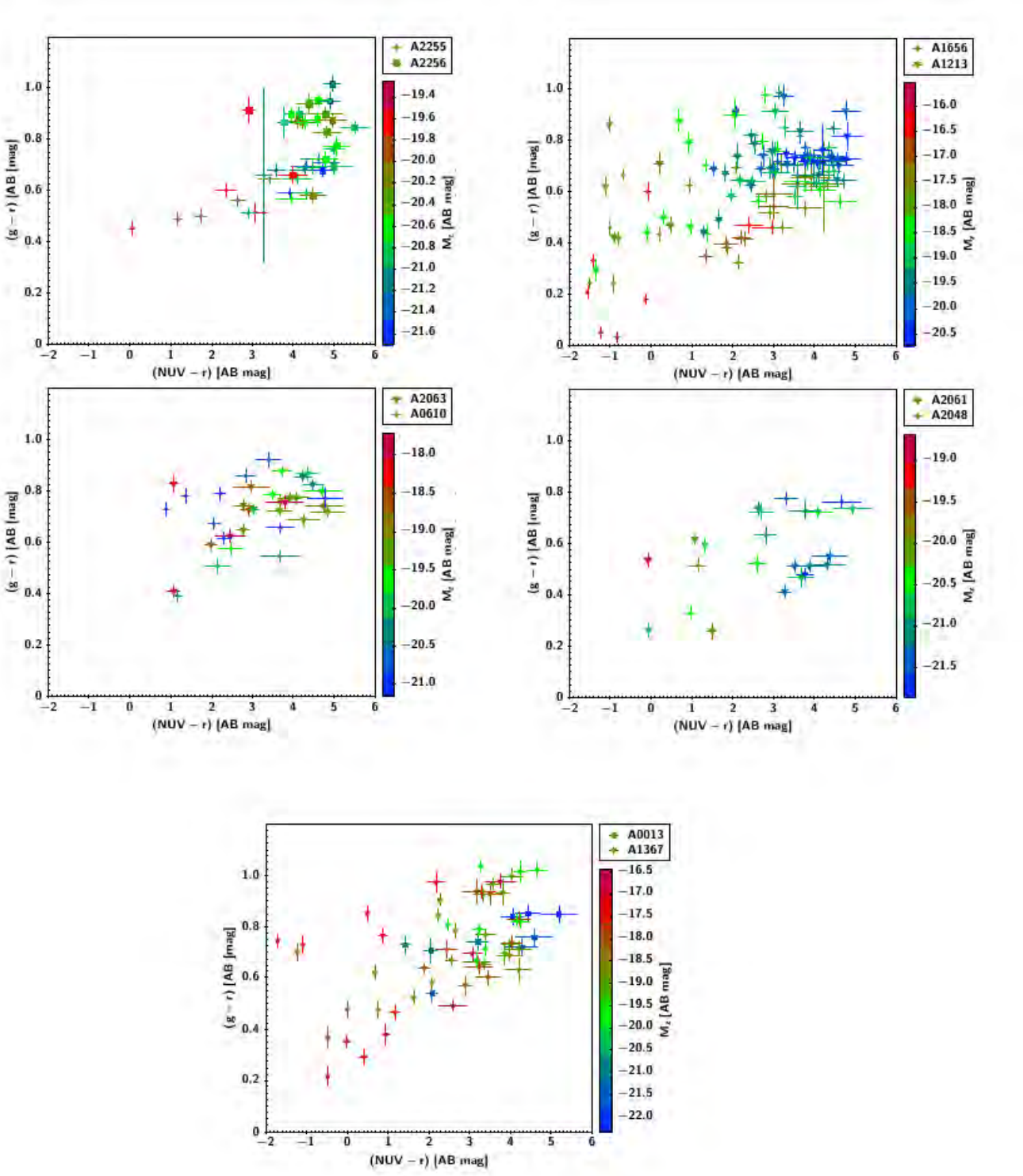

Figure 6.3: The UV-optical colour-colour-magnitude relations of galaxy clusters. The (g-r), (NUV-r) colour-colour relations are colour-coded according to the z-band luminosity M_z. GALEX and corresponding SDSS data was found only for member galaxies in the above clusters.

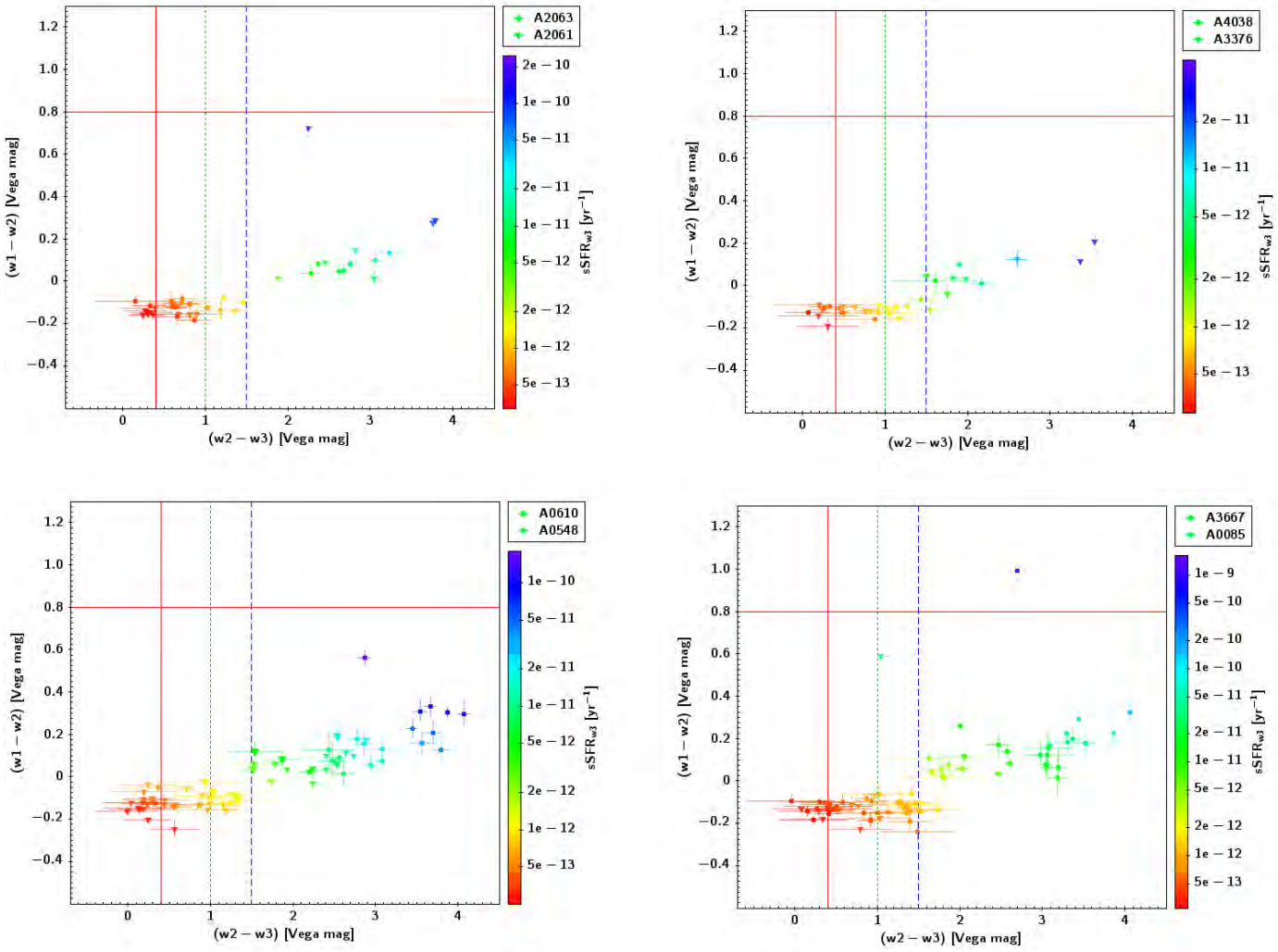

Figure 6.4: W3 IR specific star formation as a function of IR colours in our sample of galaxy clusters. The vertical dot dashed lines represent the $(W2-W3)$ colour-morphology thresh holds as inferred from Figure 4.1 viz.: early types $(W2-W3<1.0)$, S0 galaxies (bounded within green and blue dot dashed lines), and late types in the region from, and to the right, of the blue dot dashed line. The solid horizontal red line is the $(W1-W2)=0.8$ mag threshold for non-AGN galaxies (Stern et al. 2012[226]). Only those galaxy clusters whose galaxies had WISE photometry are illustrated.

Appendix C

This section displays the mid-IR (via WISE photometry) colour-colour relations with respect to obscured, W3 derived specific star formation ($sSFR_{w3}$) in each of the clusters in our sample.

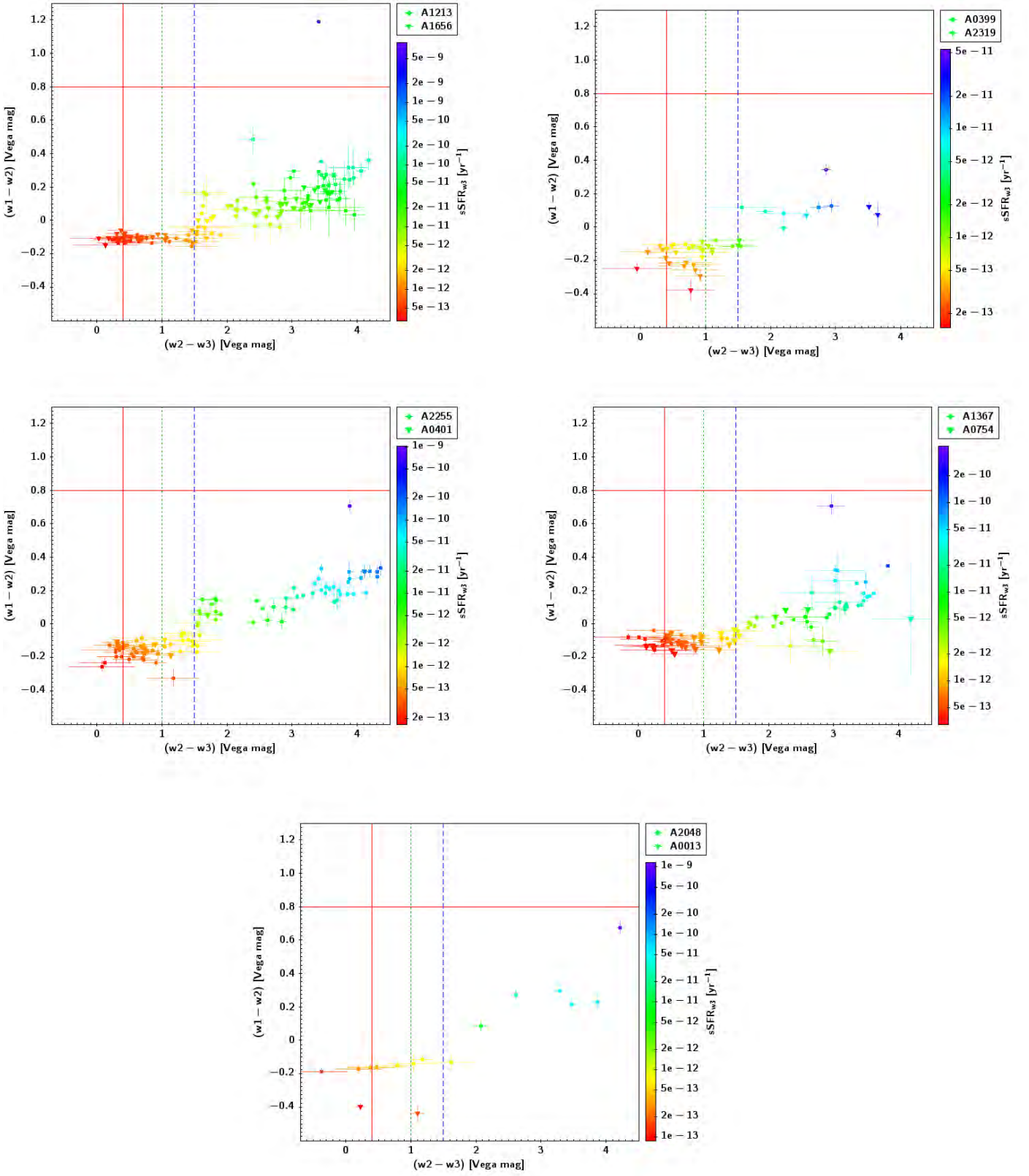

Figure 6.5: W3 IR specific star formation as a function of IR colours in our sample of galaxy clusters, continued from Figure 6.4. The vertical dot dashed lines represent the $(W2-W3)$ colour-morphology thresh holds as inferred from Figure 4.1 viz.: early types $(W2-W3<1.0)$, S0 galaxies (bounded within green and blue dot dashed lines), and late types in the region from, and to the right, of the blue dot dashed line. The solid horizontal red line is the $(W1-W2)=0.8$ mag threshold for non-AGN galaxies (Stern et al. 2012[226]). Only those galaxy clusters whose galaxies had WISE photometry are illustrated.

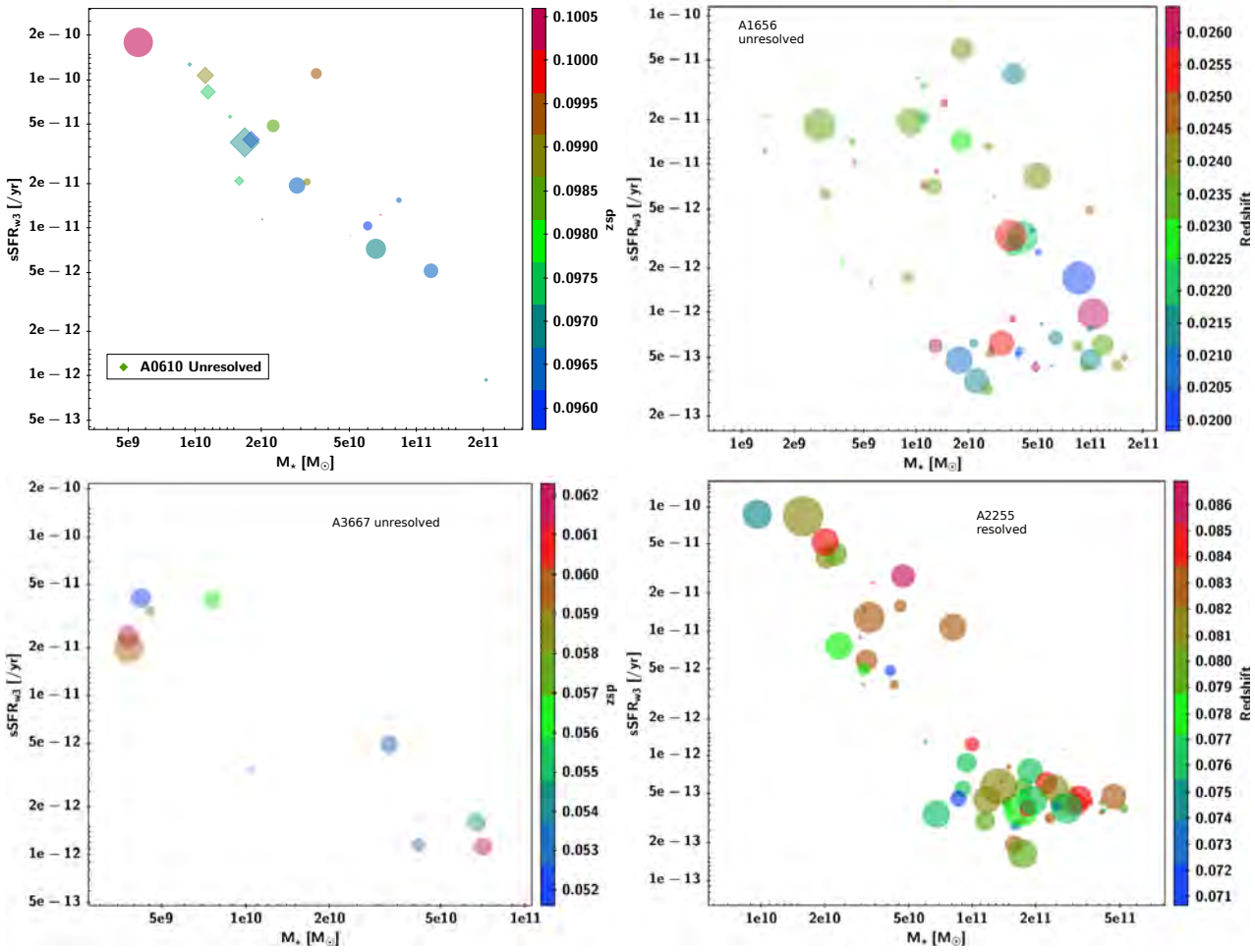

Figure 6.6: W3 IR specific star formation of galaxies as a function of galaxy stellar mass, location within the parent cluster, and galaxy redshift. The sizes of the data points are proportional to projected separations relative to cluster centres. In cases of clusters that have large numbers of galaxies, resolved and unresolved galaxies are plotted separately.

Appendix D

In this section we present graphical results of the sSFR-location distribution of galaxies. The sSFR of galaxies in each cluster is illustrated as a function of stellar mass, galaxy redshift (radial velocity) and galaxy-to-centre projected distance, D_{proj}.

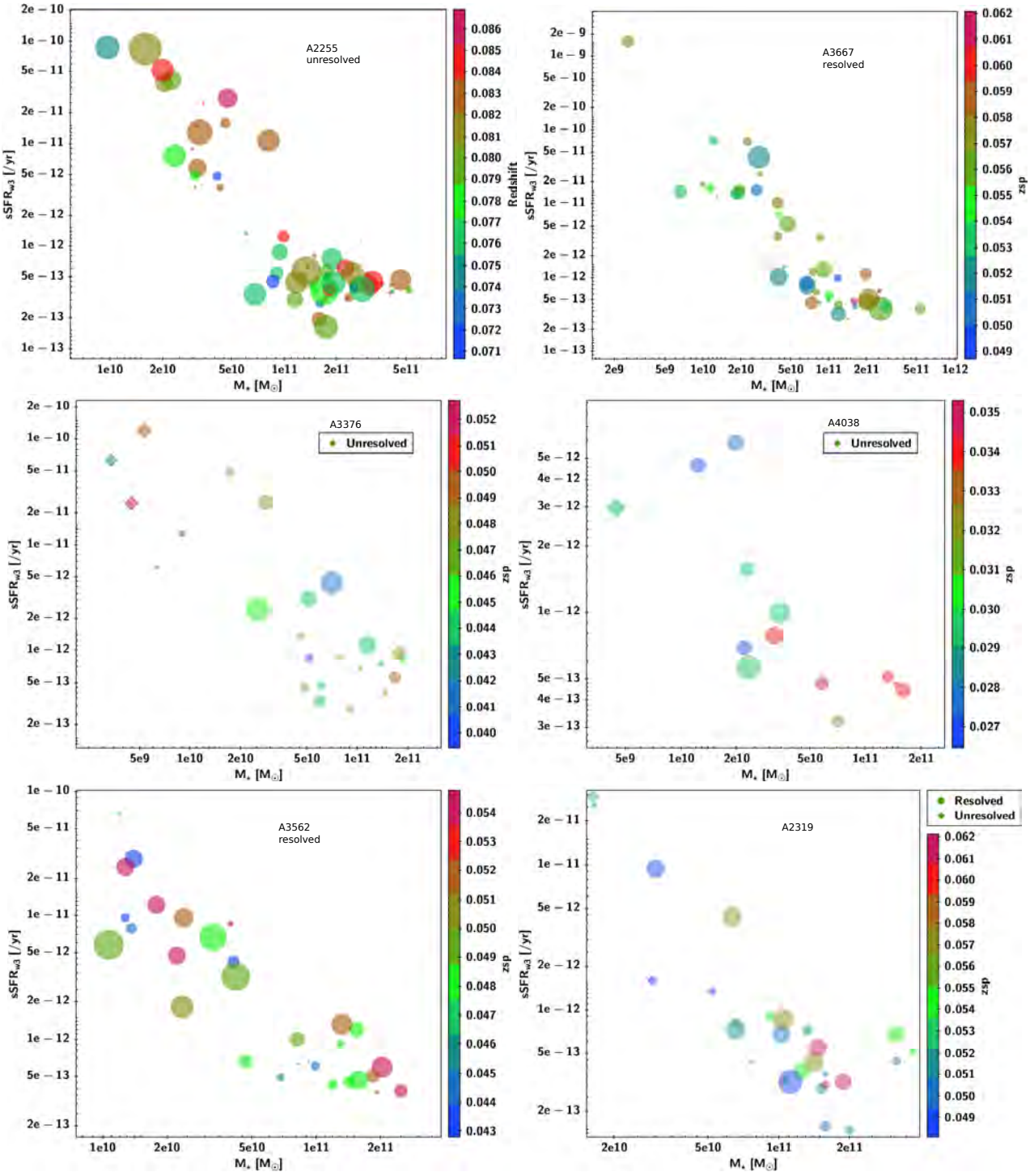

Figure 6.7: W3 IR specific star formation of galaxies as a function of galaxy stellar mass, location within the parent cluster, and galaxy redshift. The sizes of the data points are proportional to projected separations relative to cluster centres. In cases of clusters that have large numbers of galaxies, resolved and unresolved galaxies are plotted separately.

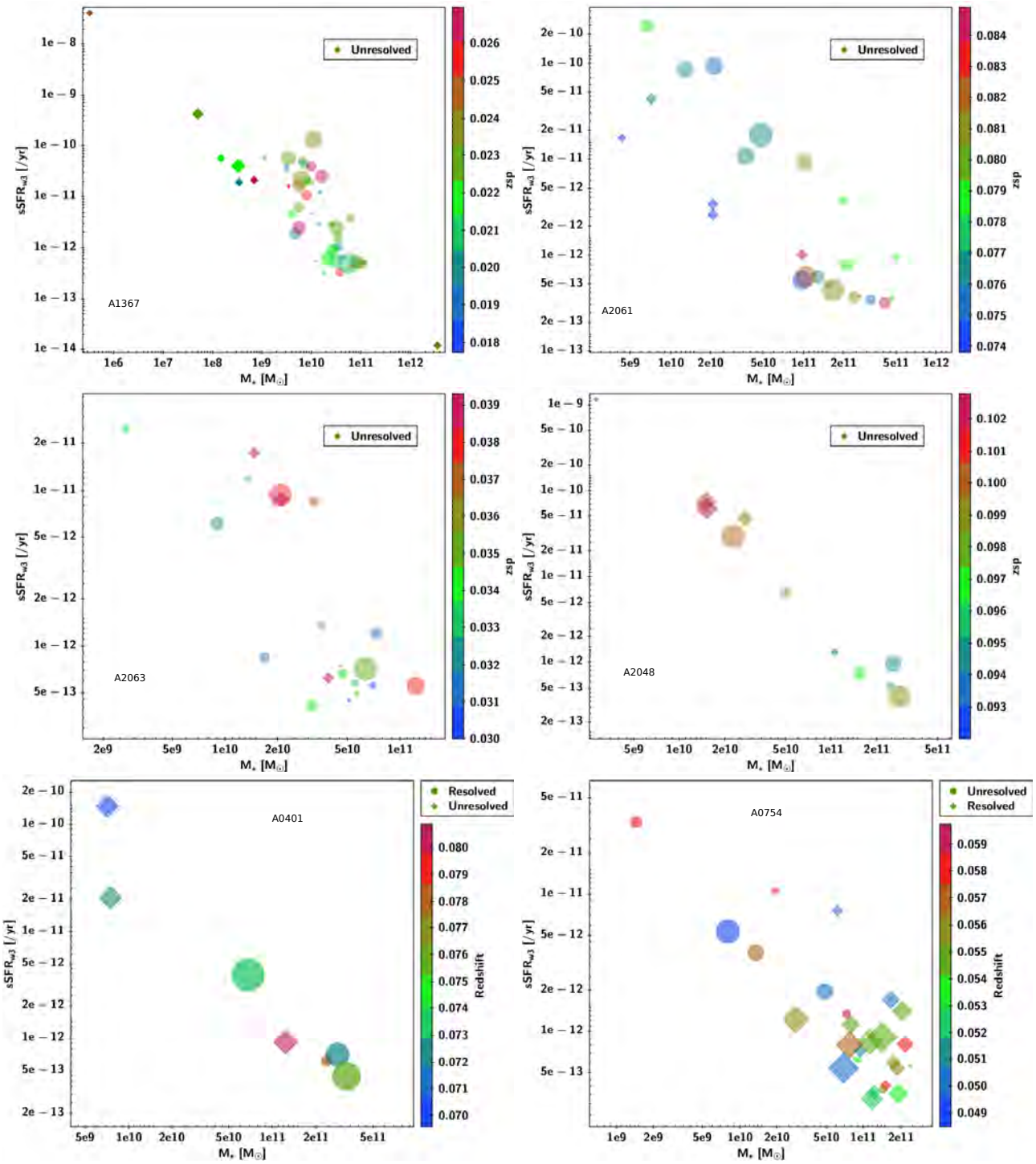

Figure 6.8: W3 IR specific star formation of galaxies as a function of galaxy stellar mass, location within the parent cluster, and galaxy redshift. The sizes of the data points are proportional to projected separations relative to cluster centres. In cases of clusters that have large numbers of galaxies, resolved and unresolved galaxies are plotted separately.

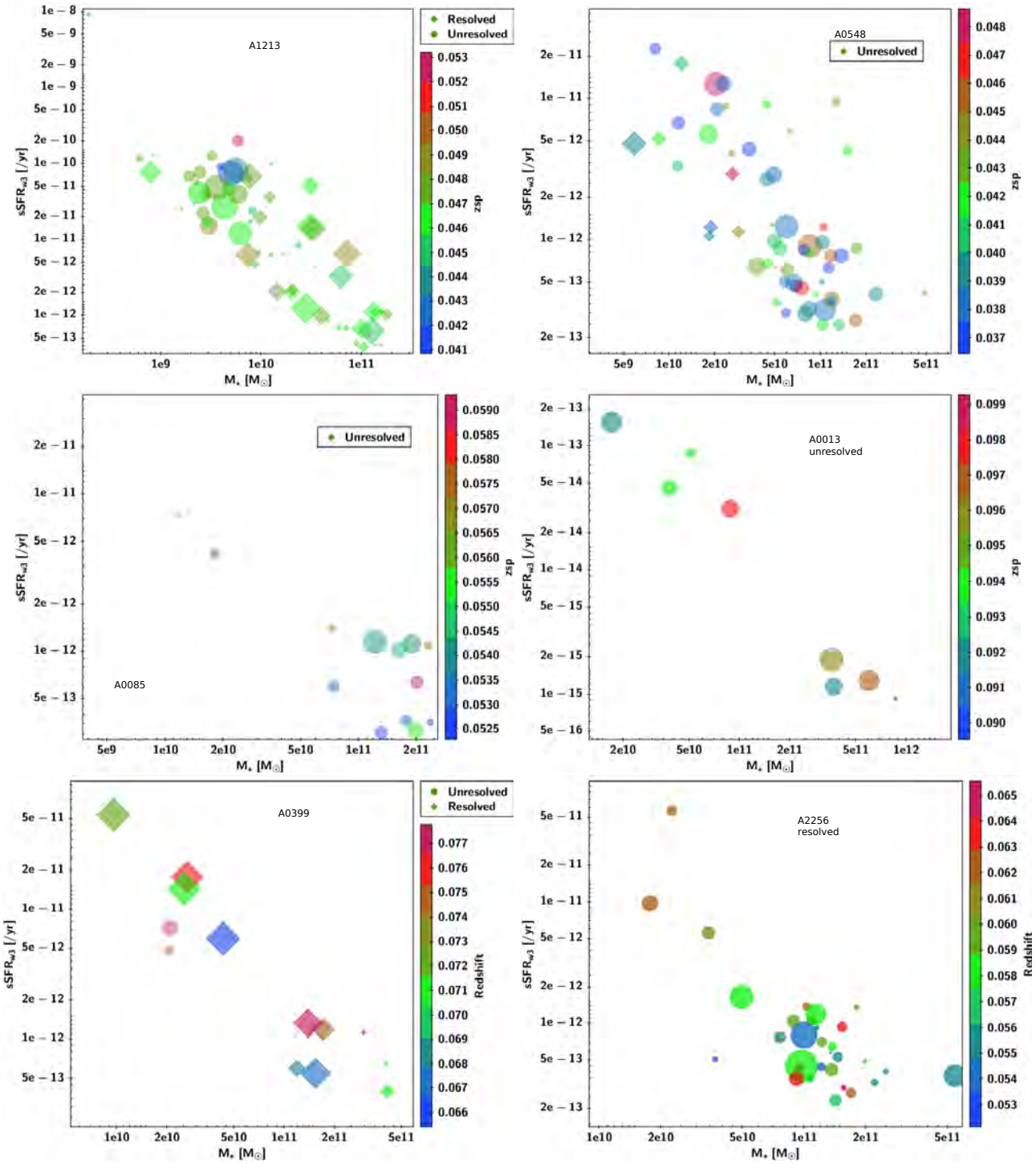

Figure 6.9: W3 IR specific star formation of galaxies as a function of galaxy stellar mass, location within the parent cluster, and galaxy redshift. The sizes of the data points are proportional to projected separations relative to cluster centres. In cases of clusters that have large numbers of galaxies, resolved and unresolved galaxies are plotted separately.

Bibliography

[1] G. O. Abell, *The Distribution of Rich Clusters of Galaxies.*, ApJS, 3 (1958), p. 211.

[2] G. O. Abell, H. G. Corwin, Jr., and R. P. Olowin, *A catalog of rich clusters of galaxies*, Astrophysical Journal Supplement Series, (1989).

[3] M. Ackermann, M. Ajello, A. Allafort, L. Baldini, J. Ballet, and et al., *GeV Gamma-ray Flux Upper Limits from Clusters of Galaxies*, ApJL, 717 (2010), pp. L71–L78.

[4] C. P. Ahn, R. Alexandroff, C. Allende Prieto, S. F. Anderson, T. Anderton, B. H. Andrews, É. Aubourg, S. Bailey, E. Balbinot, R. Barnes, and et al., *The Ninth Data Release of the Sloan Digital Sky Survey: First Spectroscopic Data from the SDSS-III Baryon Oscillation Spectroscopic Survey*, ApJS, 203 (2012), p. 21.

[5] D. F. Andrews and et al., *Robust Estimates of Location: Survey and Advances*, Princeton: Princeton University Press., 1972.

[6] S. Arnouts, E. Le Floc'h, J. Chevallard, B. D. Johnson, O. Ilbert, M. Treyer, H. Aussel, P. Capak, D. B. Sanders, N. Scoville, H. J. McCracken, B. Milliard, L. Pozzetti, and M. Salvato, *Encoding of the infrared excess in the NUVrK color diagram for star-forming galaxies*, A&A, 558 (2013), p. A67.

[7] B. Nikolic, *Nuclear Starbursts*, PhD thesis, University of Cambridge, 2005.

[8] M. Bacchi, L. Feretti, G. Giovannini, and F. Govoni, *Deep images of cluster radio halos*, A&A, 400 (2003), pp. 465–476.

[9] J. Bagchi, F. Durret, G. B. L. Neto, and S. Paul, *Giant Ringlike Radio Structures Around Galaxy Cluster Abell 3376*, Science, 314 (2006), pp. 791–794.

[10] I. K. Baldry, K. Glazebrook, J. Brinkmann, Ž. Ivezić, R. H. Lupton, R. C. Nichol, and A. S. Szalay, *Quantifying the Bimodal Color-Magnitude Distribution of Galaxies*, ApJ, 600 (2004), pp. 681–694.

[11] M. L. Balogh, I. K. Baldry, R. Nichol, C. Miller, R. Bower, and K. Glazebrook, *The Bimodal Galaxy Color Distribution: Dependence on Luminosity and Environment*, ApJ, 615 (2004), pp. L101–L104.

[12] S. Bardelli, A. Pisani, M. Ramella, E. Zucca, and G. Zamorani, *A substructure analysis of the A3558 cluster complex*, Mon. Not. R. Astron. Soc., 300 (1998), pp. 589–598.

[13] S. Bardelli, T. Venturi, E. Zucca, S. De Grandi, S. Ettori, and S. Molendi, *Abell 3560, a galaxy cluster at the edge of a major merging event*, A&A, 396 (2002), pp. 65–72.

[14] S. Barway, Y. Wadadekar, K. Vaghmare, and a. K. Kembhavi, *Luminosity-dependent star formation history of S0 galaxies: evidence from GALEX-SDSS-2MASS-WISE colours*, Mon. Not. R. Astron. Soc., 432 (2013), pp. 430–437.

[15] L. P. Bautz and W. W. Morgan, *On the Classification of the Forms of Clusters of Galaxies*, ApJL, 162 (1970), p. L149.

[16] T. Beers, K. Flynn, and K. Gebhardt, *Measures of location and scale for velocities in clusters of galaxies-A robust approach*, Astron. J., (1990).

[17] M. Bernardi, R. C. Nichol, R. K. Sheth, C. J. Miller, and J. Brinkmann, *Evolution and environment of early-type galaxies*, Evol. Environ. EARLY-TYPE GALAXIES, (2006), pp. 1288–1317.

[18] P. N. Best, *Radio-Loud AGN Feedback in Elliptical Galaxies*, in Cosmic Frontiers, N. Metcalfe and T. Shanks, eds., vol. 379 of Astronomical Society of the Pacific Conference Series, Dec. 2007, p. 213.

[19] L. Bianchi, J. Herald, B. Efremova, L. Girardi, A. Zabot, P. Marigo, A. Conti, and B. Shiao, *GALEX catalogs of UV sources: statistical properties and sample science applications: hot white dwarfs in the Milky Way*, Ap&SS, 335 (2011), pp. 161–169.

[20] H. Böhringer, P. Schuecker, L. Guzzo, C. A. Collins, W. Voges, R. G. Cruddace, A. Ortiz-Gil, G. Chincarini, S. De Grandi, A. C. Edge, H. T. MacGillivray, D. M. Neumann, S. Schindler, and P. Shaver, *The ROSAT-ESO Flux Limited X-ray (REFLEX) Galaxy cluster survey. V. The cluster catalogue*, A&A, 425 (2004), pp. 367–383.

[21] A. Bonafede, M. Brüggen, R. van Weeren, F. Vazza, G. Giovannini, H. Ebeling, A. C. Edge, M. Hoeft, and U. Klein, *Discovery of radio haloes and double relics in distant MACS galaxy clusters: clues to the efficiency of particle acceleration*, MNRAS, 426 (2012), pp. 40–56.

[22] W. Boschin, R. Barrena, M. Girardi, and M. Spolaor, *Optical analysis of the poor clusters Abell 610, Abell 725, and Abell 796, containing diffuse radio sources*, A&A, 487 (2008), pp. 33–46.

[23] M. A. Brentjens, *Deep Westerbork observations of Abell 2256 at 350 MHz*, A&A, 489 (2008), pp. 69–83.

[24] S. Brough, S. Croom, R. Sharp, a. M. Hopkins, E. N. Taylor, I. K. Baldry, M. L. P. Gunawardhana, J. Liske, P. Norberg, a. S. G. Robotham, a. E. Bauer, J. Bland-Hawthorn, M. Colless, C. Foster, L. S. Kelvin, M. a. Lara-Lopez, a. R. Lopez-Sanchez, J. Loveday, M. Owers, K. a. Pimbblet, and M. Prescott, *Galaxy And Mass Assembly: resolving the role of environment in galaxy evolution*, Monthly Notices of the Royal Astronomical Society, 435 (2013), pp. 2903–2917.

[25] M. J. I. Brown, J. Moustakas, J.-D. T. Smith, E. da Cunha, T. H. Jarrett, M. Imanishi, L. Armus, B. R. Brandl, and J. E. G. Peek, *An Atlas of Galaxy Spectral Energy Distributions from the Ultraviolet to the Mid-infrared*, ApJS, 212 (2014), p. 18.

[26] M. Brüggen, R. J. van Weeren, and H. J. A. Röttgering, *Magnetic fields and shock waves in cluster outskirts*, MmSAI, 82 (2011), p. 627.

[27] G. Brunetti, *Particle Acceleration and Non-Thermal Emission from Galaxy Clusters*, Journal of Korean Astronomical Society, 37 (2004), pp. 493–500.

[28] ——, *Cosmic rays and diffuse non-thermal emission in galaxy clusters: an introduction.*, MmSAI, 82 (2011), p. 515.

[29] V. Buat, E. Giovannoli, T. T. Takeuchi, S. Heinis, F.-T. Yuan, D. Burgarella, S. Noll, and J. Iglesias-Páramo, *Spectral energy distributions of an AKARI-SDSS-GALEX sample of galaxies*, A&A, 529 (2011), p. A22.

[30] D. A. Buote, *On the Origin of Radio Halos in Galaxy Clusters*, ApJL, 553 (2001), pp. L15–L18.

[31] J. O. Burns, K. Roettiger, J. Pinkney, R. A. Perley, F. N. Owen, and W. Voges, *Evidence for an On-going Cluster/Group Merger in Abell 2255*, ApJ, 446 (1995), p. 583.

[32] R. Cassano, G. Brunetti, and T. Venturi, *The Connection between Radio Halos and Cluster Mergers and the Statistical Properties of the Radio Halo Population*, Journal of Astrophysics and Astronomy, 32 (2011), pp. 519–527.

[33] J. Chen, J. P. Huchra, B. R. McNamara, and J. Mader, *The Mass Function of Abell Clusters*, in American Astronomical Society Meeting Abstracts, vol. 30 of Bulletin of the American Astronomical Society, Dec. 1998, p. 1307.

[34] I. V. Chilingarian, A.-L. Melchior, and I. Y. Zolotukhin, *Analytical approximations of K-corrections in optical and near-infrared bands*, Mon. Not. R. Astron. Soc., 1420 (2010), pp. no–no.

[35] I. V. Chilingarian and I. Y. Zolotukhin, *A universal ultraviolet-optical colour-colour-magnitude relation of galaxies*, Mon. Not. R. Astron. Soc., 419 (2012), pp. 1727–1739.

[36] J. Cho and C. Park, *Internal extinction in the sloan digital sky survey late-type galaxies*, The Astrophysical Journal, 693 (2009), p. 1045.

[37] T. Clarke, T. Mroczkowski, S. Brown, G. Brunetti, R. Cassano, D. Dallacasa, L. Feretti, S. Giacintucci, G. Giovannini, F. Govoni, M. Markevitch, M. Murgia, L. Rudnick, A. Scaife, V. Vacca, T. Venturi, and R. van Weeren, *White Paper: Radio Emission and Polarization Properties of Galaxy Clusters with VLASS*, ArXiv e-prints, (2014).

[38] T. E. Clarke, T. Ensslin, A. Finoguenov, H. Intema, C. Pfrommer, R. van Weeren, H. Röttgering, and R. Oonk, *The curious case of Abell 2256* ., Memorie della Societa Astronomica Italiana, 82 (2011), p. 547.

[39] T. E. Clarke and T. A. Ensslin, *Deep 1.4 GHz Very Large Array Observations of the Radio Halo and Relic in Abell 2256*, AJ, 131 (2006), pp. 2900–2912.

[40] M. S. Clemens, A. Bressan, B. Nikolic, P. Alexander, F. Annibali, and R. Rampazzo, *The star formation history of early-type galaxies as a function of mass and environment*, MNRAS, 370 (2006), pp. 702–720.

[41] M. E. Cluver, P. N. Appleton, P. Ogle, T. H. Jarrett, J. Rasmussen, U. Lisenfeld, P. Guillard, L. Verdes-Montenegro, R. Antonucci, T. Bitsakis, V. Charmandaris, F. Boulanger, E. Egami, C. K. Xu, and M. S. Yun, *Enhanced Warm H_2 Emission in the Compact Group Mid-infrared "Green Valley"*, ApJ, 765 (2013), p. 93.

[42] M. E. Cluver, T. H. Jarrett, A. M. Hopkins, S. P. Driver, J. Liske, M. L. P. Gunawardhana, E. N. Taylor, A. S. G. Robotham, M. Alpaslan, I. Baldry, M. J. I. Brown, J. A. Peacock, C. C. Popescu, R. J. Tuffs, A. E. Bauer, J. Bland-Hawthorn, M. Colless, B. W. Holwerda, M. A. Lara-López, K. Leschinski, A. R. López-Sánchez, P. Norberg, M. S. Owers, L. Wang, and S. M. Wilkins, *Galaxy and Mass Assembly (GAMA): Mid-infrared Properties and Empirical Relations from WISE*, ApJ, 782 (2014), p. 90.

[43] M. Colless and A. M. Dunn, *Structure and Dynamics of the Coma Cluster*, ApJ, 458 (1996), p. 435.

[44] L. Cortese, G. Gavazzi, and A. Boselli, *Multiple merging in the Abell cluster 1367*, Astronomy and Astrophysics, (2004), pp. 1–15.

[45] L. Cortese, D. Marcillac, J. Richard, H. Bravo-Alfaro, J.-P. Kneib, G. Rieke, G. Covone, E. Egami, J. Rigby, O. Czoske, and J. Davies, *The strong transformation of spiral galaxies infalling into massive clusters at z 0.2*, Mon. Not. R. Astron. Soc., 376 (2007), pp. 157–172.

[46] L. L. Cowie and J. Binney, *Radiative regulation of gas flow within clusters of galaxies - A model for cluster X-ray sources*, ApJ, 215 (1977), pp. 723–732.

[47] R. M. Cutri and et al., *AllWISE Data Release (Cutri+ 2013)*, VizieR Online Data Catalog, 2328 (2014), p. 0.

[48] L. P. David, A. Slyz, C. Jones, W. Forman, S. D. Vrtilek, and K. A. Arnaud, *A catalog of intracluster gas temperatures*, ApJ, 412 (1993), pp. 479–488.

[49] D. S. Davis, C. M. Bird, R. F. Mushotzky, and S. C. Odewahn, *Abell 548: an X-ray and optical analysis of substructure*, ApJ, 440 (1995), pp. 48–59.

[50] T. M. Davis and M. I. Scrimgeour, *Deriving accurate peculiar velocities (even at high redshift)*, MNRAS, 442 (2014), pp. 1117–1122.

[51] F. de Gasperin, R. J. van Weeren, M. Bruggen, F. Vazza, A. Bonafede, and H. T. Intema, *A new double radio relic in PSZ1 G096.89+24.17 and a radio relic mass-luminosity relation*, ArXiv e-prints, (2014).

[52] R. De Propris, S. Phillipps, and M. N. Bremer, *Deep luminosity functions and colour-magnitude relations for cluster galaxies at $0.2 < z < 0.6$*, MNRAS, 434 (2013), pp. 3469–3486.

[53] den Hartog, *The Dynamics of Rich Galaxy Clusters*, PhD thesis, Univ. Leiden, 1995.

[54] R. den Hartog and P. Katgert, *On the dynamics of the cores of galaxy clusters.*, MNRAS, 279 (1996), pp. 349–388.

[55] R. H. Donnelly, M. Markevitch, W. Forman, C. Jones, L. P. David, E. Churazov, and M. Gilfanov, *Temperature Structure in Abell 1367*, ApJ, 500 (1998), pp. 138–146.

[56] A. Dressler, *Galaxy morphology in rich clusters - Implications for the formation and evolution of galaxies*, ApJ, 236 (1980), pp. 351–365.

[57] A. Dressler and J. E. Gunn, *Spectroscopy of galaxies in distant clusters. II - The population of the 3C 295 cluster*, ApJ, 270 (1983), pp. 7–19.

[58] A. Dressler and S. A. Shectman, *Evidence for substructure in rich clusters of galaxies from radial-velocity measurements*, AJ, 95 (1988), pp. 985–995.

[59] F. Durret, P. Felenbok, C. Lobo, and E. Slezak, *A catalogue of velocities in the cluster of galaxies Abell 85*, A&AS, 129 (1998), pp. 281–288.

[60] F. Durret, G. B. Lima Neto, and W. Forman, *An XMM-Newton view of the cluster of galaxies Abell 85*, A&A, 432 (2005), pp. 809–821.

[61] F. Durret, C. Perrot, G. B. Lima Neto, C. Adami, and J. Bagchi, *The extraordinary cluster of galaxies Abell 3376: An optical view*, in SF2A-2012: Proceedings of the Annual meeting of the French Society of Astronomy and Astrophysics, S. Boissier, P. de Laverny, N. Nardetto, R. Samadi, D. Valls-Gabaud, and H. Wozniak, eds., Dec. 2012, pp. 461–464.

[62] F. Durret, C. Perrot, G. B. Lima Neto, C. Adami, E. Bertin, and J. Bagchi, *The merging cluster of galaxies Abell 3376: an optical view*, Astronomy & Astrophysics, 560 (2013), p. A78.

[63] H. Ebeling, A. C. Edge, H. Bohringer, S. W. Allen, C. S. Crawford, A. C. Fabian, W. Voges, and J. P. Huchra, *The ROSAT Brightest Cluster Sample - I. The compilation of the sample and the cluster log N-log S distribution*, MNRAS, 301 (1998), pp. 881–914.

[64] D. Eckert, S. Molendi, and S. Paltani, *The cool-core bias in X-ray galaxy cluster samples. I. Method and application to HIFLUGCS*, A&A, 526 (2011), p. A79.

[65] M. Einasto, L. J. Liivamägi, E. Tempel, E. Saar, E. Tago, P. Einasto, I. Enkvist, J. Einasto, V. J. Martínez, P. Heinämäki, and P. Nurmi, *The Sloan Great Wall. Morphology and Galaxy Content*, ApJ, 736 (2011), p. 51.

[66] D. Elbaz, E. Daddi, D. Le Borgne, M. Dickinson, D. M. Alexander, R.-R. Chary, J.-L. Starck, W. N. Brandt, M. Kitzbichler, E. MacDonald, M. Nonino, P. Popesso, D. Stern, and E. Vanzella, *The reversal of the star formation-density relation in the distant universe*, A&A, 468 (2007), pp. 33–48.

[67] T. A. Ensslin, *Acceleration processes in the large-scale structure*, in IAU Joint Discussion, vol. 12 of IAU Joint Discussion, Aug. 2006.

[68] S. Ettori, S. Bardelli, S. De Grandi, S. Molendi, G. Zamorani, and E. Zucca, *BeppoSAX-ROSAT PSPC observations of the Shapley supercluster: A3562*, MNRAS, 318 (2000), pp. 239–249.

[69] A. C. Fabian and P. E. J. Nulsen, *Subsonic accretion of cooling gas in clusters of galaxies*, MNRAS, 180 (1977), pp. 479–484.

[70] D. Fadda, M. Girardi, G. Giuricin, F. Mardirossian, and M. Mezzetti, *The Observational Distribution of Internal Velocity Dispersions in Nearby Galaxy Clusters*, ApJ, 473 (1996), p. 670.

[71] B. L. Fanaroff and J. M. Riley, *The morphology of extragalactic radio sources of high and low luminosity*, MNRAS, 167 (1974), pp. 31P–36P.

[72] C. Fanti, R. Fanti, L. Feretti, A. Ficarra, I. M. Gioia, G. Giovannini, L. Gregorini, F. Mantovani, B. Marano, L. Padrielli, P. Parma, P. Tomasi, and G. Vettolani, *Radio and optical observations of 9 nearby Abell clusters - A262, A347, A569, A576, A779, A1213, A1228, A2162, A2666*, A&A, 105 (1982), pp. 200–218.

[73] L. Feretti, *Radio Observations of Clusters of Galaxies*, in Matter and Energy in Clusters of Galaxies, S. Bowyer and C.-Y. Hwang, eds., vol. 301 of Astronomical Society of the Pacific Conference Series, 2003, p. 143.

[74] L. Feretti, M. Bacchi, O. B. Slee, G. Giovannini, F. Govoni, H. Andernach, and G. Tsarevsky, *Diffuse radio sources in the cluster of galaxies Abell 548b*, MNRAS, 368 (2006), pp. 544–552.

[75] L. Feretti, H. Boehringer, G. Giovannini, and D. Neumann, *The radio and X-ray properties of Abell 2255.*, A&A, 317 (1997), pp. 432–440.

[76] L. Feretti and G. Giovannini, *Clusters of Galaxies in the Radio: Relativistic Plasma and ICM/Radio Galaxy Interaction Processes*, in A Pan-Chromatic View of Clusters of Galaxies and the Large-Scale Structure, M. Plionis, O. López-Cruz, and D. Hughes, eds., vol. 740 of Lecture Notes in Physics, Berlin Springer Verlag, 2008, p. 143.

[77] L. Feretti, G. Giovannini, and H. Böhringer, *The radio and X-ray properties of Abell 2319*, New Astronomy, 2 (1997), pp. 501–515.

[78] L. Feretti, G. Giovannini, F. Govoni, and M. Murgia, *Clusters of galaxies: observational properties of the diffuse radio emission*, Astron. Astrophys. Rev., 20 (2012), pp. 1–60.

[79] C. Ferrari, F. Govoni, S. Schindler, A. M. Bykov, and Y. Rephaeli, *Observations of Extended Radio Emission in Clusters*, Space Science Reviews, 134 (2008), pp. 93–118.

[80] E. L. Fitzpatrick, *Correcting for the Effects of Interstellar Extinction*, PASP, 111 (1999), pp. 63–75.

[81] P. Flin and J. Krywult, *Substructures in Abell clusters of galaxies*, A&A, 450 (2006), pp. 9–14.

[82] F. Fontanot, G. De Lucia, P. Monaco, R. S. Somerville, and P. Santini, *The many manifestations of downsizing: hierarchical galaxy formation models confront observations*, MNRAS, 397 (2009), pp. 1776–1790.

[83] W. Forman, E. Churazov, L. David, F. Durret, C. Jones, M. Markevitch, S. Murray, M. Sun, and A. Vikhlinin, *A High Angular Resolution View of Hot Gas in Clusters, Groups, and Galaxies*, ArXiv Astrophysics e-prints, (2003).

[84] C. Fraley and A. Raftery, *How many clusters? Which clustering method? Answers via model-based cluster analysis*, Comput. J., (1998).

[85] C. Fraley and A. E. Raftery, *MCLUST Version 3 for R : Normal Mixture Modeling and Model-Based Clustering* , Tech. Rep. 504, Department of Statistics, University of Washington, 2012.

[86] D. Freedman and P. Diaconis, *On the histogram as a density estimator:l 2 theory*, Zeitschrift fr Wahrscheinlichkeitstheorie und Verwandte Gebiete, 57 (1981), pp. 453–476.

[87] Y. Fukazawa, K. Makishima, and T. Ohashi, *ASCA Compilation of X-Ray Properties of Hot Gas in Elliptical Galaxies and Galaxy Clusters: Two Breaks in the Temperature Dependences*, Publications of the Astronomical Society of Japan, 56 (2004), pp. 965–1009.

[88] J. M. Gabor, C. D. Impey, K. Jahnke, B. D. Simmons, J. R. Trump, a. M. Koekemoer, M. Brusa, N. Cappelluti, E. Schinnerer, V. Smolčić, M. Salvato, J. D. Rhodes, B. Mobasher, P. Capak, R. Massey, A. Leauthaud, and N. Scoville, *AGN Host Galaxy Morphologies in COSMOS*, arXiv, (2008), p. 21.

[89] G. Gavazzi, A. Boselli, L. Mayer, J. Iglesias-Paramo, J. M. Vílchez, and L. Carrasco, *75 Kiloparsec Trails of Ionized Gas behind Two Irregular Galaxies in A1367*, ApJL, 563 (2001), pp. L23–L26.

[90] G. Gavazzi, A. Contursi, L. Carrasco, A. Boselli, R. Kennicutt, M. Scodeggio, and W. Jaffe, *The radio and optical structure of three peculiar galaxies in A 1367.*, A&A, 304 (1995), p. 325.

[91] G. Gavazzi, L. Cortese, A. Boselli, J. Iglesias-Paramo, J. M. Vílchez, and L. Carrasco, *Capturing a Star Formation Burst in Galaxies Infalling onto the Cluster A1367*, ApJ, 597 (2003), pp. 210–217.

[92] G. Gavazzi and G. Trinchieri, *Radio and X-ray observations of the radio halo source in A1367*, ApJ, 270 (1983), pp. 410–416.

[93] K. Gebhardt and T. C. Beers, *Bound populations around cD galaxies and cD velocity offsets in clusters of galaxies*, ApJ, 383 (1991), pp. 72–89.

[94] S. Giacintucci and M. Markevitch, *Mapping the particle acceleration in the cool core of the galaxy cluster RX J1720. 1+ 2638*, arXiv Prepr. arXiv ..., (2014).

[95] G. Giovannini, a. Bonafede, L. Feretti, F. Govoni, M. Murgia, F. Ferrari, and G. Monti, *Radio halos in nearby (z ¡ 0.4) clusters of galaxies*, Astron. Astrophys., 507 (2009), pp. 1257–1270.

[96] G. Giovannini and L. Feretti, *Halo and relic sources in clusters of galaxies*, New Astron., 5 (2000), pp. 335–347.

[97] G. Giovannini and L. Feretti, *Diffuse Radio Sources and Cluster Mergers: Radio Halos and Relics*, in Merging Processes in Galaxy Clusters, L. Feretti, I. M. Gioia, and G. Giovannini, eds., vol. 272 of Astrophysics and Space Science Library, June 2002, pp. 197–227.

[98] G. Giovannini, L. Feretti, and H. Andernach, *VLA observations of the extended source near Coma A*, A&A, 150 (1985), pp. 302–306.

[99] G. Giovannini, L. Feretti, and C. Stanghellini, *The Coma cluster radio source 1253 + 275, revisited*, A&A, 252 (1991), pp. 528–537.

[100] G. Giovannini, L. Feretti, T. Venturi, K.-T. Kim, and P. P. Kronberg, *The halo radio source Coma C and the origin of halo sources*, ApJ, 406 (1993), pp. 399–406.

[101] M. Girardi, E. Escalera, D. Fadda, G. Giuricin, F. Mardirossian, and M. Mezzetti, *Optical Substructures in 48 Galaxy Clusters: New Insights from a Multiscale Analysis*, ApJ, 482 (1997), pp. 41–62.

[102] M. Girardi, G. Giuricin, F. Mardirossian, M. Mezzetti, and W. Boschin, *Optical Mass Estimates of Galaxy Clusters*, ApJ, 505 (1998), pp. 74–95.

[103] C. Goodall, *Understanding Robust and Exploratory Data Analysis*, Wiley, New York, 1983.

[104] F. Govoni, L. Feretti, G. Giovannini, H. Böhringer, T. H. Reiprich, and M. Murgia, *Radio and X-ray diffuse emission in six clusters of galaxies*, A&A, 376 (2001), pp. 803–819.

[105] F. Govoni, M. Murgia, L. Feretti, G. Giovannini, D. Dallacasa, and G. B. Taylor, *A2255: The first detection of filamentary polarized emission in a radio halo*, A&A, 430 (2005), pp. L5–L8.

[106] A. W. Graham, S. P. Driver, V. Petrosian, C. J. Conselice, M. A. Bershady, S. M. Crawford, and T. Goto, *Total Galaxy Magnitudes and Effective Radii from Petrosian Magnitudes and Radii*, AJ, 130 (2005), pp. 1535–1544.

[107] D. Gruber and Y. Rephaeli, *RXTE Spectrum of A2319*, ArXiv Astrophysics e-prints, (2001).

[108] J. E. Gunn and J. R. Gott, III, *On the Infall of Matter Into Clusters of Galaxies and Some Effects on Their Evolution*, ApJ, 176 (1972), p. 1.

[109] J. E. Gunn, W. A. Siegmund, E. J. Mannery, R. E. Owen, C. L. Hull, R. F. Leger, L. N. Carey, G. R. Knapp, D. G. York, W. N. Boroski, S. M. Kent, R. H. Lupton, C. M. Rockosi, M. L. Evans, P. Waddell, J. E. Anderson, J. Annis, J. C. Barentine, L. M. Bartoszek, S. Bastian, S. B. Bracker, H. J. Brewington, C. I. Briegel, J. Brinkmann, Y. J. Brown, M. A. Carr, P. C. Czarapata, C. C. Drennan, T. Dombeck, G. R. Federwitz, B. A. Gillespie, C. Gonzales, S. U. Hansen, M. Harvanek, J. Hayes, W. Jordan, E. Kinney, M. Klaene, S. J. Kleinman, R. G. Kron,

J. Kresinski, G. Lee, S. Limmongkol, C. W. Lindenmeyer, D. C. Long, C. L. Loomis, P. M. McGehee, P. M. Mantsch, E. H. Neilsen, Jr., R. M. Neswold, P. R. Newman, A. Nitta, J. Peoples, Jr., J. R. Pier, P. S. Prieto, A. Prosapio, C. Rivetta, D. P. Schneider, S. Snedden, and S.-i. Wang, *The 2.5 m Telescope of the Sloan Digital Sky Survey*, AJ, 131 (2006), pp. 2332–2359.

[110] C. P. Haines, P. Merluzzi, a. Mercurio, a. Gargiulo, N. Krusanova, G. Busarello, F. La Barbera, and M. Capaccioli, *Shapley Optical Survey - II. The effect of environment on the colour-magnitude relation and galaxy colours*, Mon. Not. R. Astron. Soc., 371 (2006), pp. 55–66.

[111] M. J. Henriksen and M. L. Markevitch, *Abell 754: A Non–Head-On Collision of Subclusters*, ApJL, 466 (1996), p. L79.

[112] J. P. Henry and U. G. Briel, *An X-ray temperature map of Abell 754: A major merger*, ApJL, 443 (1995), pp. L9–L12.

[113] J. D. Hernández-Fernández, J. Iglesias-Páramo, and J. M. Vílchez, *Uv To Far-Ir Catalog of a Galaxy Sample in Nearby Clusters: Spectral Energy Distributions and Environmental Trends*, Astrophys. J. Suppl. Ser., 199 (2012), p. 22.

[114] J. Hill and W. Oegerle, *Dynamics of cD clusters of galaxies. I-Redshift data for seven clusters*, Astron. J., 106 (1993).

[115] E. Hubble, *A Relation between Distance and Radial Velocity among Extra-Galactic Nebulae*, Proceedings of the National Academy of Science, 15 (1929), pp. 168–173.

[116] D. S. Hudson, R. Mittal, T. H. Reiprich, P. E. J. Nulsen, H. Andernach, and C. L. Sarazin, *What is a cool-core cluster? a detailed analysis of the cores of the X-ray flux-limited HIFLUGCS cluster sample*, A&A, 513 (2010), p. A37.

[117] M. J. Hudson, J. R. Lucey, R. J. Smith, D. J. Schlegel, and R. L. Davies, *Streaming motions of galaxy clusters within 12 000 km s 1 - III. A standardized catalogue of Fundamental Plane data*, Mon. Not. R. Astron. Soc., 327 (2001), pp. 265–295.

[118] Y. L. Jaffé, A. Aragón-Salamanca, G. De Lucia, P. Jablonka, G. Rudnick, R. Saglia, and D. Zaritsky, *The colour-magnitude relation of elliptical and lenticular galaxies in the ESO Distant Cluster Survey*, Mon. Not. R. Astron. Soc., 410 (2011), pp. 280–292.

[119] F. Jansen, D. Lumb, B. Altieri, J. Clavel, M. Ehle, C. Erd, C. Gabriel, M. Guainazzi, P. Gondoin, R. Much, R. Munoz, M. Santos, N. Schartel, D. Texier, and G. Vacanti, *XMM-Newton observatory. I. The spacecraft and operations*, A&A, 365 (2001), pp. L1–L6.

[120] T. H. Jarrett, M. Cohen, F. Masci, E. Wright, D. Stern, D. Benford, a. Blain, S. Carey, R. M. Cutri, P. Eisenhardt, C. Lonsdale, a. Mainzer, K. Marsh, D. Padgett, S. Petty, M. Ressler, M. Skrutskie, S. Stanford, J. Surace, C. W. Tsai, S. Wheelock, and D. L. Yan, *The Spitzer - Wise Survey of the Ecliptic Poles*, Astrophys. J., 735 (2011), p. 112.

[121] T. H. Jarrett, F. Masci, C. W. Tsai, S. Petty, M. E. Cluver, R. J. Assef, D. Benford, A. Blain, C. Bridge, E. Donoso, P. Eisenhardt, B. Koribalski, S. Lake, J. D. Neill, M. Seibert, K. Sheth, S. Stanford, and E. Wright, *Extending the Nearby Galaxy Heritage with WISE: First Results from the WISE Enhanced Resolution Galaxy Atlas*, AJ, 145 (2013), p. 6.

[122] T. E. Jeltema and S. Profumo, *Implications of Fermi Observations For Hadronic Models of Radio Halos in Clusters of Galaxies*, ApJ, 728 (2011), p. 53.

[123] N. N. Jetha, M. J. Hardcastle, and I. Sakelliou, *Jet speeds in wide-angle tailed radio galaxies*, Mon. Not. R. Astron. Soc., 368 (2006), pp. 609–618.

[124] M. Johnston-Hollitt, *Detection of magnetic fields and diffuse radio emission in Abell 3667 and other rich southern clusters of galaxies*, PhD thesis, University of Adelaide, 2003.

[125] M. Johnston-Hollitt, R. W. Hunstead, and E. Corbett, *The optical morphology of A3667 re-examined*, A&A, 479 (2008), pp. 1–8.

[126] C. Jones and W. Forman, *The structure of clusters of galaxies observed with Einstein*, ApJ, 276 (1984), pp. 38–55.

[127] L. R. Jones, T. J. Ponman, A. Horton, A. Babul, H. Ebeling, and D. J. Burke, *The nature and space density of fossil groups of galaxies*, MNRAS, 343 (2003), pp. 627–638.

[128] R. Kale and K. S. Dwarakanath, *Spectral Index Studies of the Diffuse Radio Emission in Abell 2256: Implications for Merger Activity*, ApJ, 718 (2010), pp. 939–946.

[129] R. Kale, K. S. Dwarakanath, J. Bagchi, and S. Paul, *Spectral and polarization study of the double relics in Abell 3376 using the Giant Metrewave Radio Telescope and the Very Large Array*, MNRAS, 426 (2012), pp. 1204–1211.

[130] S. J. Kannappan, J. M. Guie, and A. J. Baker, *E/S0 Galaxies on the Blue Color-Stellar Mass Sequence at z = 0: Fading Mergers or Future Spirals?*, AJ, 138 (2009), pp. 579–597.

[131] K. N. Kanov, C. L. Sarazin, and A. K. Hicks, *Chandra Observation of the Interaction of the Radio Source and Cooling Core in Abell 2063*, ApJ, 653 (2006), pp. 184–192.

[132] A. E. Kass, R. E. Raftery, *Bayes factors*, J. Amer. Statist. Assoc., 90 (1995), pp. 773–795.

[133] S. Kaviraj, K. Schawinski, J. E. G. Devriendt, I. Ferreras, S. Khochfar, S.-J. Yoon, S. K. Yi, J.-M. Deharveng, A. Boselli, T. Barlow, T. Conrow, K. Forster, P. G. Friedman, D. C. Martin, P. Morrissey, S. Neff, D. Schiminovich, M. Seibert, T. Small, T. Wyder, L. Bianchi, J. Donas, T. Heckman, Y.-W. Lee, B. Madore, B. Milliard, R. M. Rich, and A. Szalay, *UV-Optical Colors As Probes of Early-Type Galaxy Evolution*, ApJS, 173 (2007), pp. 619–642.

[134] J. C. Kempner and C. L. Sarazin, *Radio Halo and Relic Candidates from the Westerbork Northern Sky Survey*, ApJ, 548 (2001), pp. 639–651.

[135] K.-T. Kim, P. P. Kronberg, P. E. Dewdney, and T. L. Landecker, *The halo and magnetic field of the Coma cluster of galaxies*, ApJ, 355 (1990), pp. 29–37.

[136] R. Kiuchi, M. Mori, G. V. Bicknell, R. W. Clay, P. G. Edwards, R. Enomoto, S. Gunji, S. Hara, T. Hara, T. Hattori, S. Hayashi, Y. Higashi, Y. Hirai, K. Inoue, C. Itoh, S. Kabuki, F. Kajino, H. Katagiri, A. Kawachi, T. Kifune, H. Kubo, J. Kushida, Y. Matsubara, T. Mizukami, Y. Mizumoto, R. Mizuniwa, H. Muraishi, Y. Muraki, T. Naito, T. Nakamori, S. Nakano, D. Nishida, K. Nishijima, M. Ohishi, Y. Sakamoto, A. Seki, V. Stamatescu, T. Suzuki, D. L. Swaby, T. Tanimori, G. Thornton, F. Tokanai, K. Tsuchiya, S. Watanabe, Y. Yamada, E. Yamazaki, S. Yanagita, T. Yoshida, T. Yoshikoshi, and Y. Yukawa, *CANGAROO-III Search for TeV Gamma Rays from Two Clusters of Galaxies*, ApJ, 704 (2009), pp. 240–246.

[137] A. R. Klemola, *Groups and clusters of southern galaxies.*, AJ, 74 (1969), pp. 804–806.

[138] G. P. Knopp, J. P. Henry, and U. G. Briel, *ROSAT PSPC Observations of Abell 3667*, ApJ, 472 (1996), p. 125.

[139] T. Kodama and N. Arimoto, *Origin of the colour-magnitude relation of elliptical galaxies.*, A&A, 320 (1997), pp. 41–53.

[140] T. Kodama, R. G. Bower, and E. F. Bell, *The colour-magnitude relation of early-type galaxies in the Hubble Deep Field*, MNRAS, 306 (1999), pp. 561–566.

[141] S. S. Komissarov and A. G. Gubanov, *Relic radio galaxies: evolution of synchrotron spectrum*, A&A, 285 (1994), pp. 27–43.

[142] J. Kormendy and S. Djorgovski, *Surface photometry and the structure of elliptical galaxies*, Annual review of astronomy and astrophysics, 27 (1989), pp. 235–277.

[143] M. P. Kowalski, M. P. Ulmer, R. G. Cruddace, and K. S. Wood, *An X-ray survey of clusters of galaxies. IV - A survey of southern clusters and a compilation of upper limits for both Abell and southern clusters*, ApJS, 56 (1984), pp. 403–506.

[144] A. V. Kravtsov and S. Borgani, *Formation of Galaxy Clusters*, Annu. Rev. Astron. Astrophys., 50 (2012), pp. 353–409.

[145] J. Krempec-Krygier and B. Krygier, *Interaction of Abell Cluster 2063 and the Group of Galaxies MKW3s*, Acta Astronomica, 49 (1999), pp. 403–420.

[146] M. I. Large, D. S. Mathewson, and C. G. T. Haslam, *A High-Resolution Survey of the Coma Cluster of Galaxies at 408 Mc./s.*, Nature, 183 (1959), pp. 1663–1664.

[147] S. M. Lea, J. Silk, E. Kellogg, and S. Murray, *Thermal-Bremsstrahlung Interpretation of Cluster X-Ray Sources*, ApJL, 184 (1973), p. L105.

[148] F. Leisch, *A toolbox for k-centroids cluster analysis*, Computational Statistics and Data Analysis, 51 (2006), pp. 526–544.

[149] G. B. Lima Neto, V. Pislar, and J. Bagchi, *BeppoSAX observation of the rich cluster of galaxies Abell 85*, A&A, 368 (2001), pp. 440–450.

[150] G. B. Lima Neto, V. Pislar, F. Durret, D. Gerbal, and E. Slezak, *The rich cluster of galaxies ABCG85. II. X-ray analysis using the ROSAT HRI.*, A&A, 327 (1997), pp. 81–89.

[151] Y.-T. Lin and J. J. Mohr, *K-band Properties of Galaxy Clusters and Groups: Brightest Cluster Galaxies and Intracluster Light*, ApJ, 617 (2004), pp. 879–895.

[152] R. R. Lindner, A. J. Baker, J. P. Hughes, N. Battaglia, N. Gupta, K. Knowles, T. A. Marriage, F. Menanteau, K. Moodley, E. D. Reese, and R. Srianand, *The Radio Relics and Halo of El Gordo, a Massive z = 0.870 Cluster Merger*, ApJ, 786 (2014), p. 49.

[153] F. K. Liu and G. Z. Xie, *A finding list of extragalactic radio jets and statistical results*, Astron. Astrophys. Suppl. Ser., 95 (1992), pp. 249–268.

[154] R. E. G. Machado and G. B. Lima Neto, *Simulations of the merging galaxy cluster Abell 3376*, Monthly Notices of the Royal Astronomical Society, 430 (2013), pp. 3249–3260.

[155] M. Maechler, P. Rousseeuw, A. Struyf, M. Hubert, and K. Hornik, *cluster: Cluster Analysis Basics and Extensions*, 2013. R package version 1.14.4 — For new features, see the 'Changelog' file (in the package source).

[156] K. G. Malmquist, Lund Medd. Ser. II, 22 (1920), pp. 1–39.

[157] F. Marini, S. Bardelli, E. Zucca, S. De Grandi, A. Cappi, S. Ettori, L. Moscardini, G. Tormen, and A. Diaferio, *BeppoSAX temperature maps of galaxy clusters in the Corona Borealis supercluster: A2061, A2067 and A2124*, MNRAS, 353 (2004), pp. 1219–1230.

[158] M. Markevitch, C. L. Sarazin, and A. Vikhlinin, *Physics of the Merging Clusters Cygnus A, A3667, and A2065*, ApJ, 521 (1999), pp. 526–530.

[159] M. Markevitch and A. Vikhlinin, *Dark Matter and Baryon Fraction at the Virial Radius in Abell 2256*, ApJ, 491 (1997), pp. 467–476.

[160] M. Markevitch, A. Vikhlinin, P. Mazzotta, and L. VanSpeybroeck, *Temperature Structure of Four Merging Clusters Obtained with Chandra*, ArXiv Astrophysics e-prints, (2000).

[161] P. Martini, J. S. Mulchaey, and D. D. Kelson, *The Distribution of Active Galactic Nuclei in Clusters of Galaxies*, ApJ, 664 (2007), pp. 761–776.

[162] W. G. Mathews and J. N. Bregman, *Radiative accretion flow onto giant galaxies in clusters*, ApJ, 224 (1978), pp. 308–319.

[163] A. Mazure, P. Katgert, R. den Hartog, A. Biviano, P. Dubath, E. Escalera, P. Focardi, D. Gerbal, G. Giuricin, B. Jones, O. Le Fevre, M. Moles, J. Perea, and G. Rhee, *The ESO Nearby Abell Cluster Survey. II. The distribution of velocity dispersions of rich galaxy clusters.*, A&A, 310 (1996), pp. 31–48.

[164] N. Menci, A. Fontana, E. Giallongo, A. Grazian, and S. Salimbeni, *The Abundance of Distant and Extremely Red Galaxies: The Role of AGN Feedback in Hierarchical Models*, ApJ, 647 (2006), pp. 753–762.

[165] N. Menci, A. Fontana, E. Giallongo, and S. Salimbeni, *Bimodal Color Distribution in Hierarchical Galaxy Formation*, ApJ, 632 (2005), pp. 49–57.

[166] D. Merritt, *Internal dynamics of galaxy clusters*, Minnesota Lect. Clust. Galaxies ..., (1988).

[167] S. Molendi and F. Pizzolato, *Is the Gas in Cooling Flows Multiphase?*, ApJ, 560 (2001), pp. 194–200.

[168] C. Moss, M. Whittle, and J. E. Pesce, *Tidally induced star formation in Abell 1367*, Mon. Not. R. Astron. Soc., 300 (1998), pp. 205–220.

[169] F. Mosteller and J. W. Tukey, *Data analysis and regression. A second course in statistics*, 1977.

[170] M. Murgia, F. Govoni, L. Feretti, and G. Giovannini, *A double radio halo in the close pair of galaxy clusters Abell 399 and Abell 401*, arXiv Prepr. arXiv ..., 86 (2009), pp. 1–6.

[171] M. Murgia, F. Govoni, L. Feretti, and G. Giovannini, *A double radio halo in the close pair of galaxy clusters Abell 399 and Abell 401*, A&A, 509 (2010), p. A86.

[172] T. Nagayama, P. A. Woudt, C. Nagashima, Y. Nakajima, D. Kato, M. Kurita, T. Nagata, H. Nakaya, M. Tamura, K. Sugitani, K. Wakamatsu, and S. Sato, *A deep near-infrared survey around the giant radio galaxy PKS 1343-601*, MNRAS, 354 (2004), pp. 980–990.

[173] M. Neyrinck, *Zobov: a parameter-free void-finding algorithm*, Mon. Not. R. Astron. ..., 000 (2008).

[174] K. G. Noeske, B. J. Weiner, S. M. Faber, C. Papovich, D. C. Koo, R. S. Somerville, K. Bundy, C. J. Conselice, J. A. Newman, D. Schiminovich, E. Le Floc'h, A. L. Coil, G. H. Rieke, J. M. Lotz, J. R. Primack, P. Barmby, M. C. Cooper, M. Davis, R. S. Ellis, G. G. Fazio, P. Guhathakurta, J. Huang, S. A. Kassin, D. C. Martin, A. C. Phillips, R. M. Rich, T. A. Small, C. N. A. Willmer, and G. Wilson, *Star Formation in AEGIS Field Galaxies since z=1.1: The Dominance of Gradually Declining Star Formation, and the Main Sequence of Star-forming Galaxies*, ApJL, 660 (2007), pp. L43–L46.

[175] S. E. Nuza, M. Hoeft, R. J. van Weeren, S. Gottlöber, and G. Yepes, *How many radio relics await discovery?*, Mon. Not. R. Astron. Soc., 420 (2012), pp. 2006–2019.

[176] A. A. O'Donoghue, J. A. Eilek, and F. N. Owen, *Flow dynamics and bending of wide-angle tailed radio sources*, ApJ, 408 (1993), pp. 428–445.

[177] W. Oegerle, J. Hill, and M. Fitchett, *Observations of high dispersion clusters of galaxies: Constraints on Cold Dark Matter*, Astron. J., (1995).

[178] W. R. Oegerle and J. M. Hill, *Dynamics of cD Clusters of Galaxies. IV. Conclusion of a Survey of 25 Abell Clusters*, AJ, 122 (2001), pp. 2858–2873.

[179] M. S. Owers, W. J. Couch, and P. E. Nulsen, *Substructure in the cold front cluster abell 3667*, The Astrophysical Journal, 693 (2009), p. 901.

[180] M. S. Owers, P. E. J. Nulsen, and W. J. Couch, *Minor Merger-induced Cold Fronts in Abell 2142 and RXJ1720.1+2638*, ApJ, 741 (2011), p. 122.

[181] C. B. Peres, A. C. Fabian, A. C. Edge, S. W. Allen, R. M. Johnstone, and D. A. White, *A ROSAT study of the cores of clusters of galaxies - I. Cooling flows in an X-ray flux-limited sample*, MNRAS, 298 (1998), pp. 416–432.

[182] J. R. Peterson, F. B. S. Paerels, J. S. Kaastra, M. Arnaud, T. H. Reiprich, A. C. Fabian, R. F. Mushotzky, J. G. Jernigan, and I. Sakelliou, *X-ray imaging-spectroscopy of Abell 1835*, A&A, 365 (2001), pp. L104–L109.

[183] V. Petrosian, *Surface brightness and evolution of galaxies*, ApJL, 209 (1976), pp. L1–L5.

[184] K. A. Pimbblet, S. S. Shabala, C. P. Haines, A. Fraser-McKelvie, and D. J. E. Floyd, *The drivers of AGN activity in galaxy clusters: AGN fraction as a function of mass and environment*, MNRAS, 429 (2013), pp. 1827–1839.

[185] K. a. Pimbblet, I. Smail, A. C. Edge, E. O'Hely, W. J. Couch, and A. I. Zabludoff, *The Las Campanas/Anglo-Australian Telescope Rich Cluster Survey - III. Spectroscopic studies of X-ray bright galaxy clusters at z˜ 0.1*, Mon. Not. R. Astron. Soc., 366 (2006), pp. 645–666.

[186] K. a. Pimbblet, I. Smail, T. Kodama, W. J. Couch, A. C. Edge, A. I. Zabludoff, and E. O'Hely, *The Las Campanas/AAT Rich Cluster Survey - II. The environmental dependence of galaxy colours in clusters at z 0.1*, Mon. Not. R. Astron. Soc., 331 (2002), pp. 333–350.

[187] V. Pislar, F. Durret, D. Gerbal, G. B. Lima Neto, and E. Slezak, *The rich cluster of galaxies ABCG 85. I. X-ray analysis.*, A&A, 322 (1997), pp. 53–65.

[188] R. F. Pizzo, A. G. de Bruyn, G. Bernardi, and M. A. Brentjens, *Deep multi-frequency rotation measure tomography of the galaxy cluster A2255*, A&A, 525 (2011), p. A104.

[189] Planck Collaboration, P. A. R. Ade, N. Aghanim, M. Arnaud, M. Ashdown, F. Atrio-Barandela, J. Aumont, C. Baccigalupi, A. Balbi, A. J. Banday, and et al., *Planck intermediate results. X. Physics of the hot gas in the Coma cluster*, A&A, 554 (2013), p. A140.

[190] B. M. Poggianti, *Color, spectral and morphological transformations of galaxies in clusters*, Astrophysics and Space Science, 285 (2003), pp. 121–131.

[191] S. C. Porter, S. Raychaudhury, K. a. Pimbblet, and M. J. Drinkwater, *Star formation in galaxies falling into clusters along supercluster-scale filaments*, Mon. Not. R. Astron. Soc., 1160 (2008), pp. 1152–1160.

[192] M. Pović, M. Sánchez-Portal, A. M. P. García, A. Bongiovanni, J. Cepa, M. Huertas-Company, M. A. Lara-López, M. F. Lorenzo, A. Ederoclite, E. Alfaro, H. Castañeda, J. Gallego, J. I. González-Serrano, and J. J. González, *AGN-Host Galaxy Connection: Morphology and Colours of X-ray Selected AGN at z ¡ 2*, arXiv, (2012), p. 24.

[193] W. H. Press and P. Schechter, *Formation of Galaxies and Clusters of Galaxies by Self-Similar Gravitational Condensation*, ApJ, 187 (1974), pp. 425–438.

[194] D. Proust, A. Mazure, L. Sodre, H. Capelato, and G. Lund, *New measurements of radial velocities in clusters of galaxies. II*, A&AS, 72 (1988), pp. 415–425.

[195] D. Proust, H. Quintana, E. R. Carrasco, A. Reisenegger, E. Slezak, H. Muriel, R. Dünner, L. Sodré, Jr., M. J. Drinkwater, Q. A. Parker, and C. J. Ragone, *The Shapley Supercluster: the Largest Matter Concentration in the Local Universe*, The Messenger, 124 (2006), p. 30.

[196] H. Quintana and A. Ramirez, *Redshifts of 165 Abell and southern rich clusters of galaxies*, ApJS, 96 (1995), pp. 343–358.

[197] R Core Team, *R: A Language and Environment for Statistical Computing*, R Foundation for Statistical Computing, Vienna, Austria, 2013.

[198] T. H. Reiprich and H. Böhringer, *The Mass Function of an X-Ray Flux-limited Sample of Galaxy Clusters*, ApJ, 567 (2002), pp. 716–740.

[199] I. F. Riad, R. C. Kraan-Korteweg, and P. A. Woudt, *The effect of dust extinction on the observed properties of galaxies in the near-infrared*, MNRAS, 401 (2010), pp. 924–932.

[200] G. T. Richards, X. Fan, H. J. Newberg, M. A. Strauss, D. E. Vanden Berk, D. P. Schneider, B. Yanny, A. Boucher, S. Burles, J. A. Frieman, J. E. Gunn, P. B. Hall, Ž. Ivezić, S. Kent, J. Loveday, R. H. Lupton, C. M. Rockosi, D. J. Schlegel, C. Stoughton, M. SubbaRao, and D. G. York, *Spectroscopic Target Selection in the Sloan Digital Sky Survey: The Quasar Sample*, AJ, 123 (2002), pp. 2945–2975.

[201] H. J. Rood and G. N. Sastry, *"Tuning Fork" Classification of Rich Clusters of Galaxies*, Publications of the Astronomical Society of the Pacific, 83 (1971), p. 313.

[202] H. J. A. Rottgering, M. H. Wieringa, R. W. Hunstead, and R. D. Ekers, *The extended radio emission in the luminous X-ray cluster A3667*, MNRAS, 290 (1997), pp. 577–584.

[203] L. Rudnick and J. A. Lemmerman, *An Objective Survey of Mpc-scale Radio Emission in 0.03 ¡ z ¡ 0.3 Bright X-ray Clusters*, ApJ, 697 (2009), pp. 1341–1357.

[204] D. Ryu, H. Kang, J. Cho, and S. Das, *Turbulence and Magnetic Fields in the Large-Scale Structure of the Universe*, Science, 320 (2008), pp. 909–.

[205] I. Sakelliou and T. J. Ponman, *The binary cluster system Abell 399/401*, MmSAI, 75 (2004), p. 547.

[206] ——, *XMM-Newton observations of Abell 2255: a test case of a merger after 'core crossing'*, MNRAS, 367 (2006), pp. 1409–1416.

[207] S. Salimbeni, E. Giallongo, N. Menci, M. Castellano, A. Fontana, A. Grazian, L. Pentericci, D. Trevese, S. Cristiani, M. Nonino, and E. Vanzella, *The red and blue galaxy luminosity function in the GOODS field: Evidence for an excess of red-dwarf galaxies*, Nuovo Cimento B Serie, 122 (2007), pp. 1183–1188.

[208] J. S. Sanders, A. C. Fabian, S. W. Allen, R. G. Morris, J. Graham, and R. M. Johnstone, *Cool X-ray emitting gas in the core of the Centaurus cluster of galaxies*, MNRAS, 385 (2008), pp. 1186–1200.

[209] C. L. Sarazin, *The Energy Spectrum of Primary Cosmic-Ray Electrons in Clusters of Galaxies and Inverse Compton Emission*, ApJ, 520 (1999), pp. 529–547.

[210] C. L. Sarazin, A. Finoguenov, and D. R. Wik, *Merger shocks in Abell 3667 and the Cygnus A cluster*, Astronomische Nachrichten, 334 (2013), p. 346.

[211] K. Schawinski, C. M. Urry, B. D. Simmons, L. Fortson, S. Kaviraj, W. C. Keel, C. J. Lintott, K. L. Masters, R. C. Nichol, M. Sarzi, R. Skibba, E. Treister, K. W. Willett, O. I. Wong, and S. K. Yi, *The green valley is a red herring: Galaxy Zoo reveals two evolutionary pathways towards quenching of star formation in early- and late-type galaxies*, MNRAS, 440 (2014), pp. 889–907.

[212] E. F. Schlafly and D. P. Finkbeiner, *Measuring Reddening with Sloan Digital Sky Survey Stellar Spectra and Recalibrating SFD*, ApJ, 737 (2011), p. 103.

[213] D. J. Schlegel, D. P. Finkbeiner, and M. Davis, *Maps of Dust Infrared Emission for Use in Estimation of Reddening and Cosmic Microwave Background Radiation Foregrounds*, ApJ, 500 (1998), pp. 525–553.

[214] G. Schwarz, *Estimating the dimension of a model.*, Annals of Statistics, 6 (1978), pp. 461–646.

[215] D. W. Scott, *On optimal and data-based histograms*, Biometrika, 66 (1979), pp. 605–610.

[216] S. Shen, G. Kauffmann, A. von der Linden, S. D. M. White, and P. N. Best, *Radio-loud active galactic nuclei and the L_X-σ relation of galaxy groups and clusters*, MNRAS, 389 (2008), pp. 1074–1086.

[217] H. Shim, M. Im, H. M. Lee, M. G. Lee, S. J. Kim, H. S. Hwang, N. Hwang, J. Ko, J. C. Lee, S. Lim, H. Matsuhara, H. Seo, T. Wada, and T. Goto, *Merging Galaxy Cluster A2255 in Mid-Infrared*, Astrophys. J., 727 (2011), p. 14.

[218] B. W. Silverman, *Density estimation for statistics and data analysis*, Monographs on Statistics and Applied Probability, London: Chapman and Hall, 1986.

[219] S. W. Skillman, B. W. O'Shea, E. J. Hallman, J. O. Burns, and M. L. Norman, *Cosmological Shocks in Adaptive Mesh Refinement Simulations and the Acceleration of Cosmic Rays*, ApJ, 689 (2008), pp. 1063–1077.

[220] O. Slee and A. Roy, *Four extreme relic radio sources in clusters of galaxies*, Astron. . . . , (2001), pp. 1172–1193.

[221] O. B. Slee and A. L. Roy, *An extreme example of a radio relic in Abell 4038*, MNRAS, 297 (1998), pp. L86–L92.

[222] E. Slezak, F. Durret, J. Guibert, and C. Lobo, *A photometric catalogue of galaxies in the cluster Abell 85*, A&AS, 128 (1998), pp. 67–73.

[223] T. A. Small, C.-P. Ma, W. L. W. Sargent, and D. Hamilton, *The Norris Survey of the Corona Borealis Supercluster. III. Structure and Mass of the Supercluster*, ApJ, 492 (1998), pp. 45–56.

[224] L. Sodre, Jr., H. V. Capelato, J. E. Steiner, D. Proust, and A. Mazure, *The cluster of galaxies SC2008-57 (A3667)*, MNRAS, 259 (1992), pp. 233–246.

[225] L. Solovyeva, S. Anokhin, L. Feretti, J. L. Sauvageot, R. Teyssier, G. Giovannini, F. Govoni, and D. Neumann, *The dynamical state of A548 from XMM-Newton data: X-ray and radio connection*, A&A, 484 (2008), pp. 621–630.

[226] D. Stern, R. J. Assef, D. J. Benford, A. Blain, R. Cutri, A. Dey, P. Eisenhardt, R. L. Griffith, T. H. Jarrett, S. Lake, F. Masci, S. Petty, S. A. Stanford, C.-W. Tsai, E. L. Wright, L. Yan, F. Harrison, and K. Madsen, *Mid-infrared Selection of Active Galactic Nuclei with the Wide-Field Infrared Survey Explorer. I. Characterizing WISE-selected Active Galactic Nuclei in COSMOS*, ApJ, 753 (2012), p. 30.

[227] I. Strateva, Ž. Ivezić, G. R. Knapp, V. K. Narayanan, M. A. Strauss, J. E. Gunn, R. H. Lupton, D. Schlegel, N. A. Bahcall, J. Brinkmann, R. J. Brunner, T. Budavári, I. Csabai, F. J. Castander, M. Doi, M. Fukugita, Z. Győry, M. Hamabe, G. Hennessy, T. Ichikawa, P. Z. Kunszt, D. Q. Lamb, T. A. McKay, S. Okamura, J. Racusin, M. Sekiguchi, D. P. Schneider, K. Shimasaku, and D. York, *Color Separation of Galaxy Types in the Sloan Digital Sky Survey Imaging Data*, AJ, 122 (2001), pp. 1861–1874.

[228] M. Struble and H. Rood, *A compilation of redshifts and velocity dispersions for ACO clusters*, Astrophys. J. Suppl. . . . , (1999).

[229] M. Sun, M. Donahue, and G. M. Voit, *Hα Tail, Intracluster H II Regions, and Star Formation: ESO 137-001 in Abell 3627*, ApJ, 671 (2007), pp. 190–202.

[230] M. Sun and S. S. Murray, *Chandra View of the Dynamically Young Cluster of Galaxies A1367. I. Small-Scale Structures*, ApJ, 576 (2002), pp. 708–719.

[231] M. Sun, S. S. Murray, M. Markevitch, and A. Vikhlinin, *Chandra Observation of A2256: A Cluster at the Early Stage of Merging*, ApJ, 565 (2002), pp. 867–876.

[232] A. I. Terlevich, N. Caldwell, and R. G. Bower, *The colour-magnitude relation for galaxies in the Coma cluster*, MNRAS, 326 (2001), pp. 1547–1562.

[233] J. W. Tukey, *Bias and confidence in not-quite large samples (abstract)*, Ann. Math. Stat., 29: 614 (1958).

[234] R. B. Tully and J. R. Fisher, *A new method of determining distances to galaxies*, A&A, 54 (1977), pp. 661–673.

[235] E. A. Valentijn, *A Westerbork Survey of Clusters of Galaxies - Part Ten - a 610-MHZ Survey of Extended Radio Emission from 8 Abell Clusters*, A&AS, 38 (1979), p. 319.

[236] R. J. van Weeren, M. Brüggen, H. J. A. Röttgering, and M. Hoeft, *Using double radio relics to constrain galaxy cluster mergers: a model of double radio relics in CIZA J2242.8+5301*, MNRAS, 418 (2011), pp. 230–243.

[237] R. J. van Weeren, M. Brüggen, H. J. A. Röttgering, M. Hoeft, S. E. Nuza, and H. T. Intema, *Radio continuum observations of new radio halos and relics from the NVSS and WENSS surveys. Relic orientations, cluster X-ray luminosity, and redshift distributions*, A&A, 533 (2011), p. A35.

[238] R. J. van Weeren, H. J. A. Röttgering, J. Bagchi, S. Raychaudhury, H. T. Intema, F. Miniati, T. A. Ensslin, M. Markevitch, and T. Erben, *Radio observations of ZwCl 2341.1+0000: a double radio relic cluster*, A&A, 506 (2009), pp. 1083–1094.

[239] R. J. van Weeren, H. J. A. Röttgering, and M. Brüggen, *Diffuse steep-spectrum sources from the 74 MHz VLSS survey*, A&A, 527 (2011), p. A114.

[240] ——, *Diffuse steep-spectrum sources from the 74 MHz VLSS survey*, A&A, 527 (2011), p. A114.

[241] R. J. van Weeren, H. J. A. Röttgering, M. Brüggen, and A. Cohen, *A search for steep spectrum radio relics and halos with the GMRT*, A&A, 508 (2009), pp. 75–92.

[242] van Weeren R. J. Bruggen M. Rottgering H. J. A. Hoeft M. Nuza S. E. Intema H. T., *Radio continuum observations of new radio halos and relics from the NVSS and WENSS surveys*, A&A, 35 (2011), pp. 1–20.

[243] F. Vazza, K. Dolag, D. Ryu, G. Brunetti, C. Gheller, H. Kang, and C. Pfrommer, *A comparison of cosmological codes: properties of thermal gas and shock waves in large-scale structures*, MNRAS, 418 (2011), pp. 960–985.

[244] T. Venturi, S. Bardelli, D. Dallacasa, G. Brunetti, S. Giacintucci, R. W. Hunstead, and R. Morganti, *The radio halo in the merging cluster A3562*, A&A, 402 (2003), pp. 913–920.

[245] T. Venturi, M. Rossetti, S. Bardelli, S. Giacintucci, D. Dallacasa, M. Cornacchia, and N. G. Kantharia, *Radio emission at the centre of the galaxy cluster Abell 3560: evidence for core sloshing?*, A&A, 558 (2013), p. A146.

[246] A. Vikhlinin, R. A. Burenin, H. Ebeling, W. R. Forman, A. Hornstrup, C. Jones, A. V. Kravtsov, S. S. Murray, D. Nagai, H. Quintana, and A. Voevodkin, *Chandra Cluster Cosmology Project. II. Samples and X-Ray Data Reduction*, ApJ, 692 (2009), pp. 1033–1059.

[247] A. Vikhlinin, M. Markevitch, and S. S. Murray, *A Moving Cold Front in the Intergalactic Medium of A3667*, ApJ, 551 (2001), pp. 160–171.

[248] N. Visvanathan and A. Sandage, *The color-absolute magnitude relation for E and S0 galaxies. I - Calibration and tests for universality using Virgo and eight other nearby clusters*, ApJ, 216 (1977), pp. 214–226.

[249] M. A. G. Willson, *Radio observations of the cluster of galaxies in Coma Berenices - the 5C4 survey.*, Monthly Notices of the Royal Astronomical Society, 151 (1970), pp. 1–44.

[250] S. Wilson, *A multi-wavelength study of a sample of galaxy clusters*, Master's thesis, University of the North-West, South Africa, 2012.

[251] A. Wirth, L. Smarr, and J. S. Gallagher, *Dumbbell galaxies and precessing radio jets*, AJ, 87 (1982), pp. 602–615.

[252] E. L. Wright, P. R. M. Eisenhardt, A. K. Mainzer, M. E. Ressler, R. M. Cutri, T. Jarrett, J. D. Kirkpatrick, D. Padgett, R. S. McMillan, M. Skrutskie, S. A. Stanford, M. Cohen, R. G. Walker, J. C. Mather, D. Leisawitz, T. N. Gautier, III, I. McLean, D. Benford, C. J. Lonsdale, A. Blain, B. Mendez, W. R. Irace, V. Duval, F. Liu, D. Royer, I. Heinrichsen, J. Howard, M. Shannon, M. Kendall, A. L. Walsh, M. Larsen, J. G. Cardon, S. Schick, M. Schwalm, M. Abid, B. Fabinsky, L. Naes, and C.-W. Tsai, *The Wide-field Infrared Survey Explorer (WISE): Mission Description and Initial On-orbit Performance*, AJ, 140 (2010), pp. 1868–1881.

[253] T. K. Wyder, D. C. Martin, D. Schiminovich, M. Seibert, T. Budavári, M. A. Treyer, T. A. Barlow, K. Forster, P. G. Friedman, P. Morrissey, S. G. Neff, T. Small, L. Bianchi, J. Donas, T. M. Heckman, Y.-W. Lee, B. F. Madore, B. Milliard, R. M. Rich, A. S. Szalay, B. Y. Welsh, and S. K. Yi, *The UV-Optical Galaxy Color-Magnitude Diagram. I. Basic Properties*, ApJS, 173 (2007), pp. 293–314.

[254] H. B. Yuan, X. W. Liu, and M. S. Xiang, *Empirical extinction coefficients for the GALEX, SDSS, 2MASS and WISE passbands*, MNRAS, 430 (2013), pp. 2188–2199.

[255] Q. Yuan, X. Zhou, and Z. Jiang, *Multicolor Photometry of the Galaxies in A2255 by the Beijing-Arizona-Taiwan-Connecticut Survey and Sloan Digital Sky Survey*, ApJS, 149 (2003), pp. 53–66.

[256] A. I. Zabludoff and D. Zaritsky, *A Collision of Subclusters in Abell 754*, ApJL, 447 (1995), p. L21.

[257] F. Zwicky, E. Herzog, and P. Wild, *Catalogue of galaxies and of clusters of galaxies, Vol. 2*, 1963.

[258] F. Zwicky, E. Herzog, P. Wild, M. Karpowicz, and C. T. Kowal, *Catalogue of galaxies and of clusters of galaxies, Vol. I*, 1961.